Fall 2014

# Control of morphology Al-Fe-Si phase in Al-Si-Cu hypoeutectic alloy

Meng Wang
*Purdue University*

Graduate School Form 30
(Updated 11/20/2014)

# PURDUE UNIVERSITY
## GRADUATE SCHOOL
## Thesis/Dissertation Acceptance

This is to certify that the thesis/dissertation prepared

By Meng Wang

Entitled
CONTROL OF MORPHOLOGY OF AL-FE-SI PHASE IN AL-SI-CU HYPOEUTECTIC ALLOY

For the degree of Doctor of Philosophy

Is approved by the final examining committee:

Qingyou Han

David Johnson

Helen McNally

Milan Rakita

To the best of my knowledge and as understood by the student in the Thesis/Dissertation Agreement, Publication Delay, and Certification/Disclaimer (Graduate School Form 32), this thesis/dissertation adheres to the provisions of Purdue University's "Policy on Integrity in Research" and the use of copyrighted material.

Qingyou Han

Approved by Major Professor(s): _____

_____

Approved by: James Mohler 12/05/2014

Head of the Department Graduate Program Date

# CONTROL OF MORPHOLOGY AL-FE-SI PHASE IN AL-SI-CU HYPOEUTECTIC ALLOY

A Dissertation

Submitted to the Faculty

of

Purdue University

by

Meng Wang

In Partial Fulfillment of the

Requirements for the Degree

of

Doctor of Philosophy

December 2014

Purdue University

West Lafayette, Indiana

# ACKNOWLEDGEMENTS

I would like to thank my advisor Dr. Qingyou Han for his unconditional support, encouragement, unlimited patience, trust in me, and countless insightful discussions from which I learned a lot. His scientific enthusiasm and need to know why and how things work served me as an inspiration to persevere. I am indebted to Dr. David Johnson for giving me the use of Thermo-Calc software. This software turned out to be the main tool in this research. Thanks to Dr. Helen McNally for her guidance. Thanks to Dr. Milan Rakita for accepting on short notice to serve as my committee member and giving very useful help.

I am indebted to Dr. Wilson Xu, who gave me great help for my research.

I am thankful to Professor Joseph Kmec for revision of my dissertation.

I am thankful to all those people in my research group, including Dr Zhiwei Liu, Dr Jie Song, Dr Yanxiong Liu, Wei Dai, Fei He, Fei Yin, Hengyu Zhu, Pu Wang, Yanfei Liu, Pengyu Zhu, Derrick Myers, Ryan Houck, and Ian McAdams. I express great acknowledge the donation of master alloys from Dr. Greg Hildeman.

My true love and gratitude go to my parents, Keqi Wang and Jing Mo, and all my other family members. My girl friend, Yang Chen, gave me the greatest help and support to finish my Ph. D. study.

TABLE OF CONTENTS

Page

Page

Page

# LIST OF TABLES

Table Page

Table Page

Table Page

# LIST OF FIGURES

Figure Page

Figure Page

# ABSTRACT

Wang, Meng. Ph.D., Purdue University, December 2014. Control of Morphology of Al-Fe-Si Phase in Al-Si-Cu Hypoeutectic Alloy. Major Professor: Qingyou Han.

Aluminum-Silicon (Al-Si) alloys are one of the most versatile aluminum alloys. Iron is considered one of the most harmful elements in Al-Si diecasting alloy because its presence leads to the precipitation of many AlFeSi intermetallic phases and unacceptable mechanical properties, such as reduction in ductility. Thus controlling the fraction and morphology of AlFeSi phase, especially the β-AlFeSi phase is an important way to improve the ductility of Al-Si die casting alloys.

In this dissertation, thermodynamics calculation of AlFeSi phase formation and fraction change during solidification process were conducted using Thermo-Calc software. A series of experiments, including adjusting cooling rates, addition of alloying elements, and heat treatment were conducted and effective methods to eliminate the detrimental effect of β-AlFeSi phase were examined.

Thermodynamics calculations, provided many worthwhile findings, including that the formation temperature and fraction of α-AlFeSi and β-AlFeSi are mainly affected by the content of Mn and Fe elements; that both elements can effectively increase the formation temperature of both AlFeSi phases; that addition of Mn can reduce the amount of more detrimental β-AlFeSi, while Fe addition facilitates the formation of both α-

AlFeSi and β-AlFeSi; that Mg addition can reduce the formation temperature of β-AlFeSi, which means it can reduce the size of β-AlFeSi; that other elements do not have a significant effect on the formation and fraction of α-AlFeSi, β-AlFeSi, fcc α-Al and Si phase. Thus the findings show that an effective method for reducing β-AlFeSi phase is to reduce Fe content, control the amount of Mn content, and increase Mg content.

With low Mn and Fe, β-AlFeSi phase is a stable phase and can be formed with low cooling rates. Thus increasing cooling rates will effectively reduce the amount of β-AlFeSi phase. With the addition of Mn or Fe, α-AlFeSi is more stable and high cooling rates can facilitate the formation of β-AlFeSi phase in reverse. The reason lies in high content Mn and Fe increase the stability of α-AlFeSi phase. Thus increasing cooling rate method should not be used for high Fe, high Mn Al-Si alloy.

Addition of Ca and Sr is shown to result in a reduction of the β-AlFeSi phase. They have the effect of fragmentation by the rejection of Si at the β-phase/Al matrix interface. On the other hand, with addition of Ca and Sr, the introduced $Al_2CaSi_2$/$Al_2SrSi_2$ can be the substrate of α-AlFeSi. From the experiment results, the Sr and Ca addition should be controlled between 0.05 and 0.1%.

Addition of K seems to have the most beneficial effect on β-AlFeSi phase modification. $K_2O$ is formed to be the nucleation substrate of α-AlFeSi and, because of the solution ability of K in aluminum, no introduced intermetallics formed. It is proved that 1%K addition can effectively modify β-AlFeSi phase.

The study also shows that the high-temperature short-time heat treatment can lead to an effective reduction of the size the fraction of β-AlFeSi phase. The reduction of β-AlFeSi phase is because of not only the decomposition of β-AlFeSi but also the transformation of

β-AlFeSi to α-AlFeSi for A380 alloy. Heat treatment at 525 ℃ for 1 hour is enough to eliminate all the β-AlFeSi. However, the treatment temperature cannon be to to high to avoid other detrimental effect.

In summary, the effective way to reduce the detrimental effect of β-AlFeSi include the increase of the cooling rate, control of the content Fe and Mn, addition of Sr/Ca/K element, and short time high temperature heat treatment.

# CHAPTER 1. INTRODUCTION

## 1.1 Background

Aluminum-Silicon alloys are one of the most widely used aluminum alloys. Based on the Si concentration the Al-Si alloy systems are divided into three categories: hypoeutectic (<11.6% Si), eutectic (11.6-13% Si) and hypereutectic (14-25% Si). Hypoeutectic alloys are most widely used because of their excellent casting properties and comparatively high strength-weight ratio. (Taylor, 1995)

Of all the casting methods, die casting is a high-efficiency, high-quality process. Die casting is production method that forces liquid alloy into a mold under high pressure. Using die-casting method to manufacture parts is easy and inexpensive, which is suitable for small size parts. Die castings usually have a very good surface and size and can make dimensional perfect products. The die casting method is used extensively by the automobile manufacturing and other industries. A number of Al-Si die casting alloys, such as A319, A380, A383, A390 et al., are the main currently used die casting aluminum alloys.

In most Al-Si die casting aluminum alloys, Fe is a both beneficial and a detrimental element. With iron, soldering can be inhibited, while the brittle AlFeSi phase will also degrade mechanical properties and induce pores and defects in aluminum-

silicon alloys. It is a key topic to control the content and morphology of Fe intermetallics in current aluminum silicon die casting research.

## 1.2 Statement of Purpose

Aluminum is remarkable for its low density high strength and its resistance to chemical reaction. Structural components made of aluminum alloys are widely used in automotive, food, military and other industry fields. The price of aluminum is 1/5 of that of the same weight of titanium. So it is and will still be one of the most important light-weight metals.

Aluminum-Silicon casting alloys are the most extensively used one of all the Al alloys. The main impurities that exist in secondary Al-Si casting alloys are Fe, Zn, Mg. Iron is considered one of the most harmful elements since its presence leads to the precipitation of many AlFeSi intermetallics in the form of long, sharp angled platelets or needles. These intermetallic phases severely degrade the tensile strength and ductility of the alloys. Moreover, because they often form during solidification of the eutectic stage these phases may affect castability by interfering with interdendritic feeding and thus promote porosity.

To offset the dentrimental effect of of these impurities and intermetallics, four methods have been developed by the casting industry. The first is to reduce the content of iron. Some low-iron alloys, such as Silafont-36, Mercalloy 362 and 367, have been developed and applied in die casting (Hartlieb, 2013). The second method is element alloying. Elements including Mn, Cr, Ca, Be, Sr, Mg, Co, are added to Al-Si alloys to reduce the amount or change the morphology of β-AlFeSi phase (Zhang, Gao, Damoha,

& Robertson, 2012). The third method involves controlling the cooling rates during casting. It has been proved that increasing the cooling rates will effectively change the morphology of AlFeSi phase (Zhang et al., 2012). Finally, the last method used involves heat treatment. Because solution treatment usually results in surface blistering or dimensional instability of die casting parts, this method has limited application for die-casting. (Gustafsson, Thorvaldsson, & Dunlop, 1986; Kim, Park, Han, & Lee, 2006).

In this dissertation, these methods of controlling and modifying AlFeSi intermetallics morphology in A380 alloy are systematically studied. The nucleation and growth of AlFeSi phase and mechanical properties of modified A380 alloy are investigated. Optimizing method of controlling the fraction and morphology of AlFeSi phase in Al-Si hypoeutectic alloys are also studied.

## 1.3 Significance

The following areas were considered to be significant to this study:

1. There is plenty of research on the element alloying to alter the morphology of AlFeSi phase in Al-Si alloy, especially Mn and Sr. Because there is little research on some other elements, such as Ca and K, the effect of these elements on A380 series alloys on AlFeSi phase is studied. And these elements could both refine the AlFeSi phase and eutectic Si phase, which will effectively increase the mechanical properties, including both strength and ducitlity.
2. The thermodynamics simulation in our study is adopted with newest TCAL 2 software. In this study, the AlFeSi phase formation under Level condition and

Scheil condition are studied. Thus it will be an economical way to guide the alloy design.

3. There is little report on heat treatment on the morphology change of AlFeSi phase in A380 series alloys. In this study, the heat treatment is systematically studied. It is also a simple way to both reduce the size of AlFeSi phase and improve the toughness of alloy.
4. The optimized conditions for reducing and inhibiting the formation of AlFeSi in A380 series alloys are obtained and analyzed in this study. So it will answer what is the best way to reduce the detrimental effect of β-AlFeSi in Al-Si die casting alloys.

## 1.4 Research Questions

The focus of this research is on AlFeSi phase formation and phase evolution in Al-Si eutectic die casting alloys, with concentration on how to reduce and control the morphology of AlFeSi phases, especially β-AlFeSi phase, in Al-Si alloy under die casting conditions.

Areas of the concern includes: a) the desired alloying elements and content to actively affect AlFeSi phases in A380 alloy; b) phase revolution sequence of AlFeSi phase in A380 alloy; c) the effect of heat treatment on AlFeSi phase; d) the optimized conditions for inhibiting the formation of AlFeSi.

## 1.5 Assumptions

Assumptions for this study include:

1. All the fabrication of casting, and microstructure observation are conducted under the same environment.
2. The fabricated material is uniform, without macroscopic or microscopic deficiency.
3. Errors in measurements are considered to be too small to influence conclusions based on their readings.
4. The composition of the material is the same as the nominal one.

## 1.6 Limitations

The limitations for this study include:

1. The simuation results are based on Thermo-Calc TCAL 2 database.
2. All the test results are restricted by the current experimental conditions.

## 1.7 Delimitation

The delimitations for this study include:

1. The matrix alloy is confined to uniform commercial A380 alloy.
2. All the materials are limited to ASMS criteria.

## 1.8 Definition of Key Terms

Die casting-a versatile process for producing engineered metal parts by forcing molten metal under high pressure into reusable steel molds (Doehler, 1951).

Hardness-measurement of how resistant solid matter is to various kinds of permanent shape change when a force is applied (Anderson, 1970).

Heat treatment-a group of industrial and metalworking processes used to alter the physical, and sometimes chemical, properties of a material related to high temperature process (Groover, 2010).

Intermetallic compounds-solid phases containing two or more metallic elements, with optionally one or more non-metallic elements, whose crystal structure differs from that of the other constituents (Schulze, 1967).

Solution heat treatment-a process in which an alloy or metal is heated to a suitable temperature, is held at that temperature long enough to allow a certain constituent to enter into solid solution, and is then cooled rapidly to hold that constituent in solution (Cambell, 1991).

Ultimate Tensile Strength-the maximum stress that a material can withstand while being stretched or pulled before failing or breaking (Degarmo, 2003).

## 1.9 Summary

In this chapter, the overall research situation of Al-Si-Fe phase in Al-Si alloy have been introduced, in addition of the purpose, scope, significance, research questions, limitation, delimitation and definition of key terms. In the next two chapters, literature review and methodology of the research will be conducted.

# CHAPTER 2. LITERATURE REVIEW

## 2.1 Introduction

Most aluminum scraps and ingots contain high percent of impurity. Particularly, iron is the most detrimental one because of its keeps increasing during recycling process (Green, 2007). Once the content of Fe decreases to a critical percent, the cost and the work to get rid of it are very remarkable. So the Fe-free Al-Si alloy is difficult to obtain (Crepeau, 1995).

Iron usually forms AlFe and AlFeSi intermetallics in the aluminum alloys because the solution limit of Fe in Al is low (<0.05%). The impurities include α-AlFeSi, and β-AlFeSi and $Al_3Fe$.. The AlFe and AlFeSi phase will cause the harmful effect to the mechanical properties of Aluminum-Silicon diecasting alloys. The tensile strength will be impaired by the high Fe content, and the ductility will severely decreases once the Fe content is over a critical percent (Khalifa, Samuel & Gruzleski, 2003). Therefore, many efforts have been devoted to reduce the detrimental effect raised by β-AlFeSi.

## 2.2 Introduction of β-$Al_5$FeSi Phase

### 2.2.1 Fe-rich phases in aluminum and aluminum-silicon alloys

As we have known that, the solution limitation of iron in aluminum is about 0.05%. So iron have to form other intermetallic phases (Mondolfo, 1976). There are both

binary AlFe and ternary AlFeSi in most Al-Si diecating alloys (Khalifa, Samuel, & Gruzleski, 2003). A list of Al-Fe binary and Al-Fe-Si ternary phases in Al-Si diecasting alloys are shown in Table 2.1.

Table 2.1 *Indentified Fe-rich phases in aluminum alloys*

| Fe-rich Intermetallics | Crystal structure | Refence |
|---|---|---|
| $Al_mFe$ | Bct | (Liu, Thorvalsson, & Dunlop, 1986; Khalifa, Samuel & Gruzleski, 2003) |
| $Al_6Fe$ | Orthorhomic | (Mondolfo, 1976; Khalifa, Samuel, & Gruzleski, 2003) |
| AlxFe | C-centered othorhombic | (Liu, Thorvaldsson, & Dunlop, 1986)<br>(Young & Clyne, 1981) |
| θ-$Al_3Fe$ or θ-$Al_{13}Fe_4$ | Monoclinic<br>C-Centered monoclinic | (Mondolfo, 1976; Khalifa, Samuel, & Gruzleski 2003)<br>(Liu et al., 1986) |
| α-$Al_8Fe_2Si$ or α-$Al_{12}Fe_3Si_2$<br>α-$Al_{15}Fe_3Si_2$<br>(Crepeau 1995) | Hexagonal<br>Bcc | (Mondolfo, 1976; Stefeniay, Griger, & Turmezey, 1987; Crepeau, 1995; Khalifa, Samuel, & Gruzleski, 2003;<br>(Skjerpe, 1987; Kral, Mcintyre, and Smillie, 2004) |

Table 2.1 continued *Indentified Fe-rich phases in aluminum alloys (Zhang, 2012)*

| Fe-rich Intermetallics | Crystal structure | Refence |
|---|---|---|
| β-$Al_5FeSi$<br>$Al_9Fe_2Si_2$ (Philips 1976) | Monoclinic<br>B-face centered<br>orthorhombic<br>Orthorhombic<br>Tetragonal | (Mondolfo 1976; Stefaniay, Griger, and Turmezey 1987; Crepeau 1995; Khalifa, Samuel, and Gruzleski 2003; Shabestari 2004; Lu and Dahle 2005)<br>(Carpenter and LePage 1993)<br>(Zheng et al. 2000)<br>(Kral, Mcintyre, and Smillie 2004) |
| δ-$Al_4FeSi_2$<br>δ-$Al_3FeS_{i2}$ (Panpay and Schubert 1969; Kral, Makashima and Mitchell 2006) | Tetragonal | (Mondolfo, 1976; Crepeau, 1995; Khalifa, Samuel, & Gruzleski, 2003; Kral, Nakashima, & Metchell, 2006) |
| q1-AlFeSi | C-centered orthorhombic | (Liu, Thorvaldsson, & Dunlop, 1986; Khalifa, Samuel, & Gruzleski, 2003) |
| q2-AlFeSi | monoclinic | (Liu et al., 1986) |
| γ-$Al_8FeSi$ | C-centered monoclinic | (Mondolfo, 1976; Stefeniay, Griger, & Turmezey, 1987) |
| p-$Al_8Mg_3FeSi_6$ | | (Crepeau, 1995) |
| π-$Al_8Mg_3FeSi_6$ | | (Barresi et al., 1993) |

### 2.2.1 α and β Fe-rich Phases in Aluminum and Aluminum-silicon Alloys

The most significant AlFeSi intermetalics in AlSi alloys are α-AlFeSi and β-AlFeSi. The α-AlFeSi is usually named as α-$Al_{12}Fe_3Si_2$, α-$Al_8Fe_2Si$, α-$Al_{15}Fe_3Si_2$ or just α-AlFeSi (Liu, Thorvaldsson, & Dunlop, 1986; Stefaniay, Griger, & Turmezey, 1987; Khalifa, Samuel, & Gruzleski, 2003; Mondolfo, 1976). There is a conflict about the crystal structure of α-$Al_8Fe_2Si$, Someone claimed that the α-phase was bcc while others thought it as $Al_{19}(Fe,Mn)_5Si_2$, space group Im3 (Kral, Mcintyre, & Smillie, 2004; Kral, 2005). The spatial structure of the α-phase from other sources was reported as hcp (Mondolfo 1976; Stefaniay, Griger, & Turmezey, 1987; Crepeau, 1995). As to the morphology, the α-phases are usually Chinese script, star-like or polygon (Lu & Dahle 2005; Dinnis, Taylor, & Dahle, 2005). This structure is more beneficial than the platelet or needle-like β-$Al_5FeSi$ on Al-Si alloy's ductility because of no stress concentration on the needle point. There are two distinct α-phase morphologies, namely, convoluted arm structure condensed phase and polygonal crystal phase if it solidifies as secondary phase (Dinnis, Taylor, & Dahle, 2005).

β-AlFeSi phase can be called as $Al_9Fe_2Si_2$, $Al_5FeSi$, or β-AlFeSi. The exact structure of the β-AlFeSi is contradicted. Monoclinic structure was agreed by most people (Mondolfo, 1976; Murali et al., 1994; Crepeau, 1995). Other People considered that β-phase was orthorhombic (Carpenter, & LePage, 1993); (Zheng, Vincent, & Steeds, 2000). Other claimed the β-AlFeSi was tetragonal (Kral, Mcintyre, & Smillie, 2004).

Of all the Al-Fe-Si phase, β-AlFeSi is viewed as most deleterious, and a lot of work has been done to diminish the detrimental effect. β-AlFeSi has an ununiformed platelet morphology, which is brittle and so a cuase stress concentration. Clearly, the β-

AlFeSi phase severely deteriorates the toughness of Aluminum-Silicon casting alloys, a condition that is particularly unacceptable for the die casting industry.

## 2.3 The Significance of β Phase Research

### 2.3.1 The Current Situation of β Phase in Al-Si Alloy

Most work has been made to decide the effect of the content of Fe on the properties of the alloys. It is commonly agreed that Fe has no obvious damage on the alloy's mechanical properties if the Fe content is under a low level. However, if the iron content surpasses the critical point the properties drop rapidly because of the brittle Iron-intermetallics formation. β-$Al_5FeSi$ usually forms and increases drastically with further addition of Fe content if Fe is over 0.7% (Mondolfo, 1976; Khalifa, Samuel, and Gruzleski, 2003). The critical Fe content can be change by control cooling rates and element alloying.

The critical content is also related to other factors, such as the silicon percentage in Al-Si alloy. Figure 2-1 shows the change of critical iron level in Aluminum-Silicon alloy. With the increase of Si content, the fraction of Fe increases without the formation of pre-eutectic β-phase. In regard of a determined Fe content, starting nucleation temperature of the β-Fe decreases with the increase of Si content. Also the liquidus and solidus temperature decrease. The AB line between the fcc zone and β-AlFeSi zone is the boundary where the most detrimental primary β-phase forms (Taylor, 1995; Mbuya, Odera and Ng'ang'a, 2003).

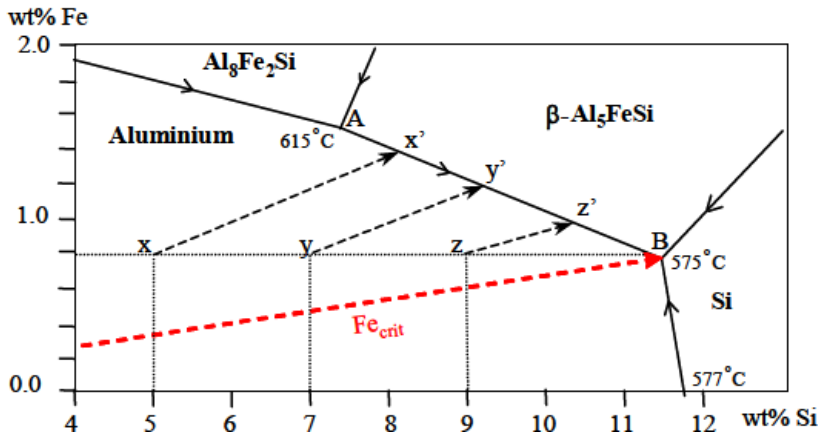


*Figure 2.1* Ternary Al-Si-Fe phase diagram showing primary Al solidification paths for all alloys with $Fe_{crit}$ iron Levels, and for 5%Si (x-x'), 7%Si (y-y')and 9%Si (z-z') alloys with 0.8%Fe. (Taylor, 1995)

The mechanism involving β-phase deterioration is not fully understood. Mascre (1955) gave out the idea restricted feeding suggesting that porosity was increased due to β-$Al_5FeSi$, so feeding channels of solidification was blocked because the platelet β-$Al_5FeSi$ are dendrite-like. Roy, Samuel, and Samuel (1996) claimed a 'pore nucleation theory' claiming that the β-AlFeSi phase can nucleate pores. Cao and Campbell (2004b, 2006) proposed double-over oxide bi-films theory, which was popular in Al-Fe-Si phase research. They considered the wetted side of the films is the good substrate in the nucleation and growth of β-AlFeSi phase. If the molten alloy is solidified, the interface of the two dried side traps the air so that the film becomes the crack. This can form β-$Al_5FeSi$ phase.

### 2.3.2 The Development of A380 and New-developed Low-Fe Al-Si Diecasting Alloy in Place of A380

Alloying and lowering the Fe content are two important ways that has been used to develop new Al-Fe-Si diecating alloys.

Traditional die casting alloys, such as, 360.0 and 380.0 which are two of the most popular die casting alloys, contain up to 2% iron according to the AFS (American Foundary Society) standard. Most die casting alloys registered with the AFS contain up to 1.3% iron (Donahue, 2011). The current practice involving on high iron die casting aluminum alloy is to replace Fe with other elements, mostly Mn (Hartlieb, 2013). This is the common method to solve Fe intermetalllcs problem in Al-Si die casting alloy.

In the 1990s Rheinfelden of Germany developed the first low Fe structural die casting alloy (Silafont-36, AA365). They lowered the Fe to 0.15% max and replaced it with Mn at 0.5-0.8% for die soldering resistance. Alcoa developed similar alloys (C601 and C611). Others such as Alusuisse/Alcan (Aural alloys) and Pechiney (Calypso alloys) have developed and commercialized similar alloys with up to around 0.2% Fe and around 0.5% Mn. In Japan, the ADC3SF (also known from Ryobi as W3 alloy) uses even lower (0.3-0.4%) Mn and special part design to overcome die soldering issues. Mercury Marine discovered that use of strontium increase die-soldering resistance of casting alloys, they applied it to the Mercalloy series of die casting alloys (AA367, 368, and 362). This practice allowed them to lower the Mn content even further to only about 0.3%. Today, use of the elements Mn and Sr is made to replace the Fe in structural die casting alloys for die soldering resistance thus reducing the very negative impacts of Fe needles on ductility and feeding behavior (Hartlieb, 2013).

## 2.4 The Nucleation and Growth of β Phase

Table 2.2 gives our the phase reactions in Al-Si-Mg cast alloys with different Fe and Mn contents from the results of Cao and Campell (2004a). Here according to the main eutectic reactions L→fcc+Si, the whole solidification is divided into four stages: namely, primary, secondary, ternary and posteutectic.

Table 2.2 *Possible sequence of Phase solidification in cast Al-11.5Si-0.4Mg alloys containing various Fe and Mn contents (Cao and Campbell 2004a)*

| Reaction | Temperature | Phase | Suggested Temperature (℃) | Solidification Stage |
|---|---|---|---|---|
| 1 | $T>T_L$ | $Al_{15}(FeMn)_3Si_2$ | | predendritic |
| 2 | | $Al_5FeSi$ | | (primary) |
| 3 | T: $T_L$- TE | Development of α-Al dendritic networks | 575-578 | dendritic |
| 4 | | Liq.→Al+ $Al_{15}(FeMn)_3Si_2$ | | Post dendritic |
| 5 | | Liq.→Al+ $Al_{15}(FeMn)_3Si_2$+ $Al_5FeSi$ | | Pre-eutectic |
| 6 | | Liq.→Al+ $Al_5FeSi$ | | |
| 7 | T:~$T_E$ | liq→Al+Si | 565 to 569 | eutectic |
| 8 | | liq→Al+Si+ $Al_5FeSi$ | (575 to 576*) | coeutectic |
| 9 | | liq→Al+Si+ $Al_{15}(FeMn)_3Si_2$ | (573 to 574*) | |
| 10 | $T<T_E$ | Liq+$Al_5FeSi$→Al+Si+ $Al_{15}(FeMn)_3Si_2$ | (565 to 567*) | Posteutectic |
| 11 | | Liq+$Al_5FeSi$→Al+Si+ $Al_8FeMg_3Si_6$ | 567 | |
| 12 | | Liq→Al+Si+$Mg_2Si$ | 546 to 554 (555*) | |
| 13 | | Liq→Al+Si+$Mg_2Si$+ $Al_8FeMg_3Si_6$ | 546 to 554(554*) | |

Cao (Cao and Campbell 2004a) points out that AlFeSi and AlFe phases in Aluminum-Silcon alloys is formed by the nucleation on double-layer oxide layers. The surface of the film becomes stimulated during the pouring, casting and other motion. The stimulation action induces a surface turbulence. There are two sides of the oxide film: dried, unbounded inner sides, and wetted bonded outer side. The inner side of the films is not wet because the air is trapped inside. The outer side is in contact with the unsolidified molten alloy so that it can be the only possible nucleate site for AlFeSi phase. Cao also gave out the relationship of nucleate site and hierarchy of Al-Si-Mg cast alloys, which is shown in Figure 2-2. It shows oxide layer can be nucleate substrates of all AlFeSi phase.

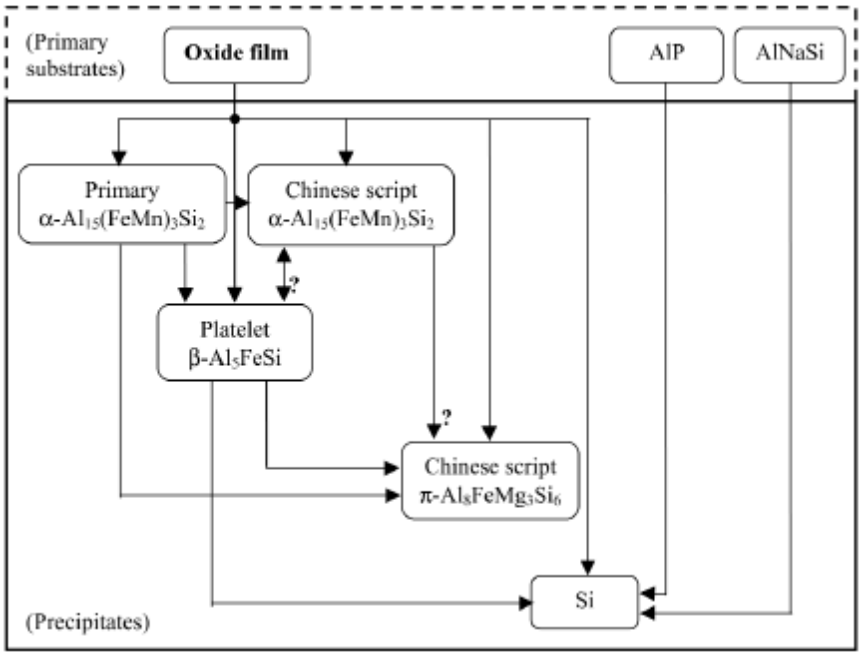


*Figure 2.2* Possible nucleation hierarchy among oxide films and main phases in Al-11.5Si-0.4Mg cast alloys containing Fe and Mn contents (arrows refer to the nucleated phase) (Cao and Campbell 2004a)

Finally, regarding the nucleation and growth of the β phase, Iglessis considered that the crystallization of AlFeSi phase is mainly controlled by growth undercooling (Iglessis, Frantz, & Gantois, 1977). However, Narayanan holds the opinion that for thinking about both the nucleation and the growth processes for the nucleation of AlFeSi phase. Therefore, if the total undercooling, the sum of the undercooling for nucleation (ΔTn) and undercooling for growth (ΔTc), is greater than the critical undercooling (ΔTcrit), the α-AlFeSi will form. Otherwise, β-AlFeSi will nucleate (Narayanan, Samuel, & Gruzleski, 1994). Yin (2001) concludes that the greater value of ΔTn or ΔTc will decide the nucleate sequence.

## 2.5 The Effect of Alloying Element on β phase

### 2.5.1 Manganese

Mn is extensively adopted as a substitute for Fe in Aluminum-Silicon cast alloys. The reason is that the crystal structure and the radius of atom of Mn is similar to that of Fe, so Mn can be substituted for Fe in AlFeSi phase (Mahta et al., 2005).

It is well known that with Mn addition, the β-AlFeSi phases can be changed from the needle-like β-AlFeSi phase to the compact size, namely Chinese script, polygon and star-like, which is less harmful to the ductility of alloy. It can improve the tensile and ductility property of Al-Si cast alloy (Mondolfo, 1976). β-AlFeSi is suppressed, and α-AlFeSi can from in prior to β phase (Mondolfo, 1976). In quaternary AlSiFeMn alloys, iron may take the place of ninety percent of manganese to form α-Al(Fe,Mn)Si (Dinnis, 2006). Commonly the morphology of α-AlFeSi is decided by cooling rate and alloying element. (Granger, Sawtell, & Kersker, 1984; Gustafsson, Thorvaldsson, and Dunlop,

1986; Narayanan, Samuel, & Gruzleski, 1994; Crepeau, 1995). Murali (1994) considered that most of β-AlFeSi can be changed into big size α-AlFeSi with high Fe and high Mn at low cooling condition in Al-Si-Mg alloy, and most Chinese script α-AlFeSi phase formed with low Fe content and low Mn at a higher cooling rate. Ashtari studied the interaction effect of Sr and Mn in A365 series alloy. With only 0.015 wt% Sr, β-$Al_5FeSi$ predominated. With addition of both trace Sr and Mn, α-AlFeSi phase began to appear (Ashtari, Tezuka, & Sato, 2003).

The best Mn:Fe ratio is still not agreed by different researchers for the nucleate and growth is are also influenced by other factors, including cooling rates, superheating temperatures and other solidified related factors. Generally, it is well accepted that to the weight ratio of Mn: Fe of 0.5 is the best portion to relief the detrimental effect of β-AlFeSi. (Colwell, & Kissling, 1961; Couture, 1981). However, it is found that α-AlFeSi is predominating with the Mn: Fe=1:6 in an Al-Si-Mg alloy (Cao, & Campbell, 2004b).

However, adding a small amount of Mn be effectively substituting Fe, in order to form α AlFeSi phase instead of β-$Al_5FeSi$ phase, higher Mn addition will cause large polygon to from, which is called “sludge”. It will also increase the total amount of AlFeSi phase and the hot tearing susceptibility (Lu, & Dahle, 2005).

### 2.5.2 Cobalt

Co, and Fe have similar atomic radius. So Co can also be added to replace Fe in AlFeSi phases. Co was effective than Mn and more addition is needed. Typically Co: Fe=0.5-1.0 was suggested to transfer almost all β-AlFeSi phase into α-AlFeSi (Couture 1981). It was reported that after the Co addition, almost all α-AlFeSi nucleated and grew

in fcc α-Al (Couture, 1981; Murali, Raman, & Murthy, 1994; Crepeau 1995; Mahta et al., 2005), which reduced the micro-segregation. Therefore, it is thought Co is much better than Mn.

### 2.5.3 Chromium

Mondolfo (1976) found that Cr was also a Fe neutralizer in Al-Si casting alloys. Mahta (2005) considered Cr is more effective, so Cr: Fe=0.3 may transfer almost all β-AlFeSi phase into α-AlFeSi. Different from Co and similar like Mn, α-AlFeSi phases was formed both in the dendrite and at the boundary of the dendrite in Al-Si casting alloys (Murali, Raman, and Murthy 1994; Mahta et al. 2005). Large amount alloying with Mn and Cr, would possibly lead to formation of the hard complex intermetallic high-temperature resistance sludge, $Al_{15}(Fe, Mn, Cr)_3Si_2$. The sludge amount can be calculated by the sludge factor. The sludge factor is the formula that integrates the combined effects of Fe, Mn, and Cr, which is shown as follows:

$$\text{Sludge Factor} = \%\ Fe + (2 \times \%\ Mn) + (3 \times \%\ Cr) \quad (2.1)$$

A sludge factor of 1.8 will not result in the formation of the sludge if the casting temperature is more than 650 °C (Czikel et al., 1985). The critical sludge factor is estimated to be 2.1 for Al-Si-Cu-Mg containing alloys (Samuel, Samuel, Villeneuve, Doty, & Valtierra 2001; Lakshmanan, Shabestari, & Gruzleski, 1995; Shabestari, 2004; Samuel, & Samuel, 1995). Sludge is highly undesirable, because once they form, they are difficult to remove using heat treatment because their higher melting points than aluminum.

### 2.5.4 Beryllium

It is considered that Be, was more effective to modify AlFeSi phase than Mn for control for the detrimental effect of β-AlFeSi phase. (Murali, Raman, & Murthy, 1995b). Crepeau and other people reported that the addition of Be 0.06-0.27wt% to reduce β-AlFeSi phase (Crepeau, 1995) was enough (Murali, Raman, & Murthy, 1995b).

Be in the Al-Si alloy can form AlFeBe or AlFeBeSi phases as $Al_8Fe_2BeSi$ or $Al_4Fe_2Be_5$ (Crepeau, 1995). The mechanism to change β-AlFeSi phase of Be is the same as that of Co that AlFeSi phases formed in the dendrite of fcc α-Al. (Murali, Raman, & Murthy, 1994, 1995a, 1995b) Particularly, trace Be addition leads to the formation of α-Al(Be,Fe)Si in Aluminum-Silicon alloys.. However, Yie (1999) reported that the β-AlFeSi phases were transformed to α-AlFeSi.

### 2.5.5 Strontium

Strontium can be used to modify Si phase in Al-Si alloy. (Closset, 1982; Shabestari, & Shahri, 2004) It is well known that eutectic silicon phases can from plate-like to a coral-like in Al-Si casting alloys. Sr can be used to transform β-AlFeSi phases to α-AlFeSi in wrought alloys (Morris, & Miners, 1975; Closset et al., 1996). In 6063 alloys with least of the addition of 0.5 wt% Sr, α-AlFeSi can therefore formed. Thus the extrusion ductility of the alloy can be improved significantly (Morris, & Miners, 1975).

More commonly, Sr has also used to refine β-AlFeSi phases in casting alloys. Many reports showed that Sr can effectively suppress the formation of β-AlFeSi phase (Tang, & Sritharan 1998; Lu, & Dahle, 2005). It was known that trace Sr addition (0.05wt%) can both transfer β-phase to α-AlFeSi and refine β-phase by the reaction of

fragmentation (Shabestari, & Gruzleski, 1996). Ashtari hold the opinion that Sr addition can only reduce the size and amount of β-phase but cannot transfer β-AlFeSi to α-AlFeSi in A380 alloy (Ashtari, Tezuka, & Sato, 2003). Other reports showed that only primary β-AlFeSi without secondary or ternary β-AlFeSi was fragmented with Sr added into low Si alloys (Samuel, 1998).

However, other studies claimed that Sr have no obvious effect on modification of β-AlFeSi phase (Ashtari, Tezuka, & Sato, 2003). Suarez-Pena and Lu have the similar conclusion form Al-Si eutectic alloys (Lu, & Dahle, 2005; Suarez-Pena, & Asensio-Lozano, 2006).

Different literature sources provide different opinions regarding the mechanism by which Sr can change the morphology of AlFeSi phase. The first assumption is that the absorption of Sr on of primary α-$Al_8Fe_2Si$. Therefore, the Sr-rich phase can prevent the dissolution of Fe. So, the reaction L+α-AlFeSi=Al+β-AlFeSi will be hindered (Mulazimoglu et al., 1994).

Closset and Cho assumed that the fragmentation β-AlFeSi is related with the change of nucleation sequence. So they maintain that the addition of Sr lead to the full saturation of the element Fe and Si, thus, thus it facilitates the formation of β-AlFeSi in advance of α-Al. Then the first nucleated β-AlFeSi can be the nucleate substrate of fcc α-Al. So the α-Al can reject Fe and Si into the residual liquid. That can facilitate the nucleation of the binary β-AlFeSi (Closset et al., 1996; Cho et al., 2008). The size of the secondary α-AlFeSi is much smaller (Suarez-Pena, & Asensio-Lozano, 2006). Another opinion is the poisoning of Sr on the possible nucleate size of β-AlFeSi, to reduce the further growth, leading to the reduction of β-AlFeSi phase. (Shabestari, & Gruzleski,

1996; Pennors et al., 1998; Cho et al., 2008) However, although these opinions can explain the size reduction of β-AlFeSi phases, but there is no persuasive explanation why β-AlFeSi can transform to α-AlFeSi with Sr addition.

### 2.5.6 Molybdenum, Nickel, and Sulfur

Molybdenum, Mo, was proved to convert platelet iron phases to compact, star-shaped compounds (Dichtl, 1970), and to be much more effective than Mn (Couture, 1981). A combined addition of Mo (0.05-0.3 wt%) and S, Sulfur (0.01-0.2 wt%) was reported to improve the mechanical properties of Al-Si alloys (Couture, 1981). Ni, Nickel was deemed as a ‘‘neutralizer’’ in some references (Mondolfo, 1976; Couture, 1981; Crepeau, 1995).

### 2.5.7 Lithium

In Al-Si-Cu-Fe alloys, Lithium is found to be effective in transferring β-AlFeSi to α-AlFeSi and refine the eutectic Si. However, the Li-containing alloys absorb gas and get more porosity. With the addition of 0.05% Li both strength and ductility of Al-Si-Cu alloy were improved significantly. (Karamouz, Azarbarmas, Emamy, & Alipour, 2013)

### 2.5.8 Potassium

The addition of the element of Potassium, K, can both transfer and refine β-AlFeSi at high cooling rates. But β-$Al_5FeSi$ is refined but not transformed to α-$Al_8Fe_2Si$ with low cooling rates. K can also modify the eutectic Si (Ashtari, Tezuka, & Sato, 2005).

### 2.5.9 Calcium

Calcium acts also as an effective Fe-corrector by refining the AlFeSi phase and the eutectic silicon, leading to an improvement of the strength and the ductility of the alloys, especially the elongation (Zaldívar-Cadena, & Flores-Valdés 2007).

The refinement of β-platelets by Ca is reported by the fragmentation of β-platelets, similar to Sr. The reason of the refinement thought to be related to the reject of Si at the interface of β-AlFeSi and fcc α-Al. With the addition of Ca, the higher diffusion rate of Si in than Fe in Al would lead to the fragment of the β-$Al_5$FeSi phase platelets with the aid of Ca.

### 2.5.10 Summary

In summary, the refinement/modification of β-AlFeSi phase can be catergoriesd into three groups: 1) substitution Fe in AlFeSi phase to transfer β-AlFeSi to α-AlFeSi, including Mn, Cr, Co and Be. It can reduce the amount of β-AlFeSi but introduce more α-AlFeSi, leading to increase of the total AlFeSi phase. 2) Prohibiting the growth of Al-Fe-Si, such as Sr and Ca. It can reduce the size of β-AlFeSi thus to prevent the dendrimental effect. 3) Promoting the nucleation and formation of α-AlFeSi, such as K. It is an ideal way to reduce the amount of β-AlFeSi. Elements from group 2 and 3 are deemed as new generation of Fe-neutralizer. However, some of these alloys, such as Sr and Ca, probable introduce other imputity. The advantage and disadvantage of each elment is listed in Table 2.3.

Table 2.3 *Advantage and Disadvantage of elements for Fe neutralizer*

| Element | Advantage | Disadvantage |
|---|---|---|
| Mn | Effective, low cost | harmful to the mechanical properties , sludge |
| Cr | More effective | harmful to the mechanical properties , sludge |
| Co | More effective | Cost, primary α-AlFeSi and Si |
| Be | More effective | Cost, pores, Be-Fe intermetallics |
| Sr | Very high effective, modification | intermetallics |
| K | effective, no sludge | pores |
| Li | effective | Cost, pores |
| Ca | Effective, low cost | intermetallics |

## 2.6 Cooling Rate

In regard of the Al-Si-Fe phase diagram, the β-AlFeSi phase keeps stable at low cooling rates for the entire range of Fe and Si variation. But at a high cooling rate, the α-AlFeSi phase can be solidified as metastable α-AlFeSi (Iglessis, Frantz, & Gantois, 1977; Narayanan, Samuel, & Gruzleski, 1994). The critical transit cooling rate increases with the increase of Fe content (Mascre, 1955). Narayanan claimed with the increase of cooling rate the formation temperature of β-AlFeSi phase decreased until it is lower than the eutectic temperature (Narayanan, Samuel, and Gruzleski, 1994).

## 2.7 Heat Treatment

Al-Fe-Si phases could be but not easily transferred with the solution heat treatment (Crepeau, 1995). Heat treatment needs a high temperature because of the lower

diffusion rate of Fe in Al.

Yin found acicular iron phase platelets can dissolve at the imperfect sites of the crystals during high temperature heat treatment and become shorter ones. At the imperfect sites of the crystal, the silicon, iron or manganese atoms are in a high-energy state and tend to transform to low-energy state, and heat treatment can accelerate the dissolving process (Yin, 2001).

## 2.8 Die casting

### 2.8.1 General Introduction

Die casting, the production of castings by applying high pressure to force molten metal into steel dies or molds is one of the most successful and breakthrough developments in modern manufacturing practice. The die casting process provides a means of producing large quantities of castings of a high level of uniformity and accuracy so that the extra machining work is either reduced or eliminated entirely. The process is applicable to castings in a wide selection of sizes, shapes, and materials (Doehler, 1951).

Die castings are smooth on both external and internal surfaces because they are formed directly against machined surface of the dies and cores. Die castings can be produced to sharp outlines and with very thin sections (in mm scale) with high strength as is difficult to achieve using sand and permanent casting method.

### 2.8.2 The Die Casting Process

The process of die casting consists several steps: 1) melting the die casting alloy in a suitable container (crucible), 2) pouring and forcing it, under pressure, into metallic

molds or dies, 3) letting the casting cool down, and then 4) opening the dies and removing the casting. Materials typically used in the die casting process include aluminum, zinc, magnesium, lead and brass.

### 2.8.3 Aluminum-base Alloys for Die Casting

Aluminum die casting alloys have the advantages of comparatively high tensile strength, light weight, resistance to corrosion and provide a nearly finished surface. These advantages lead them to a wide variety of applications. Aluminum die castings are used extensively for parts, especially in the manufacturing of automotive parts.

Silicon is the most widely useful alloying element for aluminum. It effectively lowers the melting temperature and increases the fluidity of the metal. Although the tensile and yield strengths of aluminum die casting alloys are not as high, nominally, as for other aluminum alloys, like Al-Cu or Al-Mg, their effective advantage in enabling the casting of difficult shapes is greater. The use of copper as an alloying element in the aluminum-silicon-copper series has the same effect as silicon. Alloys containing copper have better machinability than those containing silicon alone. Mg can form $Mg_2Si$ with Si to improve the tensile property. However, spinal MgO can also be formed resulting in a deterioration of ductility. Manganese is usually added to aluminum to substitute Fe to form α-Al(Mn,Fe)Si. Zinc and iron are impurities of Al-Si die casting alloy.

## 2.9 Summary

In this chapter, the problem of β-AlFeSi phase in Al-Si diecasing alloy was introduced. The current research situation in AlFeSi phase and industry application was

presented. Three methods to refine β-AlFeSi: alloying element, heat treatment and cooling rate control were discussed Elment alloying is the most effective way, while other impurity may be introduced. Heat treatment would not introduce other impurity, but it needs high solution temperature and blistering may occur. Increasing cooling rate can effectively reduce the size of AlFeSi phase, while under some situation it may lead to the increase of the fraction of β-AlFeSi phase. So how to take the advantage of these three methods is the focus work of this research.

## 2.10 Objective and Goal

The objective of the dissertation:

A. To restrain the formation and growth of β phase;

B. To change the morphology of β phase;

C. To transform β phase to α phase.

The goal of the dissertation:

To reduce the detrimental effect of β-AlFeSi phase in A380 series die-casting alloys.

# CHAPTER 3. METHODOLOGY

## 3.1 Introduction

In this dissertation, both thermodanymics simulation and casting experiment are used to study on the Al-Fe-Si phase in Al-Si diecasting alloy. Thermo-Calc$^{TM}$ software is used to simulate the thermodanymics equilibrium in Al-Si diecasting alloy. According to the simulation results, experiments were design, castings were made by controlling alloy compositions and cooling rates

## 3.2 Thermodynamics Simulation

Thermo-Calc$^{TM}$ was founded in 1997, offering a series of thermodynamics calculation software. Thermo-Calc software was developed 30 years ago and is considered as one of the best and most powerful software package for thermodynamic calculations.

While only the equilibrium situation can be simulated in Thermo-Calc software, in this dissertation, the thermodynamics calculation and phase diagrams are obtained in the following steps:

1) The effect of individual alloying element

Only one of the specified elements is changed (other elements keep constent). Thus the single element on the phase change of A380 alloys is studied. The database used is TCAL 2, which is suitable for most casting and die casting aluminum alloy. The

equilibrium, the Level and Scheil cooling curves were calculated. The range of variation for each element in this study is given in Table 3.1 and 3.2.

Table 3.1 *Range of variation of each element in calculting equilibrium phase diagram in A380 baed alloy*

| Element | Si | Fe | Mg | Cu | Zn | Mn | Ti | K | Ca | Sr |
|---|---|---|---|---|---|---|---|---|---|---|
| Viriation Range (wt%) | 4.0-12.5 | 0-2.0 | 0-1.0 | 0-4.0 | 0-4.0 | 0-2.0 | 0-0.5 | 0-3.0 | 0-0.5 | 0-0.5 |

Table 3.2 *Selected compositions for calculating Scheil and Level curves*

| Element | Si | Fe | Mg | Cu | Mn |
|---|---|---|---|---|---|
| Selected composition (wt%) | 5.0 | 0.4 | 0.1 | 1.0 | 0.2 |
| | 7.0 | 0.7 | 0.2 | 2.0 | 0.4 |
| | 9.0 | 1.0 | 0.3 | 3.0 | 0.5 |
| | 11.0 | 1.5 | 0.5 | 3.5 | 1.0 |
| | 13.0 | 2.0 | 1.0 | 4.0 | 2.0 |

2) The effect of combination change of multiple major element change

Si, Fe, Mg, Cu and Mn are considered as the main elements of A380 alloy; other elements, including Zn, Sr, Na, Ca, Ti, K et al, are treated as minor elements, because they do not have obvious effects on minimal formation of AlFeSi phase. So all five elements change are taken into consideration. The Scheil and Level cooling and phase composition was calculated. The details are given in Table 3.3 and 3.4.

Table 3.3 *Range of variation of major elements in A380 alloy for calculating equilibrium phase diagram*

| Element | Si | Fe | Mg | Cu | Mn |
|---|---|---|---|---|---|
| Variration Range (wt%) | 4.0-12.5 | 0-2.0 | 0-1.0 | 0-4.0 | 0-2.0 |

Table 3.4 *Selected compositions of element for Calculating Scheil and Level cooling curves*

| Element | Si | Fe | Mg | Cu | Mn |
|---|---|---|---|---|---|
| Selected composition (wt%) | 5.0 | 0.4 | 0.1 | 1.0 | 0.2 |
| | 7.0 | 0.7 | 0.2 | 2.0 | 0.4 |
| | 9.0 | 1.0 | 0.3 | 3.0 | 0.5 |
| | 11.0 | 1.5 | 0.5 | 3.5 | 1.0 |
| | 13.0 | 2.0 | 1.0 | 4.0 | 2.0 |

## 3.3 Experimental Design

### 3.3.1 Cooling Rates

Three different ranges of cooling rates are adopted in this study. A V-shape slope copper mold and a direct water quenching are chosen to simulate high cooling rates of die casting conditions. According to the secondary dendrite arm spacing that are measured, the cooling rates in the range of 10-50 ℃/s are specified to cover the required range of die casting cooling rates. Steel mold, copper mold, and graphite mold are used to achieve the medium cooling rates in the range of 1-10 ℃/s. Furnace cooling is used for slow cooling rates of 0.05 ℃/s. Medium and slow cooling rates are recorded by National Instruments e-CAQ-9171 data acquisition machines. The relationship between the secondary dendrite arm space, d, and the corresponding cooling rate, $\dot{t}$, can be described with the equation:

$$d = A(\dot{t})^n \tag{3.1}$$

From the study results of Samuel (1995), A and n are approximately 31 and - 0.366, respectively. So for the high cooling rate situation, since the secondary dendrite arm space is from 7-14 μm, the cooling rates calculated from Equation 3,1 for high cooling rate samples are 10-50 ℃/s approximately. The low and medium cooling rates are

calibrated directly from data collection machine and the relation of obtained cooling rates and secondary dendrite arm space is in accordance with the Equation 3.1.

### 3.3.2 Material Design

The material used in this research was a commercial Alcoa aluminum alloy A380. It is a hypoeutectic alloy, and having a relative low liquidus (593 ℃) and solidus (527 ℃) temperature. The experimental alloy was prepared by Al-Mn, Al-Sr, Al-Mg, Al-Fe, Al-Cu, Al-Ca, Al-K master alloys. The compositions of master alloys and original A380 are given in Table 3.5 and 3.6 respectively.

Table 3.5 *Compositions of Master Alloys*

| **Material** | **Major** | **Minor Element Composition(% by weight)** | | | | | | | **Al** |
|---|---|---|---|---|---|---|---|---|---|
| | | Si | Fe | Mg | Mn | Cu | Others Each | Others Total | |
| Ca10 | Ca=10% | ≤0.20 | ≤0.30 | ≤0.05 | | | ≤0.05 | ≤0.10 | Balance |
| Cu50 | Cu=50% | ≤0.10 | ≤0.15 | | | | ≤0.05 | ≤0.15 | Balance |
| Fe25 | Fe=25% | ≤0.30 | | | ≤0.20 | ≤0.05 | ≤0.05 | | Balance |
| Mg68 | Mg=68% | ≤0.10 | ≤0.15 | | | | ≤0.05 | ≤0.10 | Balance |
| Mn25 | Mn=25% | ≤0.20 | ≤0.25 | | | | ≤0.03 | ≤0.15 | Balance |

Table 3.6 *Composition of A380 alloy*

| **Element** | **Si** | **Fe** | **Cu** | **Mn** | **Mg** | **Ni** | **Zn** | **Ti** | **Al** |
|---|---|---|---|---|---|---|---|---|---|
| wt% | 9.0 | 1.0 | 3.5 | 0.4 | 0.2 | 0.3 | 0.35 | 0.08 | Bal. |

According to the simulation results and literature review, the experiments were arranged into two groups. The first one is the research on the addition of individual elemnt in table 3.7 and the second is the combination of adding two major elements shown in table 3.8.

Table 3.7 *Selected compositions of alloy varying on individual element*

| Element | Fe | Mn | Mg | Cu | Sr | K | Ca |
|---|---|---|---|---|---|---|---|
| Concentration (%) | 1.5 | 0.5 | 0.3 | 3.5 | 0.01 | 0.1 | 0.05 |
| | 2.0 | 1.0 | 0.5 | 4.0 | 0.05 | 0.5 | 0.1 |
| | - | - | - | - | 0.1 | 1.0 | 0.3 |
| | - | - | - | - | 0.2 | 2.0 | 0.5 |
| | - | - | - | - | - | 3.0 | - |

Table 3.8 *Selected compositions of alloy for variation of combined elements*

| Element | Sr+Mn | Ca+Mn | Ca+Sr |
|---|---|---|---|
| Concentration (%) | 0.1Sr+0.5Mn | 0.1Ca+1Mn | 0.1Ca+0.05Sr |
| | 0.05Sr+1Mn | | |

Table 3.9 list of all the compositions of alloy used in the dissertation

Table 3.9 *Summary of all alloys composition used in the dissertation*

| alloy | Si | Fe | Mn | Mg | Cu | Zn | Sr | Ti | K | Ca | Al |
|---|---|---|---|---|---|---|---|---|---|---|---|
| 0 | 9.0 | 1.0 | 0.4 | 0.2 | 3.5 | 3.5 | 0 | 0 | 0 | 0 | bal |
| 1 | 9.0 | **1.5** | 0.4 | 0.2 | 3.5 | 3.5 | 0 | 0 | 0 | 0 | bal |
| 2 | 9.0 | **2.0** | 0.4 | 0.2 | 3.5 | 3.5 | 0 | 0 | 0 | 0 | bal |
| 3 | 9.0 | 1.0 | **0.5** | 0.2 | 3.5 | 3.5 | 0 | 0 | 0 | 0 | bal |
| 4 | 9.0 | 1.0 | **1.0** | 0.2 | 3.5 | 3.5 | 0 | 0 | 0 | 0 | bal |
| 5 | 9.0 | 1.0 | 0.4 | **0.3** | 3.5 | 3.5 | 0 | 0 | 0 | 0 | bal |
| 6 | 9.0 | 1.0 | 0.4 | **0.5** | 3.5 | 3.5 | 0 | 0 | 0 | 0 | bal |
| 7 | 9.0 | 1.0 | 0.4 | 0.2 | **4** | 3.5 | 0 | 0 | 0 | 0 | bal |
| 8 | 9.0 | 1.0 | 0.4 | 0.2 | 3.5 | 3.5 | **0.01** | 0 | 0 | 0 | bal |
| 9 | 9.0 | 1.0 | 0.4 | 0.2 | 3.5 | 3.5 | **0.05** | 0 | 0 | 0 | bal |
| 10 | 9.0 | 1.0 | 0.4 | 0.2 | 3.5 | 3.5 | **0.1** | 0 | 0 | 0 | bal |
| 11 | 9.0 | 1.0 | 0.4 | 0.2 | 3.5 | 3.5 | **0.2** | 0 | 0 | 0 | bal |
| 12 | 9.0 | 1.0 | 0.4 | 0.2 | 3.5 | 3.5 | 0 | **0.01** | 0 | 0 | bal |
| 13 | 9.0 | 1.0 | 0.4 | 0.2 | 3.5 | 3.5 | 0 | **0.05** | 0 | 0 | bal |
| 14 | 9.0 | 1.0 | 0.4 | 0.2 | 3.5 | 3.5 | 0 | **0.1** | 0 | 0 | bal |
| 15 | 9.0 | 1.0 | 0.4 | 0.2 | 3.5 | 3.5 | 0 | **0.2** | 0 | 0 | bal |
| 16 | 9.0 | 1.0 | 0.4 | 0.2 | 3.5 | 3.5 | 0 | **0.3** | 0 | 0 | bal |
| 17 | 9.0 | 1.0 | 0.4 | 0.2 | 3.5 | 3.5 | 0 | **0.5** | 0 | 0 | bal |
| 18 | 9.0 | 1.0 | 0.4 | 0.2 | 3.5 | 3.5 | 0 | 0 | **0.1** | 0 | bal |

Table 3.9 continuned *Summary of all alloys composition used in the dissertation*

| alloy | Si | Fe | Mn | Mg | Cu | Zn | Sr | Ti | K | Ca | Al |
|---|---|---|---|---|---|---|---|---|---|---|---|
| 19 | 9.0 | 1.0 | 0.4 | 0.2 | 3.5 | 3.5 | 0 | 0 | **0.5** | 0 | bal |
| 20 | 9.0 | 1.0 | 0.4 | 0.2 | 3.5 | 3.5 | 0 | 0 | **1.0** | 0 | bal |
| 21 | 9.0 | 1.0 | 0.4 | 0.2 | 3.5 | 3.5 | 0 | 0 | **2.0** | 0 | bal |
| 22 | 9.0 | 1.0 | 0.4 | 0.2 | 3.5 | 3.5 | 0 | 0 | **3.0** | 0 | bal |
| 23 | 9.0 | 1.0 | 0.4 | 0.2 | 3.5 | 3.5 | 0 | 0 | 0 | **0.1** | bal |
| 24 | 9.0 | 1.0 | 0.4 | 0.2 | 3.5 | 3.5 | 0 | 0 | 0 | **0.3** | bal |
| 25 | 9.0 | 1.0 | **0.5** | 0.2 | 3.5 | 3.5 | **0.1** | 0 | 0 | 0 | bal |
| 26 | 9.0 | 1.0 | **0.05** | 0.2 | 3.5 | 3.5 | **1.0** | 0 | 0 | 0 | bal |
| 27 | 9.0 | 1.0 | **1** | 0.2 | 3.5 | 3.5 | 0 | 0 | 0 | **0.1** | bal |
| 28 | 9.0 | 1.0 | 0 | 0.2 | 3.5 | 3.5 | **0.05** | 0 | 0 | **0.1** | bal |

All the alloys are melted in Kerr Auto Standard Electro-melt Furnace. The use of the casting metal for one casting process is about 180 g. The molten alloys holds at 710 ℃ for 2 hours and slowly cool down to 660 ℃ for casting.

### 3.3.3 Heat treatment Design

Heat treatment is another effective way to reduce the detrimental effect of AlFeSi intermetallics. However, blistering is the main problem of heat treatment of die casting parts. In view of this, the short-time high-temperature heat treatment and water quenching is adopted. The experiment details are shown in Table 3.10.

Table 3.10 *Experiment condition for heat treatment*

| No | Solution Temperature(℃) | Solution Time(h) |
|---|---|---|
| 1 | 450 | 0.5 |
| 2 | 450 | 1 |
| 3 | 450 | 2 |
| 4 | 450 | 4 |
| 5 | 450 | 8 |
| 6 | 450 | 24 |
| 7 | 500 | 0.5 |
| 8 | 500 | 1 |
| 9 | 500 | 2 |
| 10 | 500 | 4 |
| 11 | 500 | 8 |
| 12 | 500 | 24 |
| 13 | 515 | 0.5 |
| 14 | 515 | 1 |
| 15 | 515 | 2 |
| 16 | 515 | 4 |
| 17 | 525 | 0.5 |
| 18 | 525 | 1 |
| 19 | 525 | 2 |
| 20 | 525 | 4 |

### 3.3.4 Microstructure Analysis

The as-cast samples were sectioned, grinded and polished carefully. The polished samples were etched using a solution of 0.5% HF in distilled water. Optical Images were taken by using a Leica DM LM/P 11888500 optical microscope. SEM work was conducted using by either a Hitachi S-4800 Field Emission SEM or a FEI Philips XL-40 SEM. The average size and fraction of α-AlFeSi and β-AlFeSi are calculated from 10 optical images taken from different positions of a sample with the ImageJ software.

# CHAPTER 4. RESULTS

## 4.1 Thermodynamics Simulation

The equilibrium phase diagrams and temperature vs solid fraction curves (Scheil curves and cooling curves) were derived used by Thermo-Calc software. The reason to use this method lies in the following aspects. First, it can reduce the work of the experiment. It is impossible and unnecessary to conduct experiment for hundreds of different element contents, while Thermo-Calc simulation can simply obtain the results in a short time. Second, some of the experiment data, such as solidus and liquidus temperatures, solid fraction, and solidification path etc. cannot be precisely measured from casting experiments, while thermodynamics calculation using a validated database provides fairly accurate results. The third reason is that it can also predict the phase formation and transformation during solidification.

In this section, the equilibrium phase diagrams with the single element change and Scheil and Level cooling curves are given out. In addition, the Al-Fe-Si ternary and Al-Fe-Si-xMn liquids projection and the solidification path are obtained.

### 4.1.1 The Effect of Single Element Change

In this section, only one element is changed while other elements kept consistant using an nominal compotion of A380 aluminum alloy. Figures 4.1-4.10 show phase diagrams of Al-Si-Cu-x (x=Si, Mn, Fe, Mg, Cu, Zn, Sr, K, Ca, Ti) systems.

Si is the major elements in Al-Si alloy. Compared to Al-Si wrought and other Al-Si casting alloys, A380 alloy has a higher weight percentage of Si for the requirement of castability. While increasing of Si content not only leads to the change of α-AlFeSi phase to β-AlFeSi phase, it also changes the sequence of phase formation. Figure 4.1 shows that when the content of Si is lower than 5.7%, fcc α-Al will precipitate first so that AlFeSi will precipitate as secondary phase. Once the Si content is above 5.7 percentages, the primary α-AlFeSi and/or β-AlFeSi will form first so the primary AlFeSi phase will be inevitably formed. This is in accordance with the Samuel results while in contradiction with Backerud results (Chai, & Tamminen, 1990; Samuel & Samuel, 1996).

There are four Si content points which should be paid attention to. The first one is at 5.7%. When the Si content is below 5.7%, no primary α-AlFeSi forms. While to die casting and even permanent casting aluminum silicon alloy, this Si composition is lower than most of the Al-Si cast alloys. In other words, the primary sludge α-AlFeSi is unavoidable for equilibrium casting situation. The second content point is at 9.7%. If the Si content is between 5.7-9.7%, only primary α-AlFeSi phase will form first, then fcc α-Al will precipitate followed by the nucleation of secondary β-AlFeSi phase. The nominal Si content in A380 alloy is from 7.5-9.5%, which falls into this range. The third point is at 11.8%, which is the Al-Si eutectic point. Above this point, primary Si will nucleate first in prior to the nucleation fcc α-Al. It should be avoided. The last turning point is 12.7%. Above this point β-AlFeSi will precipitate first, which will severely degrade the mechanical property.

And during the solidification process under equilibrium conditions, only four solid phases are formed (fcc α-Al, α-AlFeSi, β-AlFeSi and silicon). $Al_2Cu$ and

AlCuMgSi phase are only formed during the solid phase transformation. The nucleation sequence of A380 alloy with different Si composition is shown in Table 4.1.

Table 4.1 *Nucleation sequence of Al-Si-Cu alloy with different Si composition (Cu=3.5%, Mn=0.5%, Fe=1%, Mg=0.2%, Zn=0.35%, Al=bal.)*

| Si composition (%) | 4-5.7 | 5.7-9.7 | 9.7-11.8 | 11.8-12.7 | 12.7-13 |
|---|---|---|---|---|---|
| 1 | fcc α-Al | α-AlFeSi | α-AlFeSi | α-AlFeSi | β-AlFeSi |
| 2 | α-AlFeSi | fcc α-Al | β-AlFeSi | β-AlFeSi | α-AlFeSi |
| 3 | β-AlFeSi | β-AlFeSi | fcc α-Al | silicon | silicon |
| 4 | silicon | silicon | silicon | fcc α-Al | fcc α-Al |
| 5 | $Al_2Cu$ | $Al_2Cu$ | $Al_2Cu$ | $Al_2Cu$ | $Al_2Cu$ |
| 6 | AlCuMgSi | AlCuMgSi | AlCuMgSi | AlCuMgSi | AlCuMgSi |

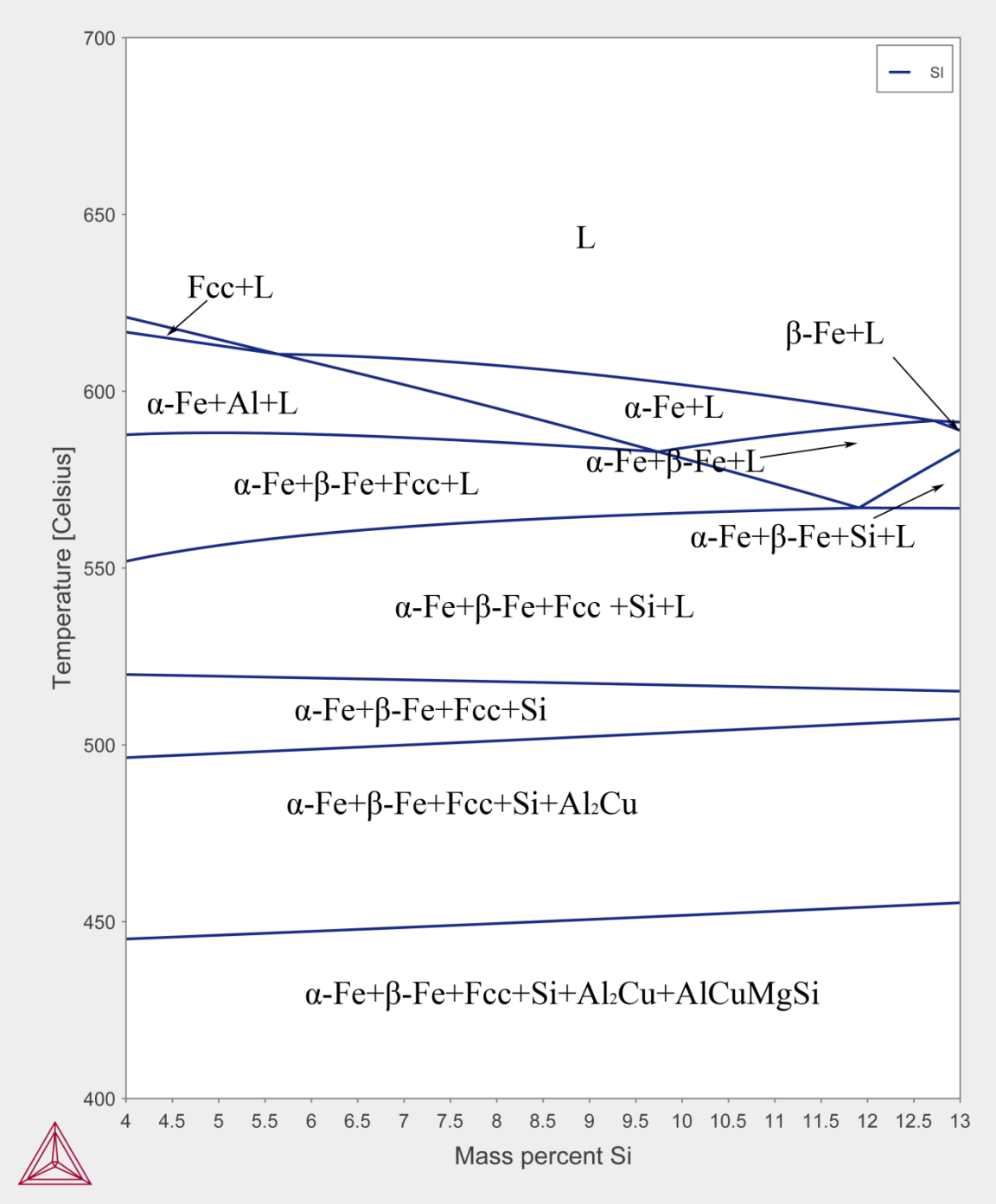


*Figure 4.1* Al-Si-Cu-xSi phase diagram
(Si=4-13%,Cu=3.5%, Mn=0.4%, Fe=1%, Mg=0.2%, Zn=0.35%, Al=bal.)

Fe is also an important element in forming AlFeSi intermetallics. Figure 4.2 is the calcularted Al-Si-Cu-xFe phase diagram and Table 4.2 lists the nucleation sequence of Al-Si-Cu alloy with different Fe contents, which is summarized from Figure 4.2. It shows that for the Fe Level within the range of 0-2%, α-AlFeSi phase will form and that β-AlFeSi cannot precipitate until the Fe Level reaches 0.11%. However, the different percentages of Fe will result in the change of nucleation sequence. The following phenomenon can be attained from Figure 4.2. 1) Only α-AlFeSi or fcc α-Al is the first precipitate phase during solidification for the Fe contents in the range of 0-2%. If the Fe Level is below 0.6%, fcc α-Al will precipitate first, otherwise α-AlFeSi will first nucleate. 2) β-AlFeSi phase always forms after α-AlFeSi phase. 3) If Fe Level is above 1.1%, primary β-AlFeSi phase will form in prior to fcc α-Al. For the 380 series alloy, the amount of Fe is from 0.7-2.0%. That means large platelet primary β-AlFeSi phase is possible to form if the Fe content is not maintained below 1.1%. 4) The starting formation temperatures of α-AlFeSi and β-AlFeSi phase increases with the increase of Fe content, while the formation temperatures of fcc α-Al and silicon phase remain constant. As mentioned above, if the Fe content is below 0.6%, fcc α-Al forms first. Thus the liquidus temperatures keep steady at around 590 ℃. However, once the Fe content is above 0.6%, the first-precipitate α-AlFeSi phase leads to a rise in liquidus temperature, and it arrives at 635 ℃ when the Fe content is up to 2 percent. That means there is sufficient time for primary β-AlFeSi to nucleate and grow up to a large size, leading to degradation of mechanical properties.

Table 4.2 *Nucleation sequence of Al-Si-Cu alloy with different Fe composition (Fe=0-2%, Si=9%,Cu=3.5%, Mn=0.5%, Mg=0.2%, Zn=0.35%, Al=bal.)*

| Fe composition (%) | 0-0.08 | 0.08-0.11 | 0.1-0.50 | 0.50-0.55 | 0.55-1.10 | 1.10-2.00 |
|---|---|---|---|---|---|---|
| 1 | fcc α-Al | fcc α-Al | fcc α-Al | α-AlFeSi | α-AlFeSi | α-AlFeSi |
| 2 | Silicon | α-AlFeSi | α-AlFeSi | fcc α-Al | fcc α-Al | β-AlFeSi |
| 3 | α-AlFeSi | silicon | silicon | Silicon | β-AlFeSi | fcc α-Al |
| 4 | $Al_2Cu$ | β-AlFeSi | β-AlFeSi | β-AlFeSi | silicon | silicon |
| 5 | AlCuMgSi | $Al_2Cu$ | $Al_2Cu$ | $Al_2Cu$ | $Al_2Cu$ | $Al_2Cu$ |
| 6 | - | AlCuMgSi | AlCuMgSi | AlCuMgSi | AlCuMgSi | AlCuMgSi |

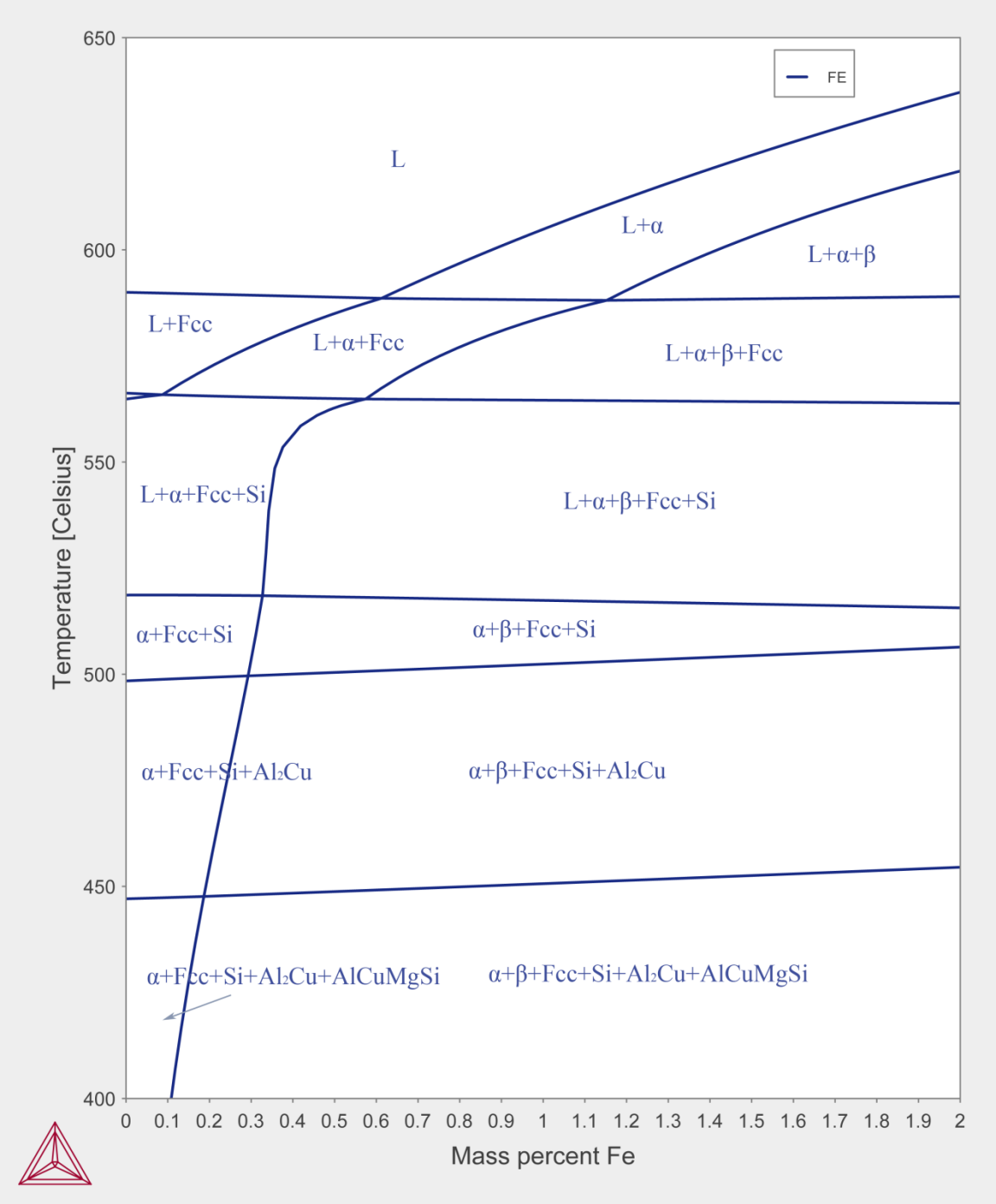


*Figure 4.2* Al-Si-Cu-xFe phase diagram
(Fe=0-2%, Si=9%,Cu=3.5%, Mn=0.4%, Mg=0.2%, Zn=0.35%, Al=bal.)

Mn is considered to be an effective Fe neutralizer because of the similarity of Mn and Fe atom structures. Mn is usually added to aluminum die casting alloys in an amount that does not exceed half the Fe content to act as a Fe corrector. (Colwell, & Kissling, 1961) As mentioned above, Mn atoms can substitute for Fe atoms in the AlFeSi phase, which leads to the formation of the compound α-Al(Fe,Mn)Si in the shape of Chinese script, thereby minimizing the deleterious effect of the needle shaped β-AlFeSi phase. Figure 4.3 shows the calulated Al-Si-Cu-xMn phase diagram and Table 4.3 lists the nucleation sequence of Al-Si-Cu alloy systems with different Mn contents.

The results shows that within the range of 0-2% Mn, α-AlFeSi and/or β-AlFeSi phase nucleates as the primary phase, the change of Mn contents only affects the solidification sequence of AlFeSi phase, while there is no effect on the phases that precipitate later such as fcc α-Al, Si, $Al_2Cu$ and AlCuMgSi. The addition of Mn promotes the formation of α-AlFeSi phase and postpones that of β-AlFeSi phase.

It can be seen that from Figure 4.3 if the Mn content is in the range of 0.25-0.38%, both primary α-AlFeSi and β-AlFeSi precipitate prior to the formation of fcc α-Al. The nominal Mn content of A380 (0.4%) is higher than that range, which means no primary β-AlFeSi precipitate will form. Mn addition can also increase the formation temperature of primary α-AlFeSi. This may lead to the formation of polygon α-AlFeSi, called sludge, which is detrimental to the mechanical property of alloys.

Table 4.3 *Nucleation sequence of Al-Si-Cu alloy with different Mn composition (Mn=0-2%, Si=4-9%, Cu=3.5%, Fe=1%, Mg=0.2%, Zn=0.35%, Al=bal.)*

| Mn composition (%) | 0-0.01 | 0.01-0.20 | 0.20-0.25 | 0.25-0.30 | 0.30-0.38 | 0.38-0.90 | 0.90-1.30 | 1.30-2.00 |
|---|---|---|---|---|---|---|---|---|
| 1 | β-AlFeSi | β-AlFeSi | β-AlFeSi | β-AlFeSi | α-AlFeSi | α-AlFeSi | α-AlFeSi | α-AlFeSi |
| 2 | fcc α-Al | fcc α-Al | fcc α-Al | α-AlFeSi | β-AlFeSi | fcc α-Al | fcc α-Al | cc α-Al |
| 3 | silicon | silicon | α-AlFeSi | fcc α-Al | fcc α-Al | β-AlFeSi | silicon | silicon |
| 4 | $Al_2Cu$ | α-AlFeSi | silicon | silicon | silicon | silicon | β-AlFeSi | $Al_2Cu$ |
| 5 | AlCuMgSi | $Al_2Cu$ | $Al_2Cu$ | $Al_2Cu$ | $Al_2Cu$ | $Al_2Cu$ | $Al_2Cu$ | β-AlFeSi |
| 6 | - | AlCuMgSi | AlCuMgSi | AlCuMgSi | AlCuMgSi | AlCuMgSi | AlCuMgSi | AlCuMgSi |

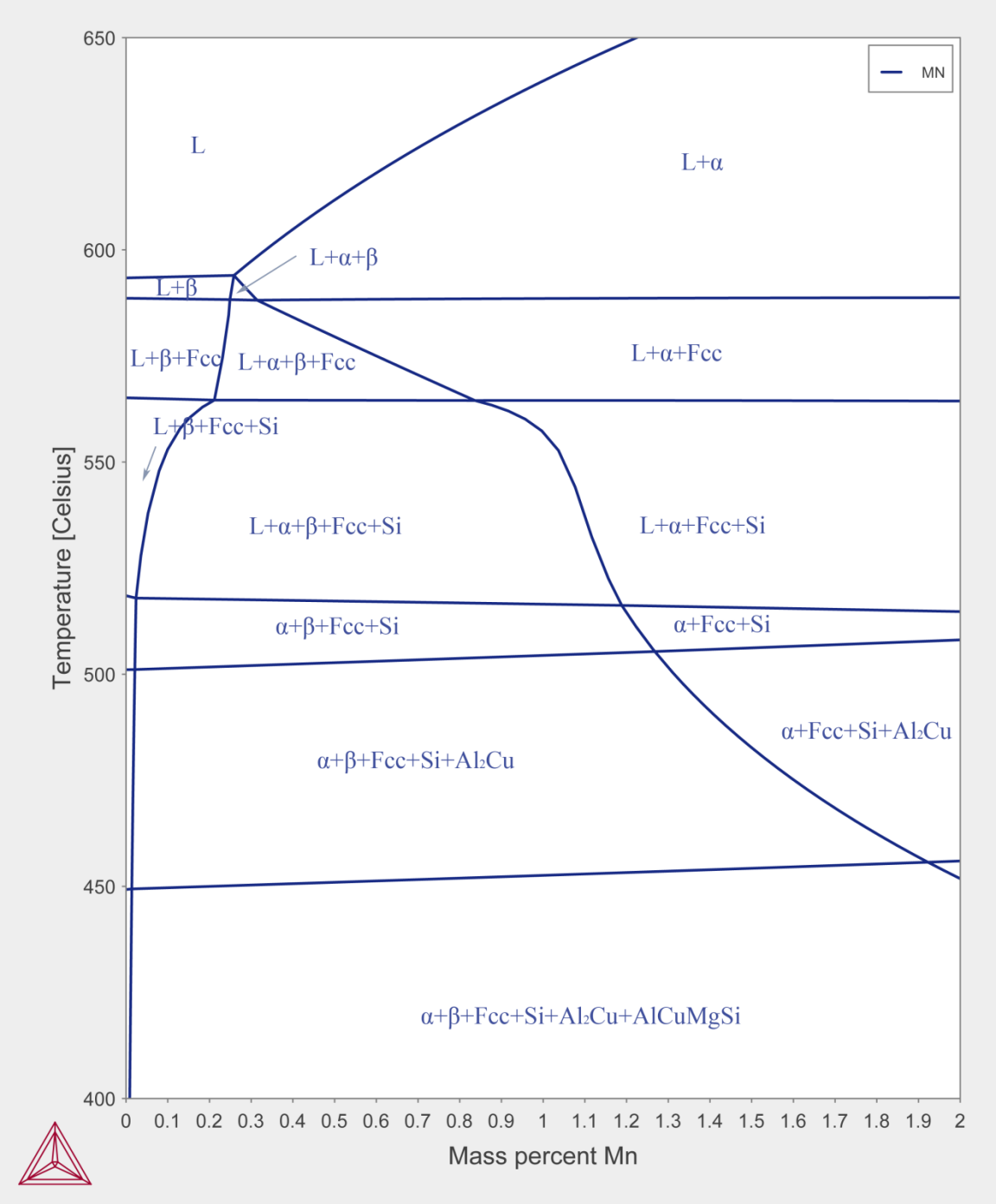


*Figure 4.3* Al-Si-Cu-xMn phase diagram
(Mn=0-2%, Si=4-9%, Cu=3.5%, Fe=1%, Mg=0.2%, Zn=0.35%, Al=bal.)

In A380 aluminum die casting alloys, Mg is viewed as an impurity specified to be below maximum of 0.1%. Mg can be oxidized in the molten alloy to form micron-sized MgO and spindle in high temperature (Samuel, 1999). In commercial aluminum alloys, Mg may react with other elements to form complex intermetallics, such as $Ai_8FeMg_3Si_6$ and $Cu_2Mg_8Si_6Al_5$. Because they can severely reduce the fluidity and ductility of the alloy, the content of Mg in aluminum diecasting alloys should be limited. Nevertheless, Mg content has no effect on formation temperature and amount of both α-AlFeSi and β-AlFeSi phase, which can be seen from Figure 4.4. However if the Mg content is above 0.65%, π-AlFeSi phase will form.

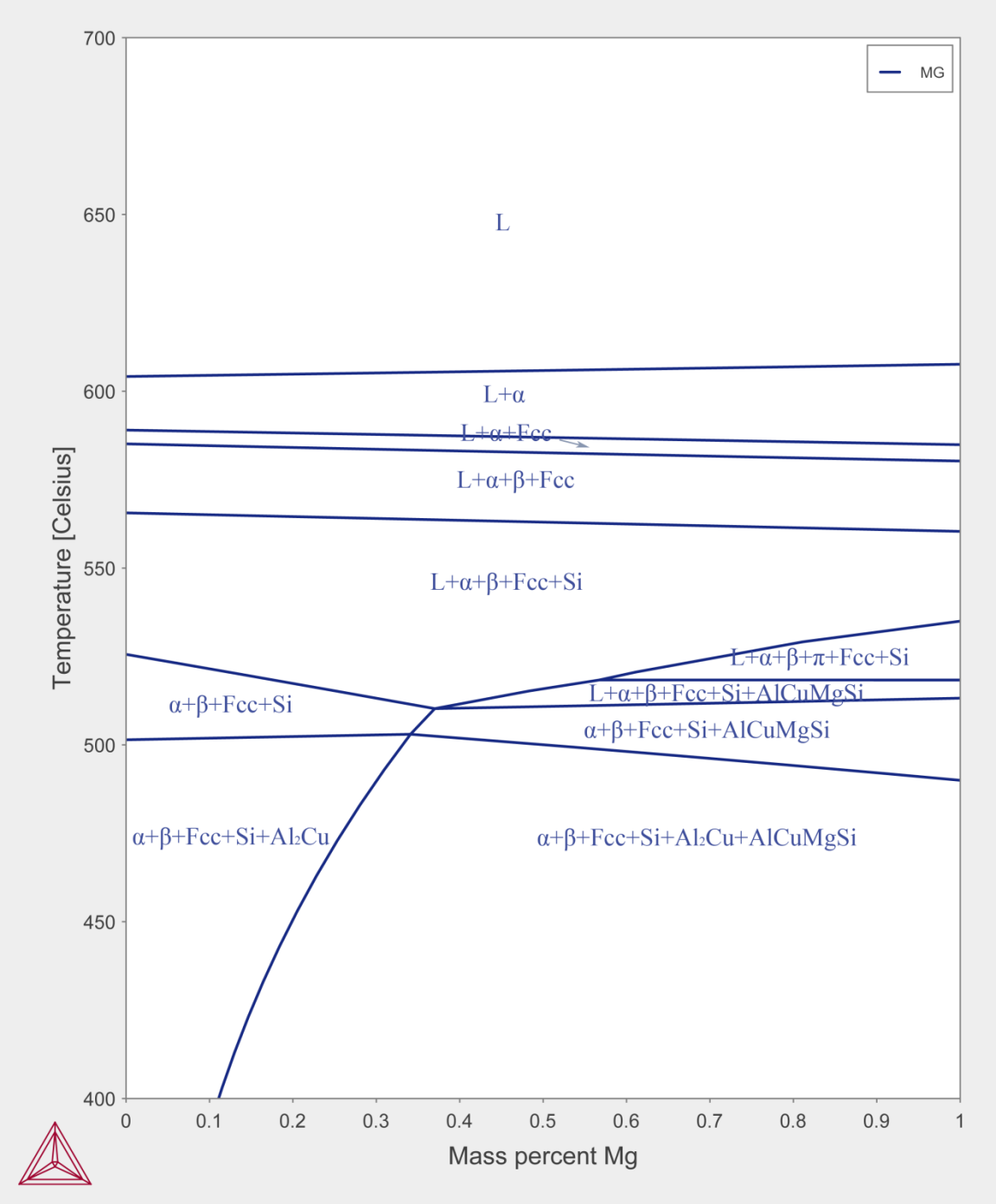


F*igure 4.4* Al-Si-Cu-xMg phase diagram
(Mg=0-1%, Si=9%, Cu=3.5%, Mn=0.4%, Fe=1%, Zn=0.35%, Al=bal.)

The content of Cu does not have a significant effect on AlFeSi phase, which is shown in Fugure 4.5.

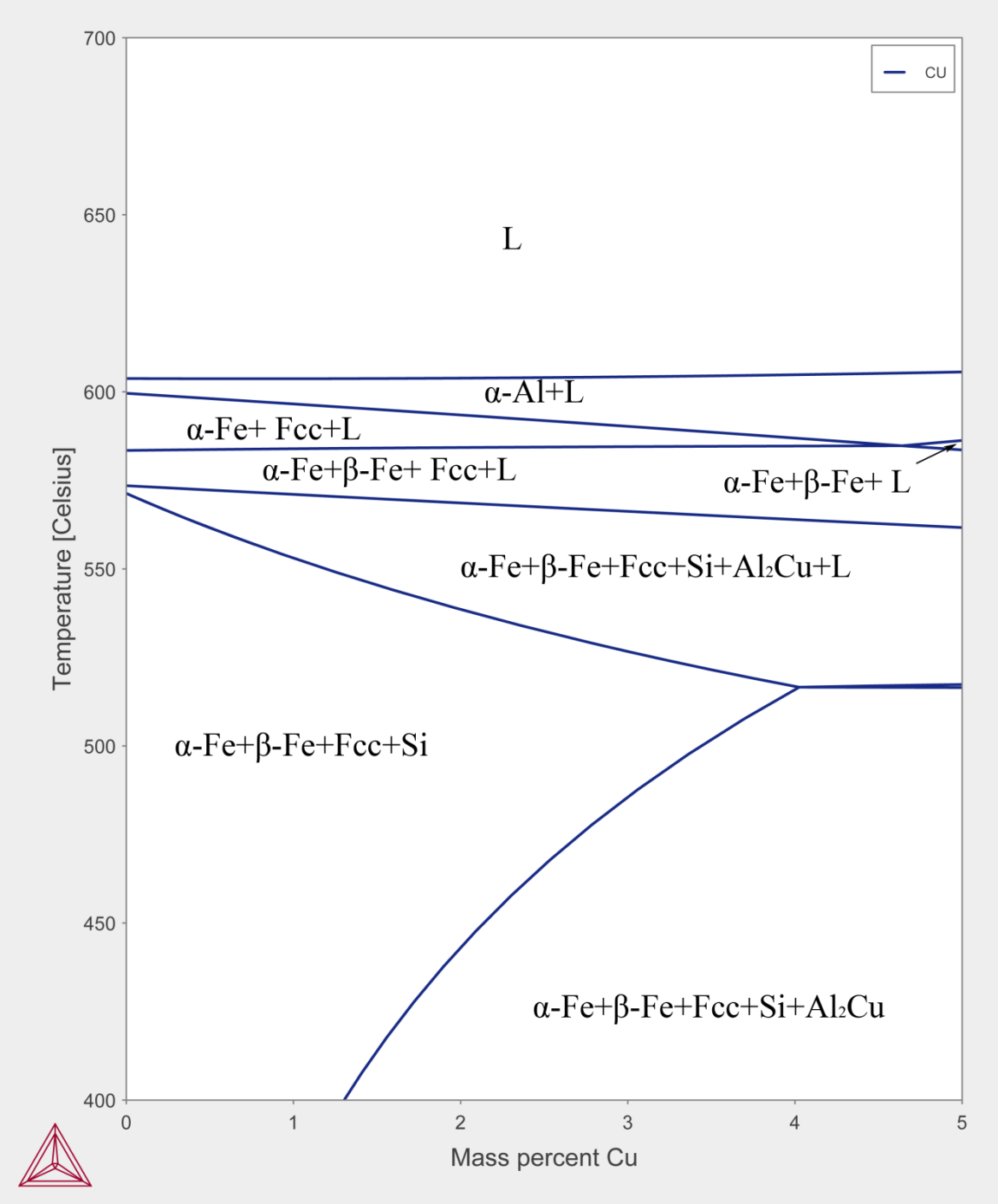


*Figure 4.5* Al-Si -xCu phase diagram
(Cu=0-4%, Si=9%, Mn=0.4%, Fe=1%, Mg=0.2%, Zn=0.35%, Al=bal.)

Zn is normally regarded as an impurity in A380 alloy. Figure 4.6 shows that zinc increases the starting formation temperature of β-AlFeSi phase and decreases that of fcc α-Al. Thus if the Zn content rises to 1.8%, primary β-AlFeSi phase will form. The content of Zn in A380 is 0.35% max, which is much lower than the critical content to form primary β-AlFeSi.

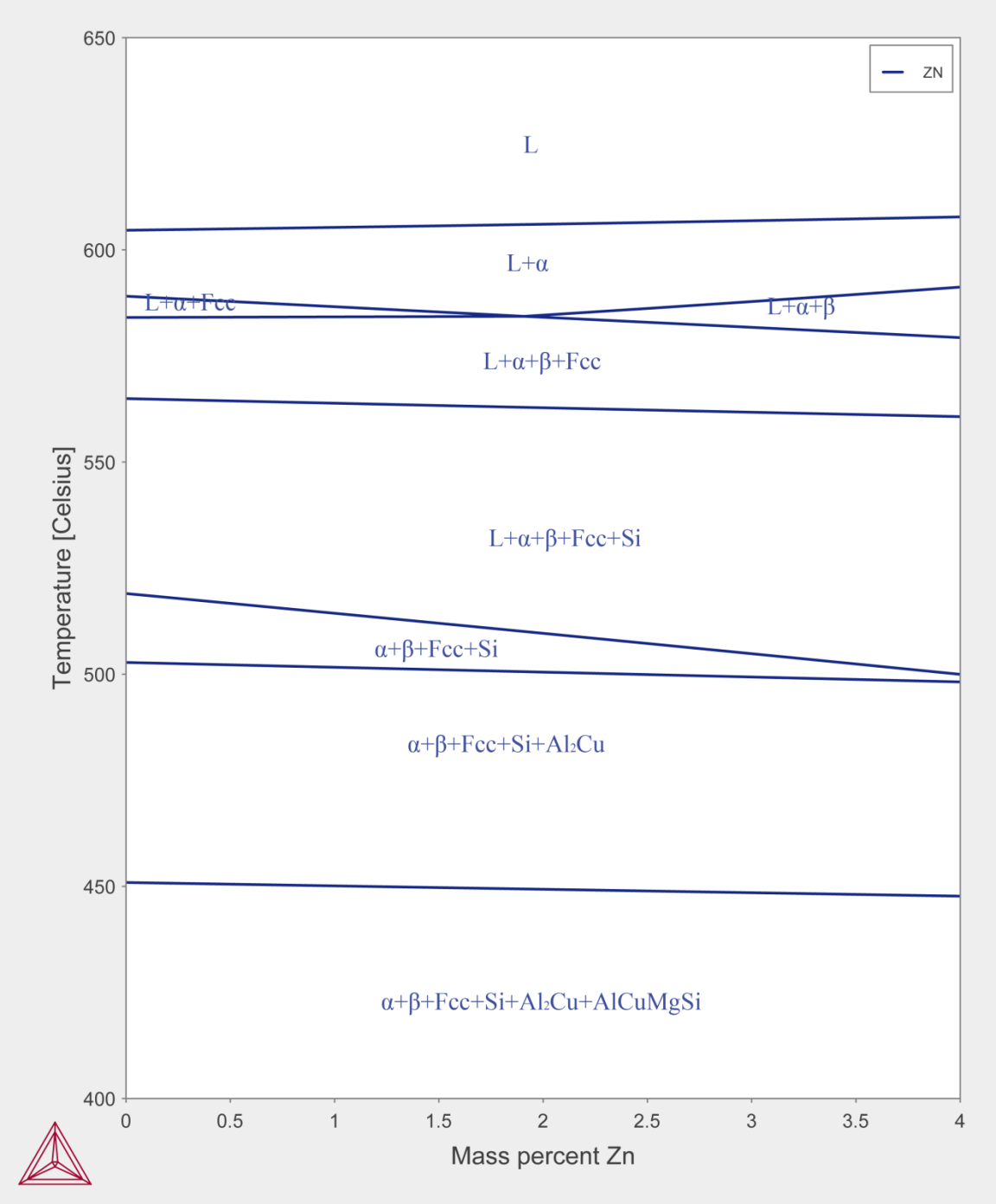


*Figure 4.6* Al-Si-Cu-xZn phase diagram
(Zn=0-4%, Si=9%,Cu=3.5%, Mn=0.4%, Fe=1%, Mg=0.2%, Al=bal.)

Other elements, including Sr, K, Ca, and Ti do not have effect on the formation on AlFeSi phase. But the Ca addition will lead to the formation of Al-Si-Ca phase, which is a hard intermetallics and detrimental to the ductility of alloy. The results are shown in Figure 4.7-4.10.

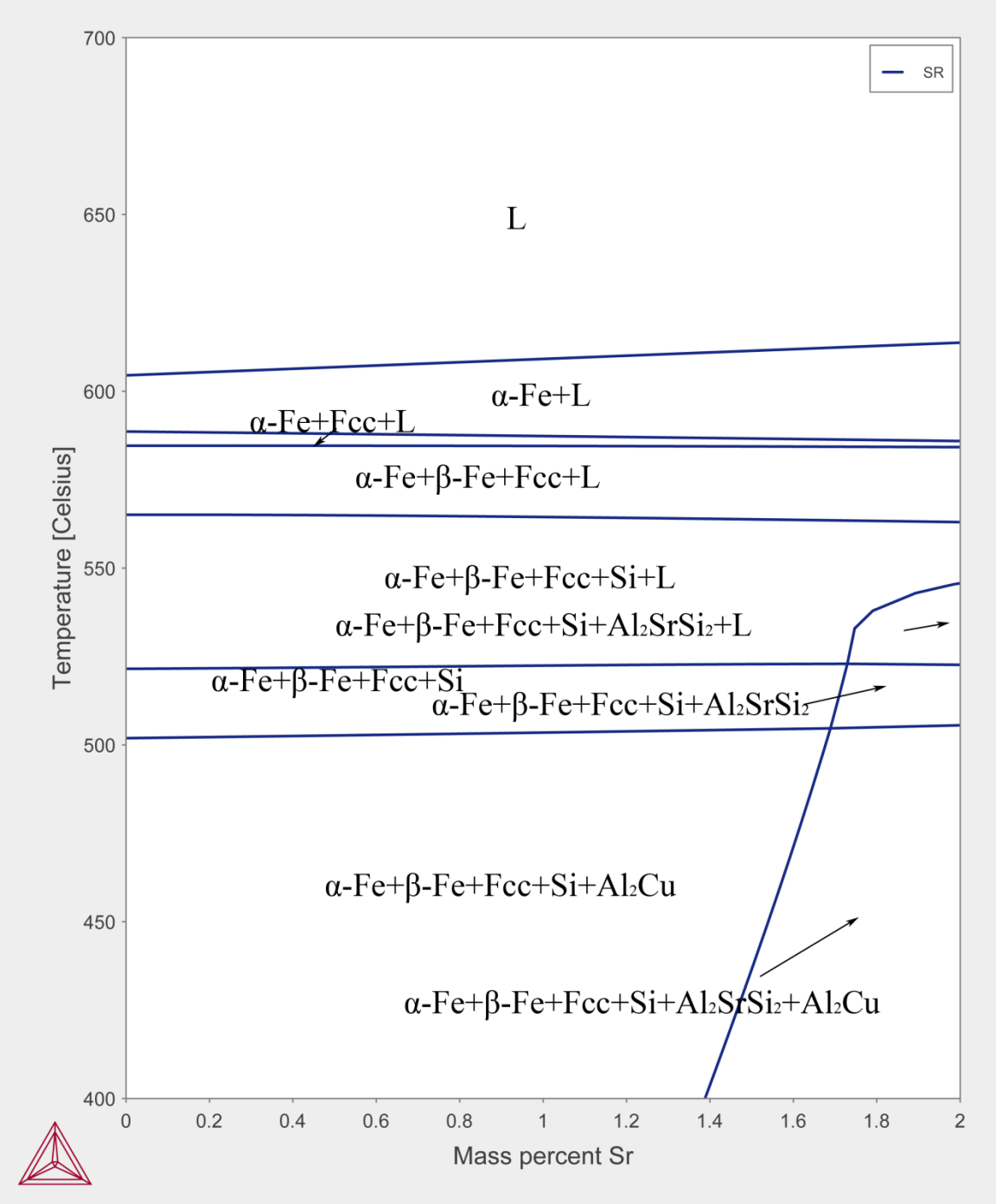


*Figure 4.7* Al-Si-Cu-xSr phase diagram
(Si=9%,Cu=3.5%, Mn=0.4%, Fe=1%, Mg=0.2%, Zn=0.35%, Al=bal.)

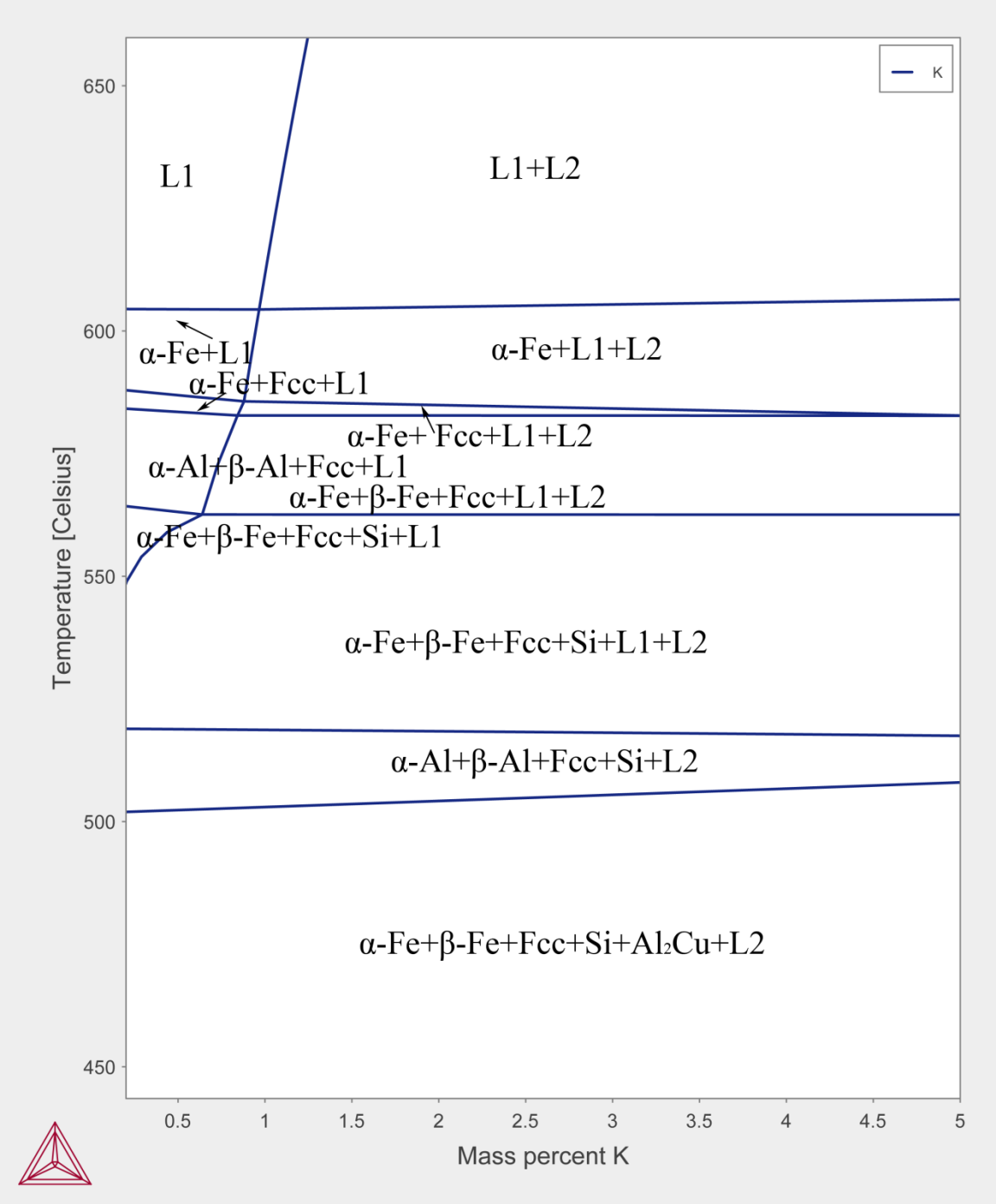


*Figure 4.8* Al-Si-Cu-xK phase diagram
(Si=9%,Cu=3.5%, Mn=0.4%, Fe=1%, Mg=0.2%, Zn=0.35%, Al=bal.)

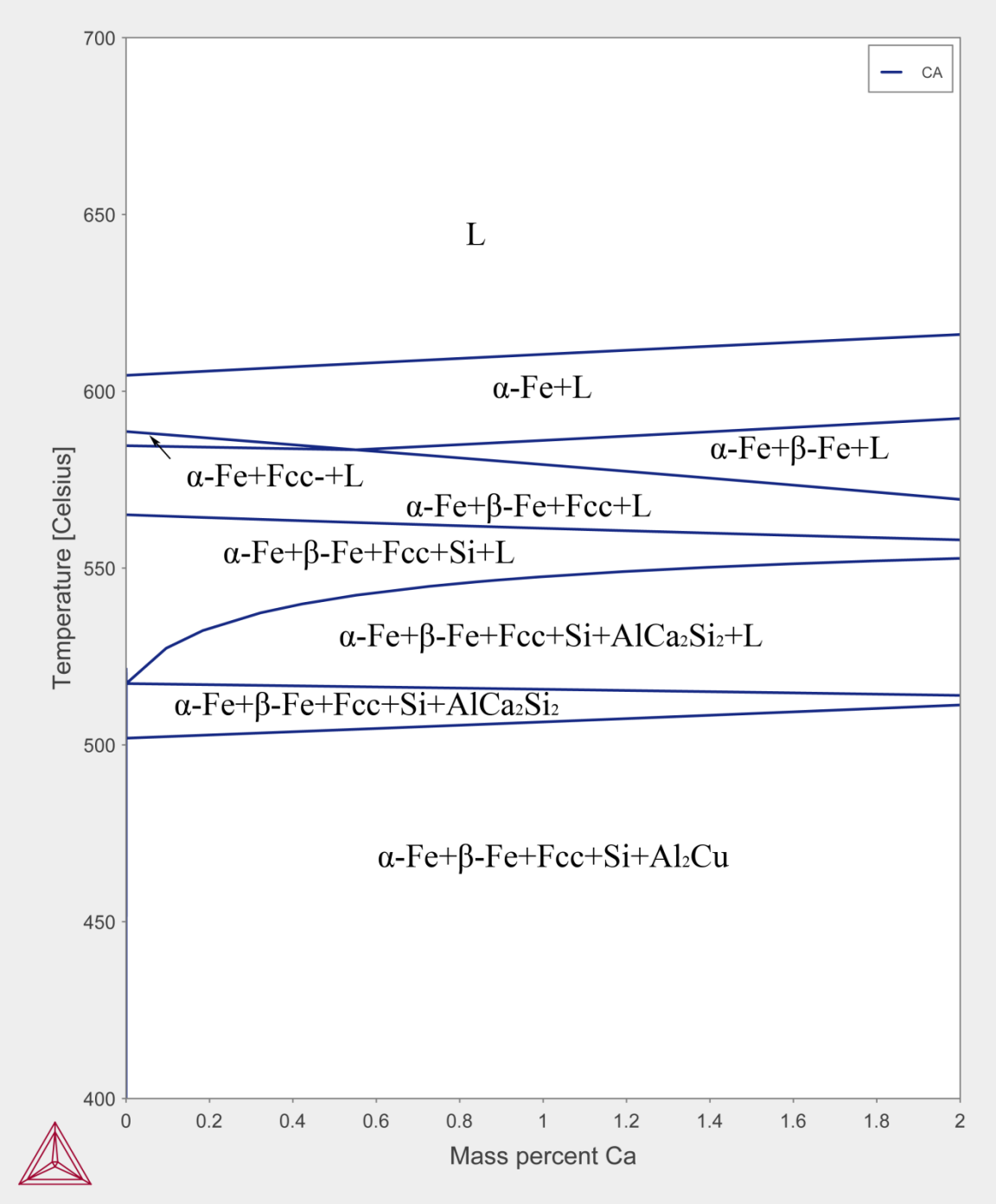


*Figure 4.9* Al-Si-Cu-xCa phase diagram
(Si=9%,Cu=3.5%, Mn=0.4%, Fe=1%, Mg=0.2%, Zn=0.35%, Al=bal.)

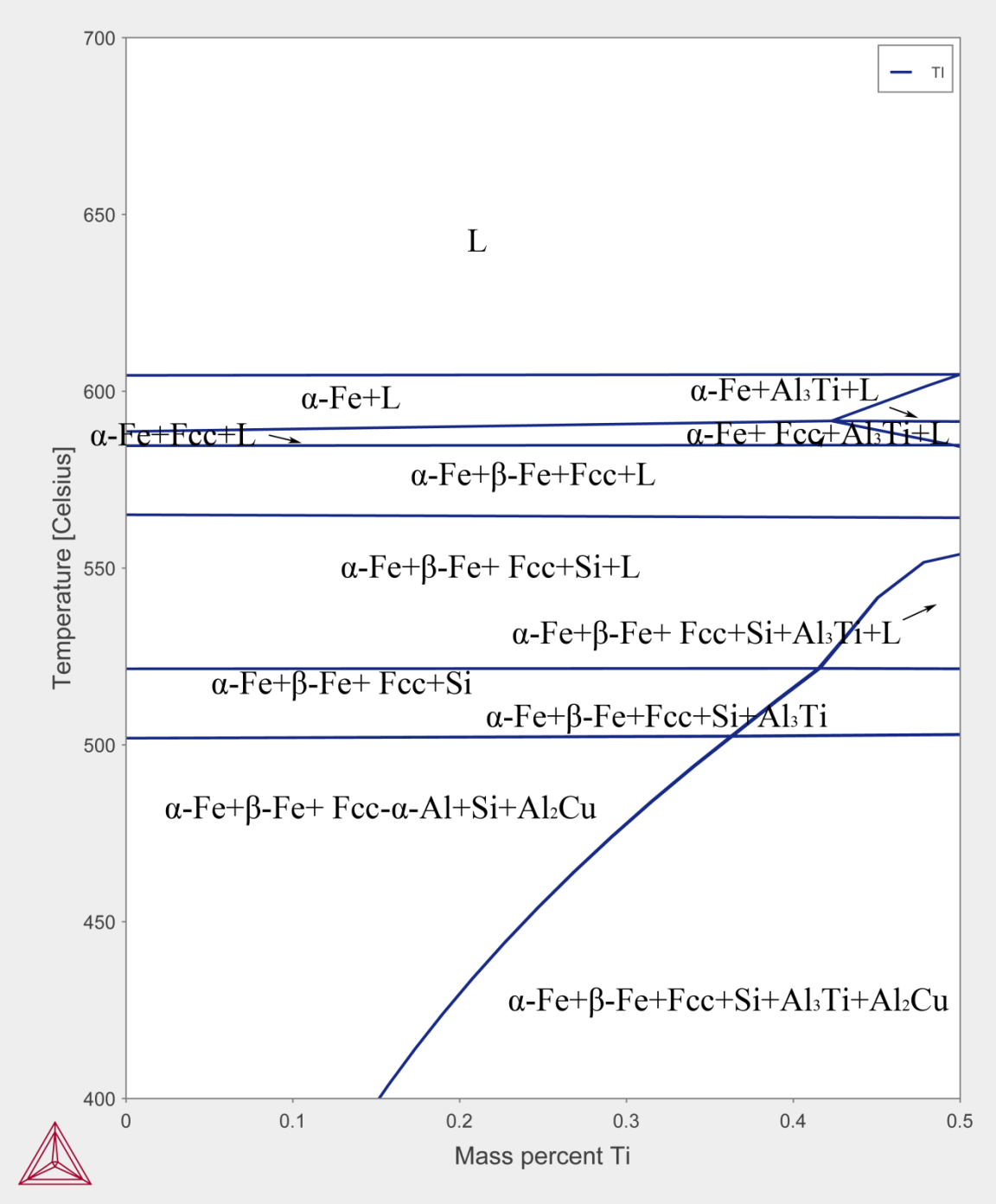


*Figure 4.10* Al-Si-Cu-xTi phase diagram
(Si=9%,Cu=3.5%, Mn=0.4%, Fe=1%, Mg=0.2%, Zn=0.35%, Al=bal.)

### 4.1.2 The Statistic Analysis of Effect of Multiple Elements Change

In section 4.1.1, the effect of single element on AlFeSi intermetallics was discussed. In this section, the effects of multiple elements on the fraction and formation temperatures of AlFeSi and other phase are studied.

In the previous section, Si, Mn, and Fe are shown to have signifcant influence on the effect of formation and solidification path of AlFeSi phase, whereas Cu and Mg have slight effect on the phase formation. In this section, the Scheil and Level curves are obtained by Thermo-Calc software. The statistical single and interaction effect of elements on the quantity and formation temperature of AlFeSi, fcc α-Al and silicon phase and its regression results are obtained by IBM SPSS software. The computal results are listed in the appendix. If the significance Level of effect of an element on is under 0.05, it is considered the effect of this element is significant. In other words, the content of this element has effect on the phase fraction or phase formation temperatures.

From Table A.1, it can be seen that only the effect of content of Si, Mn and Fe is significant, while Cu and Mg content have no effect on the fraction of α-AlFeSi phase. While the significant Level of Si is 0.036, which means compared to Mn and Fe, the effect of Si is limited. The linear regression equation of α-AlFeSi fraction can be expressed as

$$f_{\alpha(\mathrm{AlFeSi})} = -0.001\ \mathrm{Si\%} + 0.015\ \mathrm{Fe\%} + 0.043\ \mathrm{Mn\%} \quad (4.1)$$

So the fraction of α-AlFeSi is mainly affected by the amount of Mn and Fe elements in A380 series alloy. And addition of Mn is more prone to the formation of α-AlFeSi phase.

In contrast to the fraction of α-AlFeSi, the formation temperature of α-AlFeSi is

influenced by four elements. The regression can be expressed in equation 4.2:

$$T_{\alpha(AlFeSi)}\,(°C) = -2.462\ Si\% - 3.400\ Cu\% + 28.193\ Fe\% + 50.336\ Mn\% + 587.442 \quad (4.2)$$

But it can be also found that the impact factor of Si and Cu is only 2.462 and 3.4000, compared to 28.193 of Fe and 50.336 of Mn which proved the formation temperature of α-AlFeSi are mainly affected by Fe and Mn. The increase of Mn and Fe has significant effect on increasing the formation temperature of α-AlFeSi.

Similar to α-AlFeSi, the fraction and formation temperature of β-AlFeSi is only affected by the content of Fe and Mn, the regression of the fraction and formation temperature of β-AlFeSi is shown in equations 4.3 and 4.4:

$$f_{\beta(AlFeSi)} = 0.001\ Si\% + 0.022\ Fe\% - 0.012\ Mn\% \quad (4.3)$$

$$T_{\beta(AlFeSi)}(°C) = -6.077\ Mg\% + 30.450\ Fe\% - 15.008\ Mn\% + 563.98 \quad (4.4)$$

Mn prevents the formation of β-AlFeSi phase and decreases the formation temperature and reduces the tendency of formation of primary β-AlFeSi phase, while the effect of Fe is exactly opposite. It is also found that the Mg addition can effectively reduce the formation temperature of β-AlFeSi phase, which is an alternative way to reduce the detrimental effect of β-AlFeSi.

The effect of the element on the formation temperature of fcc-Al is also important. Only Si, Mg and Cu contents are significant for the formation temperature of fcc-Al, the regression equation is as follows:

$$T_{fcc-Al}(°C) = -6.399\ Si\% - 3.211\ Cu\% - 4.363\ Mg\% + 658.65 \quad (4.5)$$

It is noticed that each element will reduce the formation temperature fcc α-Al phase, while the effect of Si addition will be most significant, until the content arrives at

the eutectic point. But generally speaking, compared to the effect factors of Fe and Mn on α-AlFeSi and β-AlFeSi, the effect factors of each element on fcc α-Al are much smaller. That means the formation temperature of fcc α-Al phase are not significantly influenced by the content of elements.

Lastly, the effect of element on eutectic Si phase fraction and formation temperature is studied. The regressions results are shown in equation 4.6 and 4.7. It shows that Si phase fraction is mainly controlled by the content of Si element and the Si formation temperature can keep stable in a range of element change.

$$f_{Si} = 0.01\ \text{Si\%} - 0.006\ \text{Fe\%} - 0.005\ \text{Mg\%} - 0.008 \quad (4.6)$$

$$T_{Si}(°\text{C}) = -3.030\ \text{Cu\%} + 2.949\ \text{Si\%} - 3.591\ \text{Fe\%} - 6.281\ \text{Mg\%} + 551.23 \quad (4.7)$$

In summary, the formation temperature and fraction of α-AlFeSi and β-AlFeSi are mainly affected by the content of Mn and Fe elements. Both elements can effectively increase the formation temperature of both AlFeSi phases, which means primary α-AlFeSi and β-AlFeSi are easy to form, thus degrading the toughness of alloys. However, Mn addition can reduce the amount of the more detrimental β-AlFeSi, while Fe addition can facilitate the crystalline formation of both α-AlFeSi and β-AlFeSi. Mg addition can reduce the formation temperature of β-AlFeSi, which suggests that it can reduce the size of β-AlFeSi. On the other hand, if Mg content is above 0.5%, π-AlMgFeSi forms. It is more detrimental to the property of the alloy than β-AlFeSi. Because, other elements do not have a significant effect of the formation and fraction of α-AlFeSi, β-AlFeSi, fcc α-Al and Si phase.

### 4.1.3 Phase Fraction vs Temperature Curves

Phase evolution or phase fraction vs. temperature curves for selected alloys were also calculated under two conditions: Level and Scheil. Phase evolution simulated using Level rule represents equilibrium conditions which occur only under extremely slow cooling conditions. The Scheil curves are calculated under assumptions that there is no diffusion in the solids but complete diffusion in the liquid. Such assumptions are valid for diecasting conditions where the solid grows so fast so diffusion in solid can be ignored and the flow is so turbulent that diffusion of complete elements in the liquid can be achieved.

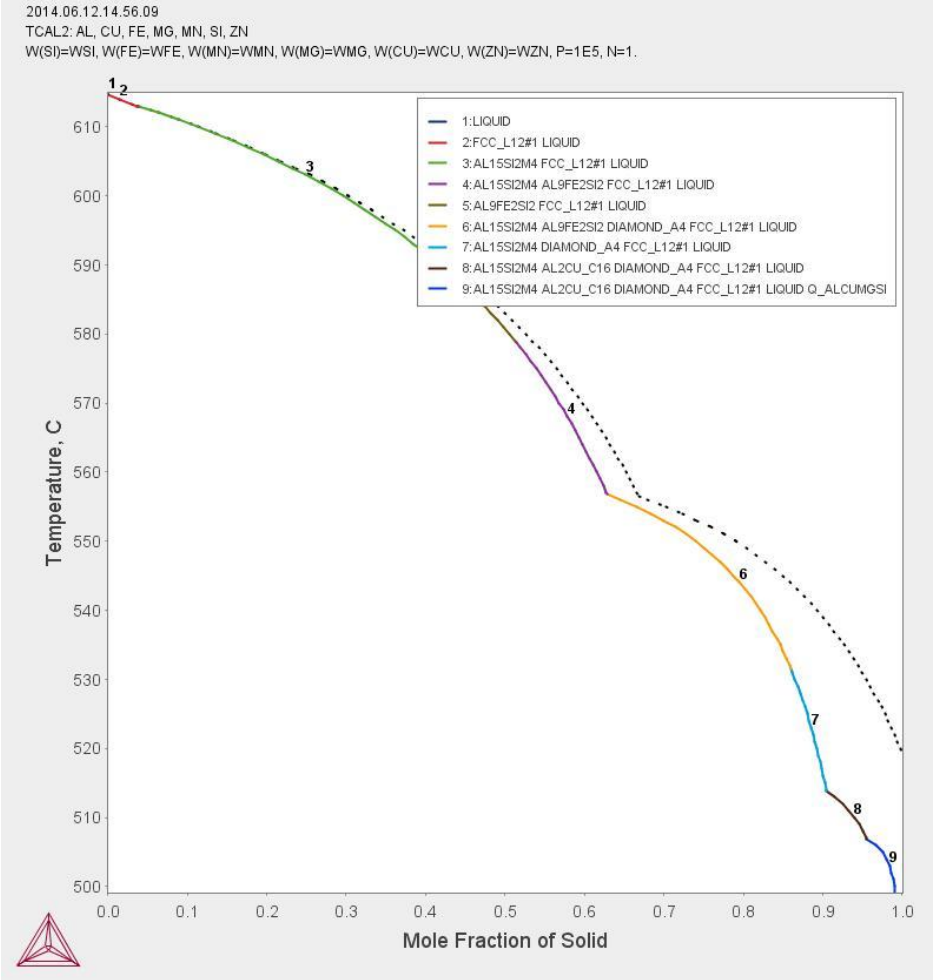
2014.06.12.14.56.09
TCAL2: AL, CU, FE, MG, MN, SI, ZN
W(SI)=WSI, W(FE)=WFE, W(MN)=WMN, W(MG)=WMG, W(CU)=WCU, W(ZN)=WZN, P=1E5, N=1.
1:LIQUID
2:FCC_L12#1 LIQUID
3:AL15SI2M4 FCC_L12#1 LIQUID
4:AL15SI2M4 AL9FE2SI2 FCC_L12#1 LIQUID
5:AL9FE2SI2 FCC_L12#1 LIQUID
6:AL15SI2M4 AL9FE2SI2 DIAMOND_A4 FCC_L12#1 LIQUID
7:AL15SI2M4 DIAMOND_A4 FCC_L12#1 LIQUID
8:AL15SI2M4 AL2CU_C16 DIAMOND_A4 FCC_L12#1 LIQUID
9:AL15SI2M4 AL2CU_C16 DIAMOND_A4 FCC_L12#1 LIQUID Q_ALCUMGSI
Temperature, C
Mole Fraction of Solid
500
510
520
530
540
550
560
570
580
590
600
610
0.0
0.1
0.2
0.3
0.4
0.5
0.6
0.7
0.8
0.9
1.0

(a)

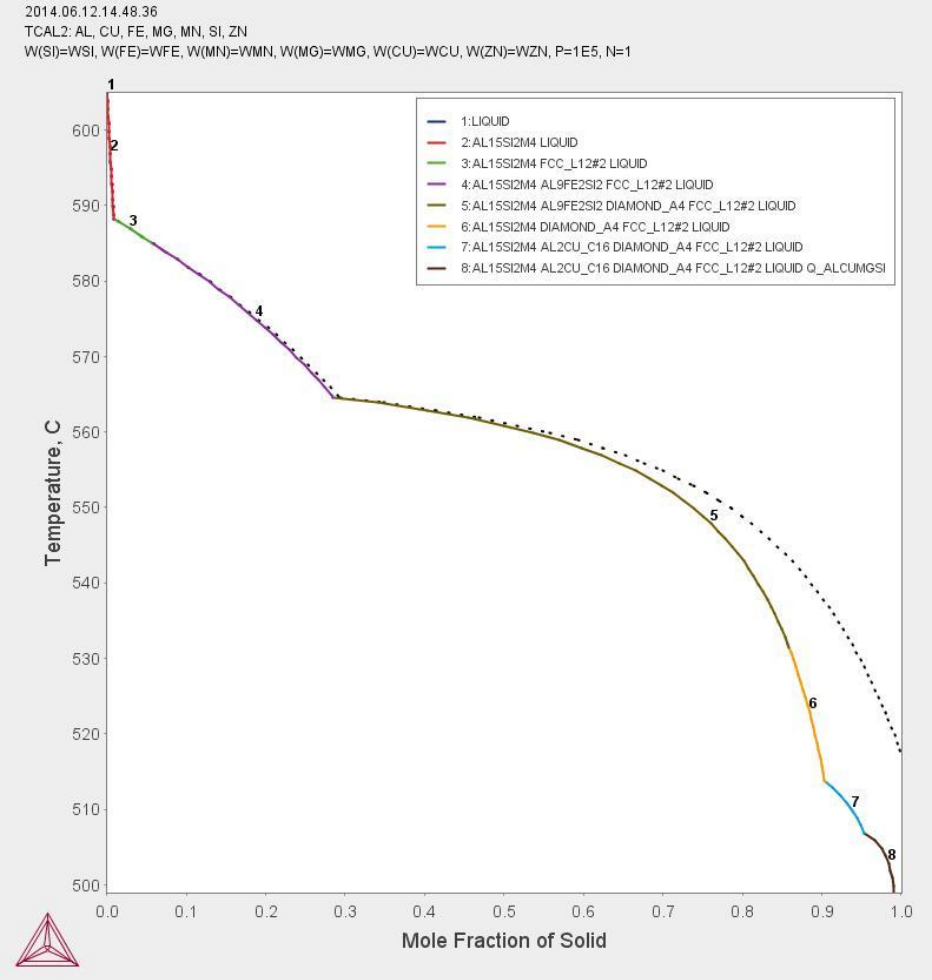
2014.06.12.14.48.36
TCAL2: AL, CU, FE, MG, MN, SI, ZN
W(SI)=WSI, W(FE)=WFE, W(MN)=WMN, W(MG)=WMG, W(CU)=WCU, W(ZN)=WZN, P=1E5, N=1
1:LIQUID
2:AL15SI2M4 LIQUID
3:AL15SI2M4 FCC_L12#2 LIQUID
4:AL15SI2M4 AL9FE2SI2 FCC_L12#2 LIQUID
5:AL15SI2M4 AL9FE2SI2 DIAMOND_A4 FCC_L12#2 LIQUID
6:AL15SI2M4 DIAMOND_A4 FCC_L12#2 LIQUID
7:AL15SI2M4 AL2CU_C16 DIAMOND_A4 FCC_L12#2 LIQUID
8:AL15SI2M4 AL2CU_C16 DIAMOND_A4 FCC_L12#2 LIQUID Q_ALCUMGSI
Temperature, C
600
590
580
570
560
550
540
530
520
510
500
0.0
0.1
0.2
0.3
0.4
0.5
0.6
0.7
0.8
0.9
1.0
Mole Fraction of Solid

(b)

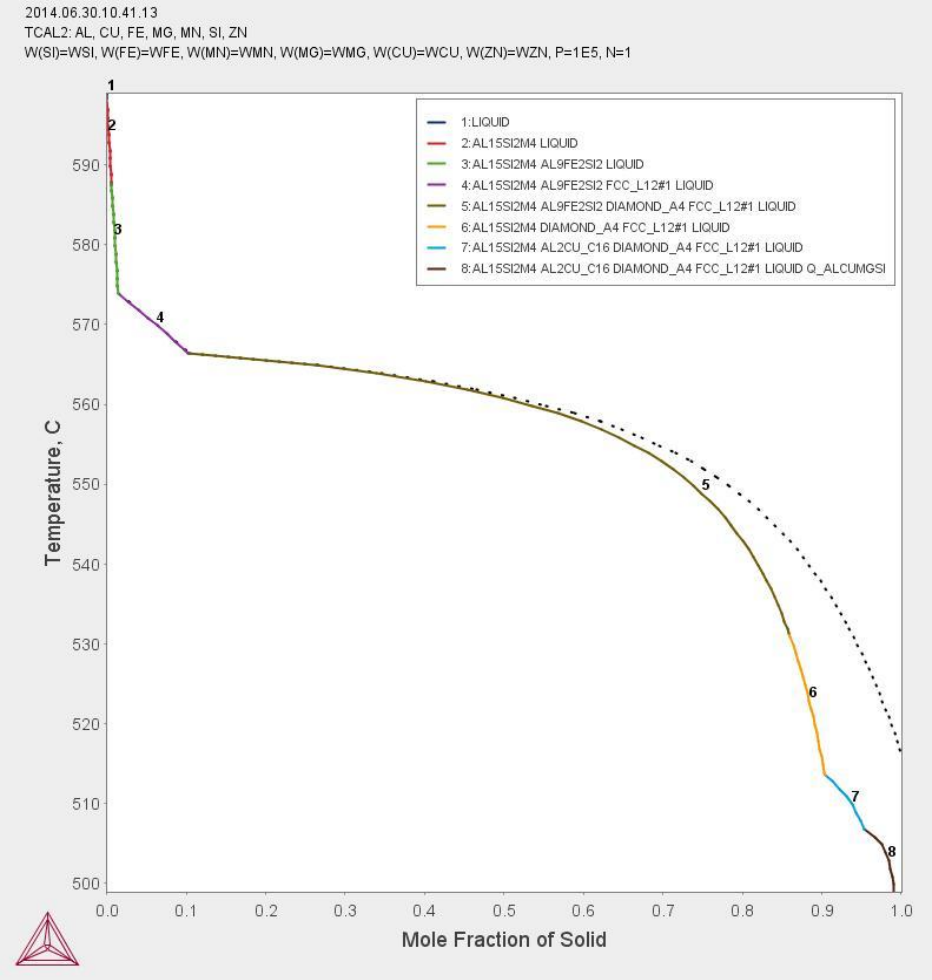


(c)

*Figure 4.11* Al-Si-Cu Scheil solidification curve
(a) Al-Si-Cu-5.0Si; (b) Al-Si-Cu-9.0Si (380); (c) Al-Si-Cu-11.0Si;
(Cu=3.5%, Mn=0.5%, Fe=1%, Mg=0.2%, Zn=0.35%, Al=bal.)

From Figure 4.11, it can be seen that the range of dendrite solidification shrinks and the range of predendrite formation of AlFeSi phase is enlarged. That means that with the addition of Si, more primary α-AlFeSi will form and less. Also the starting temperature of α-AlFeSi and fcc α-Al decreases with increasing Si addition. The starting temperature of fcc α-Al drops more faster than that of the Fe intermetallic phases with increasing Si content. And from Figure 4.11 (a) there is deflection point before the main Si eutectic formation. And Figure 4.11 (b) & (c) contains two deflection before the

formation of fcc α-Al. That is because AlFeSi phase will nucleate before the formation of fcc Al.

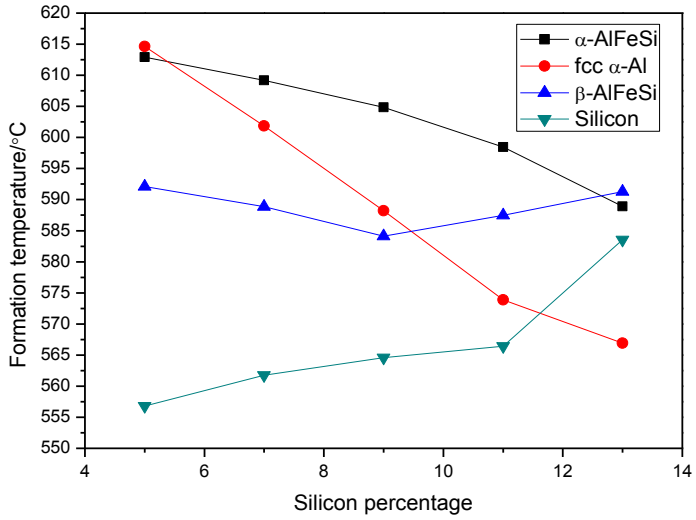


*Figure 4.12* Formation temperatures of different phases under different Si percentage in Al-Si-Cu by Scheil rule
(Cu=3.5%, Mn=0.5%, Fe=1%, Mg=0.2%, Zn=0.35%, Al=bal.)

Figure 4.12 shows the formation temperature as a function of Si. It shows that if the Si content is less than 5 percent, neither primary α-AlFeSi nor β-AlFeSi phase will form. In contrast, if Si content rises to 10 percent, primary β-AlFeSi will form. However, the fluidity of Al-Si casting alloy will be damaged with lower Si content. If Fe and Mn content remain unchanged, Si content should not be over 10 percent to avoid the formation of primary AlFeSi phase, and can be a little lower than 8 percent to reduce the fraction of AlFeSi. For other die-casting alloys, such as A383 and A384, increasing the Si content above 9 percent will increase the fluidity while sacrificing toughness for the formation of primary β-AlFeSi phase. However if fluidity is not harshly desired, low Si content is in favor of the formation of secondary β-AlFeSi in small dimension.

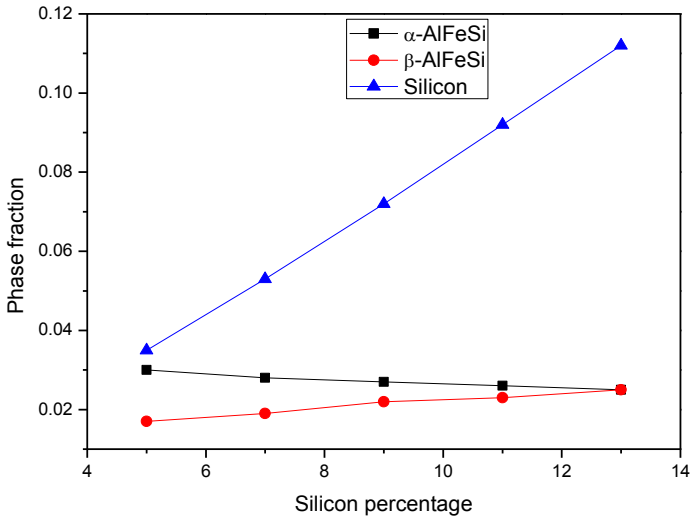


*Figure 4.13* Fraction of different phases under different Si percentage in Al-Si-Cu alloy (Cu=3.5%, Mn=0.5%, Fe=1%, Mg=0.2%, Zn=0.35%, Al=bal.)

Figure 4.13 shows the fraction of different phases under different Si percentage in Al-Si-Cu alloy. With the addition of Silicon element, the fraction of Silicon phase increases linearly, while there is slight decrease of α-AlFeSi and increase of β-AlFeSi. In summary, the addition of the element Si will have the trend to lead to the formation of primary α-AlFeSi and β-AlFeSi phase. Therefore with the condition of guaranteeing the fluidity of Al-Si alloy, the content of Si elements should be limited.

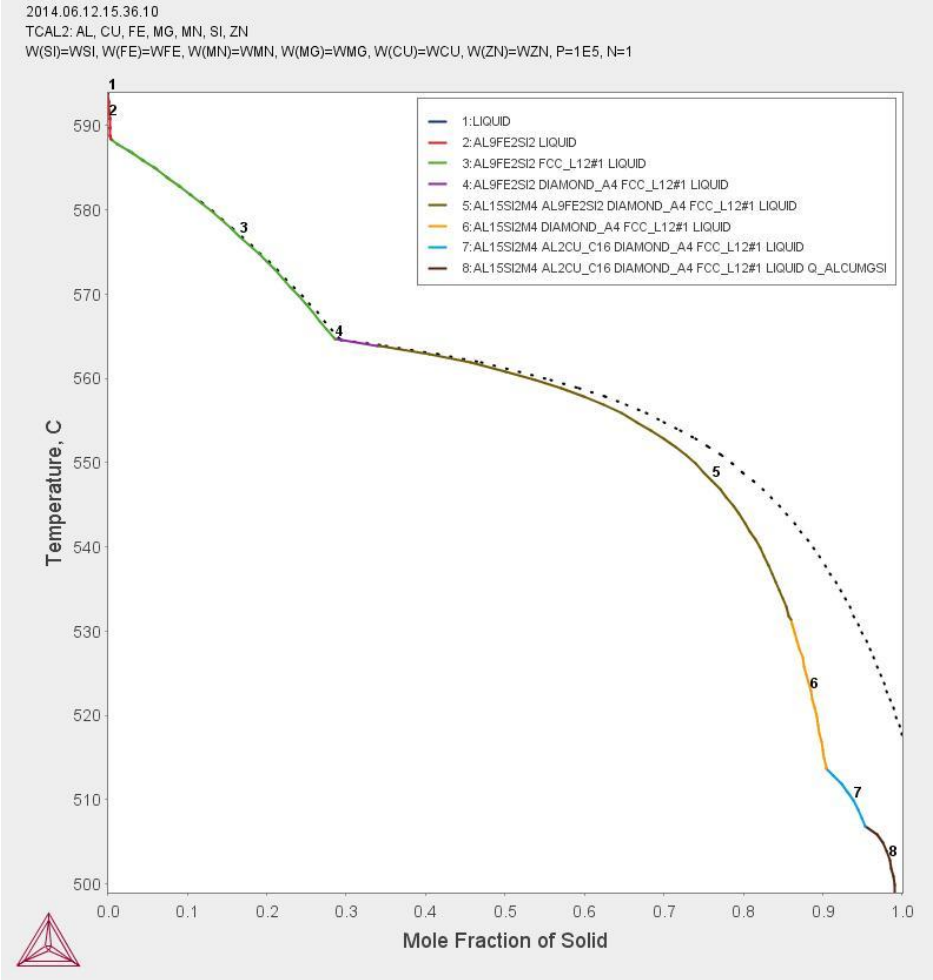
2014.06.12.15.36.10
TCAL2: AL, CU, FE, MG, MN, SI, ZN
W(SI)=WSI, W(FE)=WFE, W(MN)=WMN, W(MG)=WMG, W(CU)=WCU, W(ZN)=WZN, P=1E5, N=1
1:LIQUID
2:AL9FE2SI2 LIQUID
3:AL9FE2SI2 FCC_L12#1 LIQUID
4:AL9FE2SI2 DIAMOND_A4 FCC_L12#1 LIQUID
5:AL15SI2M4 AL9FE2SI2 DIAMOND_A4 FCC_L12#1 LIQUID
6:AL15SI2M4 DIAMOND_A4 FCC_L12#1 LIQUID
7:AL15SI2M4 AL2CU_C16 DIAMOND_A4 FCC_L12#1 LIQUID
8:AL15SI2M4 AL2CU_C16 DIAMOND_A4 FCC_L12#1 LIQUID Q_ALCUMGSI
Temperature, C
590
580
570
560
550
540
530
520
510
500
0.0
0.1
0.2
0.3
0.4
0.5
0.6
0.7
0.8
0.9
1.0
Mole Fraction of Solid
1
2
3
4
5
6
7
8

(a)

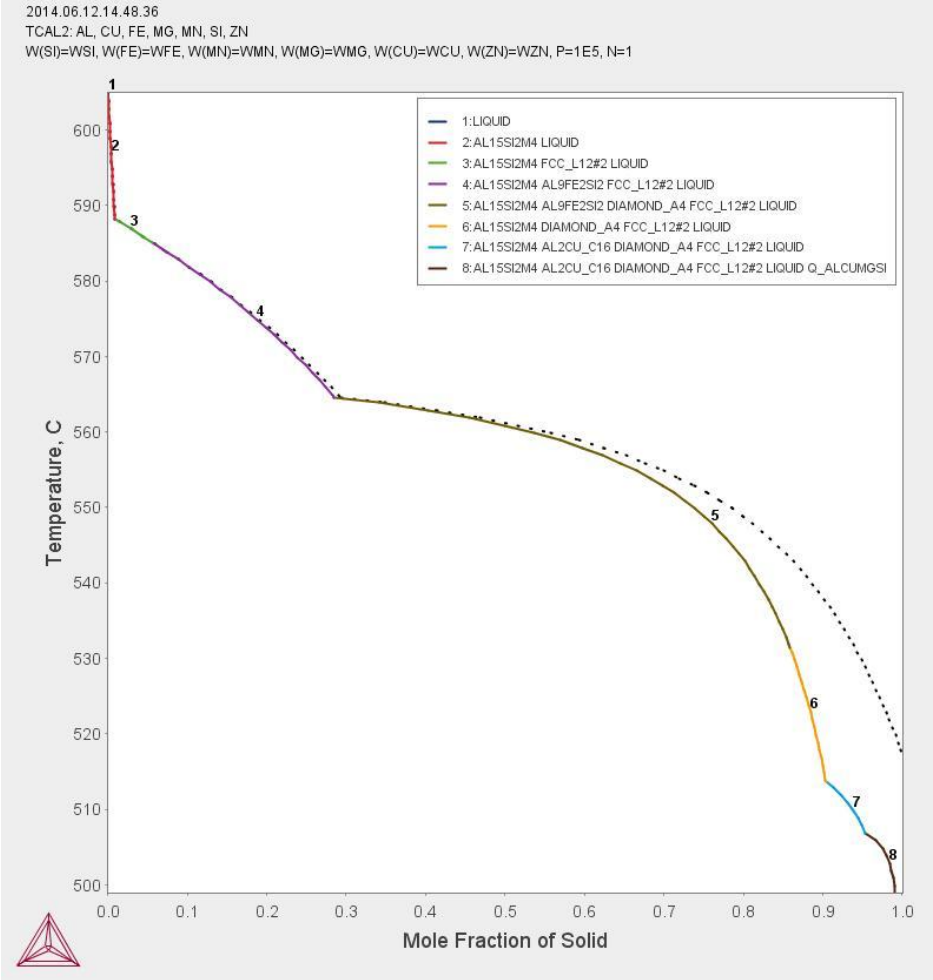
2014.06.12.14.48.36
TCAL2: AL, CU, FE, MG, MN, SI, ZN
W(SI)=WSI, W(FE)=WFE, W(MN)=WMN, W(MG)=WMG, W(CU)=WCU, W(ZN)=WZN, P=1E5, N=1
1:LIQUID
2:AL15SI2M4 LIQUID
3:AL15SI2M4 FCC_L12#2 LIQUID
4:AL15SI2M4 AL9FE2SI2 FCC_L12#2 LIQUID
5:AL15SI2M4 AL9FE2SI2 DIAMOND_A4 FCC_L12#2 LIQUID
6:AL15SI2M4 DIAMOND_A4 FCC_L12#2 LIQUID
7:AL15SI2M4 AL2CU_C16 DIAMOND_A4 FCC_L12#2 LIQUID
8:AL15SI2M4 AL2CU_C16 DIAMOND_A4 FCC_L12#2 LIQUID Q_ALCUMGSI
Temperature, C
Mole Fraction of Solid
600
590
580
570
560
550
540
530
520
510
500
0.0
0.1
0.2
0.3
0.4
0.5
0.6
0.7
0.8
0.9
1.0

(b)

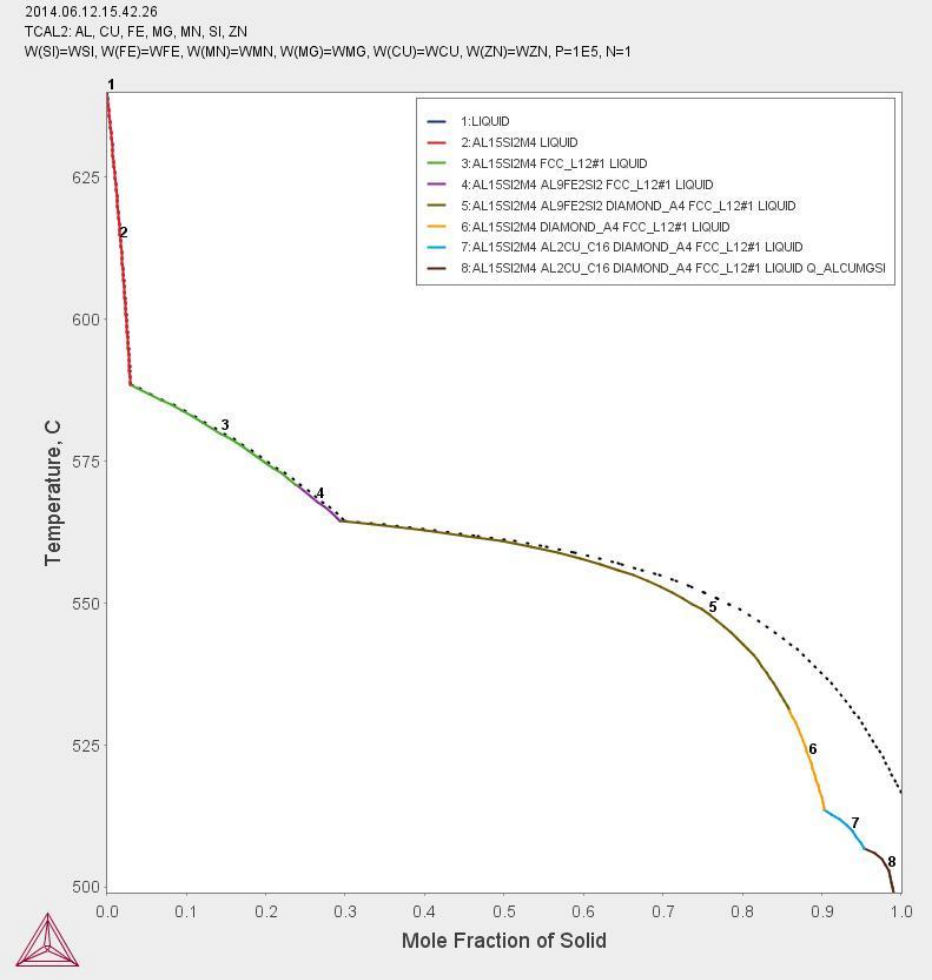


(c)

*Figure 4.14* Al-Si-Cu-xMn Scheil solidification curves
(a) Al-Si-Cu-0.2Mn; (b) Al-Si-Cu-0.4Mn(380); (c) Al-Si-Cu-1.0Mn;
(Si=9%,Cu=3.5% Fe=1%, Mg=0.2%, Zn=0.35%, Al=bal.)

From Figure 4.14, it can be seen that with the addition of Mn element, the shape of the solidification curve has not been changed. This is in agreement with the results of Pan et al (2005). Only the formation temperature and phase fraction of β-AlFeSi and α-AlFeSi is affected. With the addition of Mn, more α-AlFeSi will form and less β-AlFeSi will appear. There are always two reflection points, proving the formation of AlFeSi phase in advance of formation of fcc α-Al.

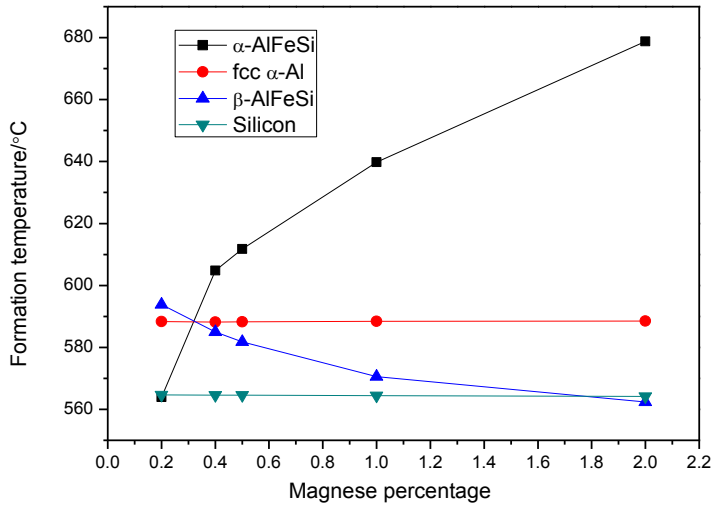


*Figure 4.15* Formation temperatures of different phases under different Mn percentage in Al-Si-Cu by Scheil rule
(Si=9%, Cu=3.5%, Fe=1%, Mg=0.2%, Zn=0.35%, Al=bal.)

Figure 4.15 shows formation temperatures of different phases under different Mn percentage in Al-Si-Cu alloy by using Level rule and Scheil rule. The content of Mn element only have an effect on the formation temperature of α-AlFeSi and of β-AlFeSi, while no effect on the formation temperature of fcc α-Al and of silicon phase. With the increase of Mn element, the formation temperature of α-AlFeSi decreases and the formation temperature of β-AlFeSi increases.

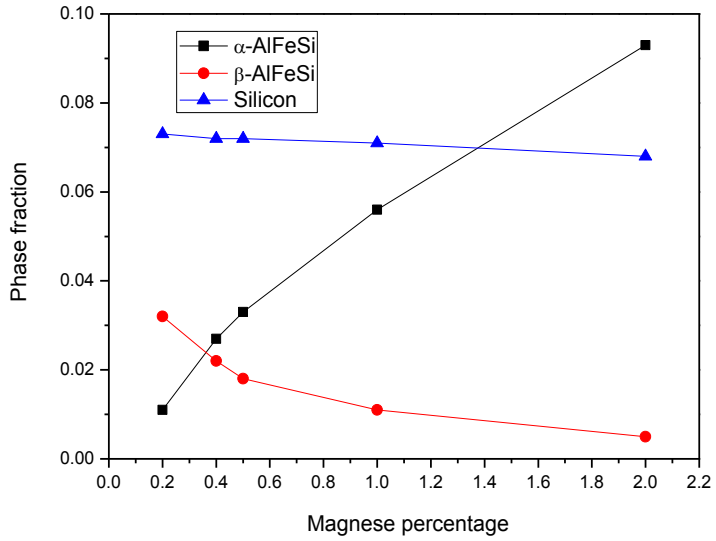


*Figure 4.16* Fraction of different phases under different Mn percentage in Al-Si-Cu alloy (Si=9%, Cu=3.5%, Fe=1%, Mg=0.2%, Zn=0.35%, Al=bal.)

Figure 4.16 shows the calculated fraction of AlFeSi phases under different Mn contents in Al-Si-Cu as Mn content is increased, the amount of α-AlFeSi increases and β-AlFeSi phase decreases. However, the amount of β-AlFeSi drops more quickly as Mn content increases, up to 0.5%. Above 0.5%, the decrease becomes more gradual with further Mn addition. Furthermore, Mn addition can lead to formation of α-AlFeSi sludge. From the plot, it can be seen that primary β-AlFeSi will be eliminated only if Mn content is above 0.38%. Thus the optimum Mn content in A380 diecasting alloy application should lie between 0.38% and 0.5%.

These simulations results agree with the experimental results of Lu and Dahle (2006) who found that β-AlFeSi intermetallic phase can be observed everywhere in the absence of Mn. With the addition of 0.3% Mn, both the amount and the size of the β-AlFeSi decrease considerably. If the content of Mn goes up to 1%, the β-AlFeSi become too small to be observed, and α-AlFeSi phase with different morphologies, including Chinese script, star-like, and polygon, sludge can be formed.

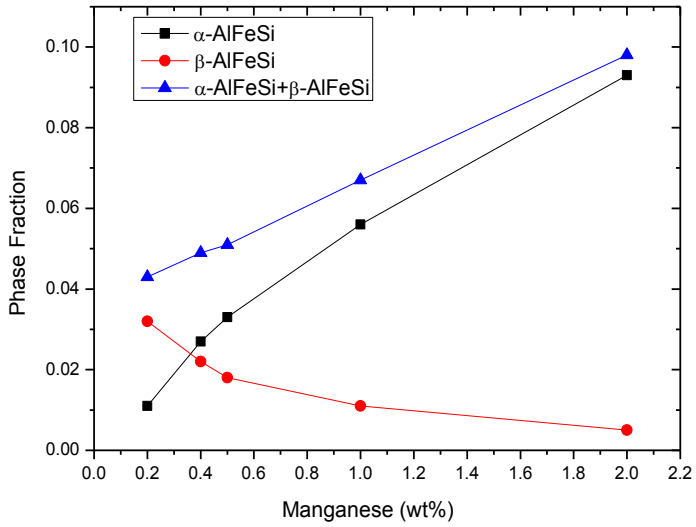


*Figure 4.17* Fraction of AlFeSi phases under different Mn content in Al-Si-Cu alloy (Si=9%, Cu=3.5%, Fe=1%, Mg=0.2%, Zn=0.35%, Al=bal.)

Figure 4.17 shows that the total amount of AlFeSi phase, including both α-AlFeSi and β-AlFeSi, also increases with increasing Mn content. Because the solubility of Mn in Al is only 0.02%, Mn must react and form Al(Mn, Fe)Si phase in Al-Si alloy, leading to the increase of amount of AlFeSi phase (Lu, & Dahle, 2005).

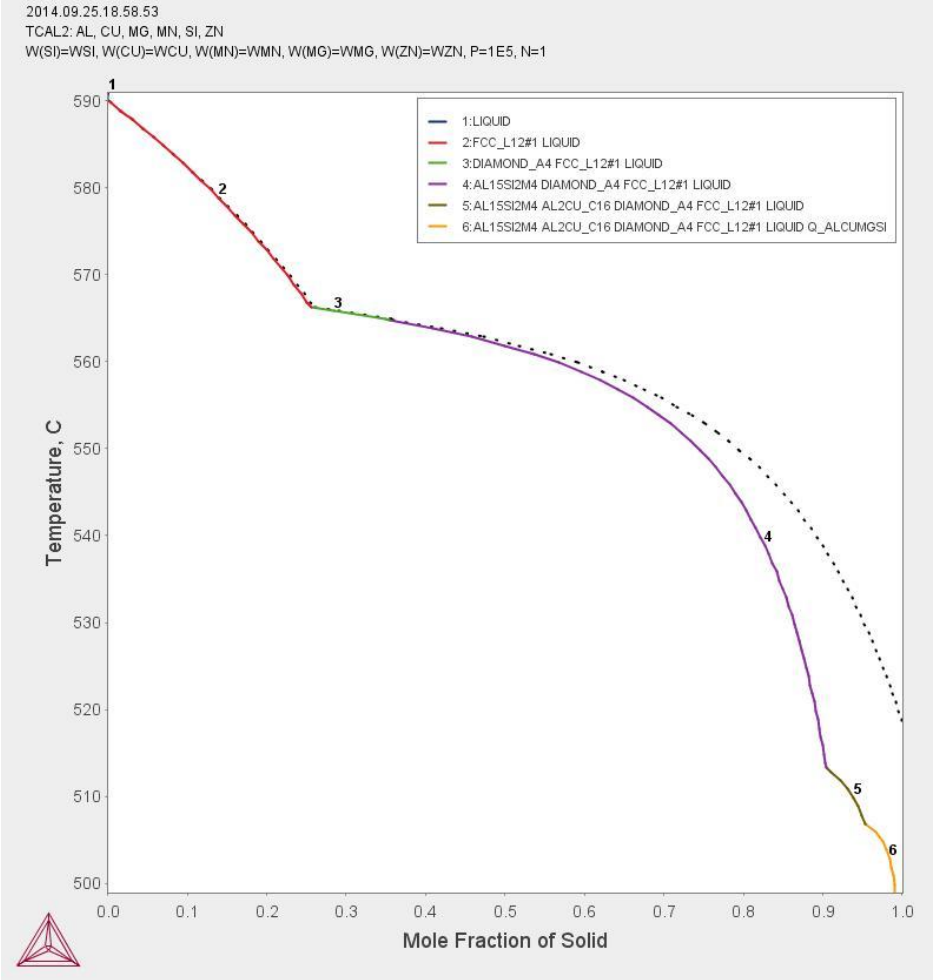
2014.09.25.18.58.53
TCAL2: AL, CU, MG, MN, SI, ZN
W(SI)=WSI, W(CU)=WCU, W(MN)=WMN, W(MG)=WMG, W(ZN)=WZN, P=1E5, N=1
1:LIQUID
2:FCC_L12#1 LIQUID
3:DIAMOND_A4 FCC_L12#1 LIQUID
4:AL15SI2M4 DIAMOND_A4 FCC_L12#1 LIQUID
5:AL15SI2M4 AL2CU_C16 DIAMOND_A4 FCC_L12#1 LIQUID
6:AL15SI2M4 AL2CU_C16 DIAMOND_A4 FCC_L12#1 LIQUID Q_ALCUMGSI
Temperature, C
590
580
570
560
550
540
530
520
510
500
0.0
0.1
0.2
0.3
0.4
0.5
0.6
0.7
0.8
0.9
1.0
Mole Fraction of Solid
1
2
3
4
5
6

(a)

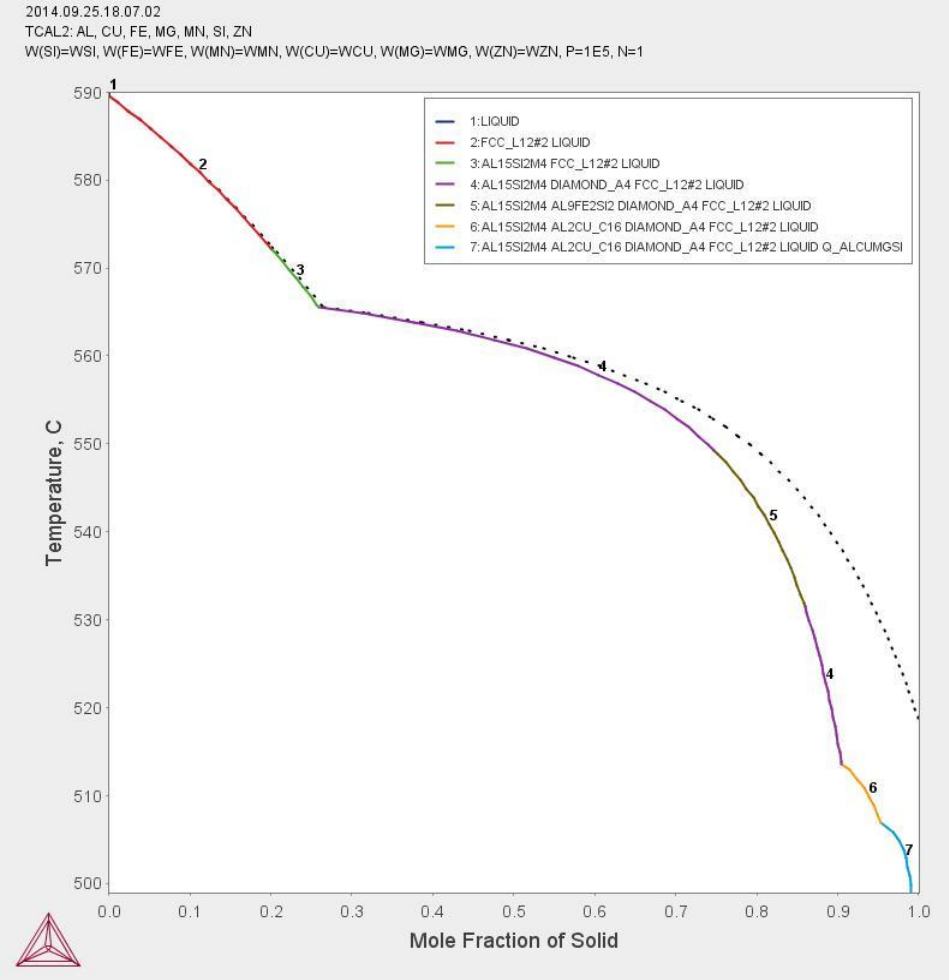
2014.09.25.18.07.02
TCAL2: AL, CU, FE, MG, MN, SI, ZN
W(SI)=WSI, W(FE)=WFE, W(MN)=WMN, W(CU)=WCU, W(MG)=WMG, W(ZN)=WZN, P=1E5, N=1
1:LIQUID
2:FCC_L12#2 LIQUID
3:AL15SI2M4 FCC_L12#2 LIQUID
4:AL15SI2M4 DIAMOND_A4 FCC_L12#2 LIQUID
5:AL15SI2M4 AL9FE2SI2 DIAMOND_A4 FCC_L12#2 LIQUID
6:AL15SI2M4 AL2CU_C16 DIAMOND_A4 FCC_L12#2 LIQUID
7:AL15SI2M4 AL2CU_C16 DIAMOND_A4 FCC_L12#2 LIQUID Q_ALCUMGSI
Temperature, C
590
580
570
560
550
540
530
520
510
500
0.0
0.1
0.2
0.3
0.4
0.5
0.6
0.7
0.8
0.9
1.0
Mole Fraction of Solid
1
2
3
4
5
4
6
7

(b)

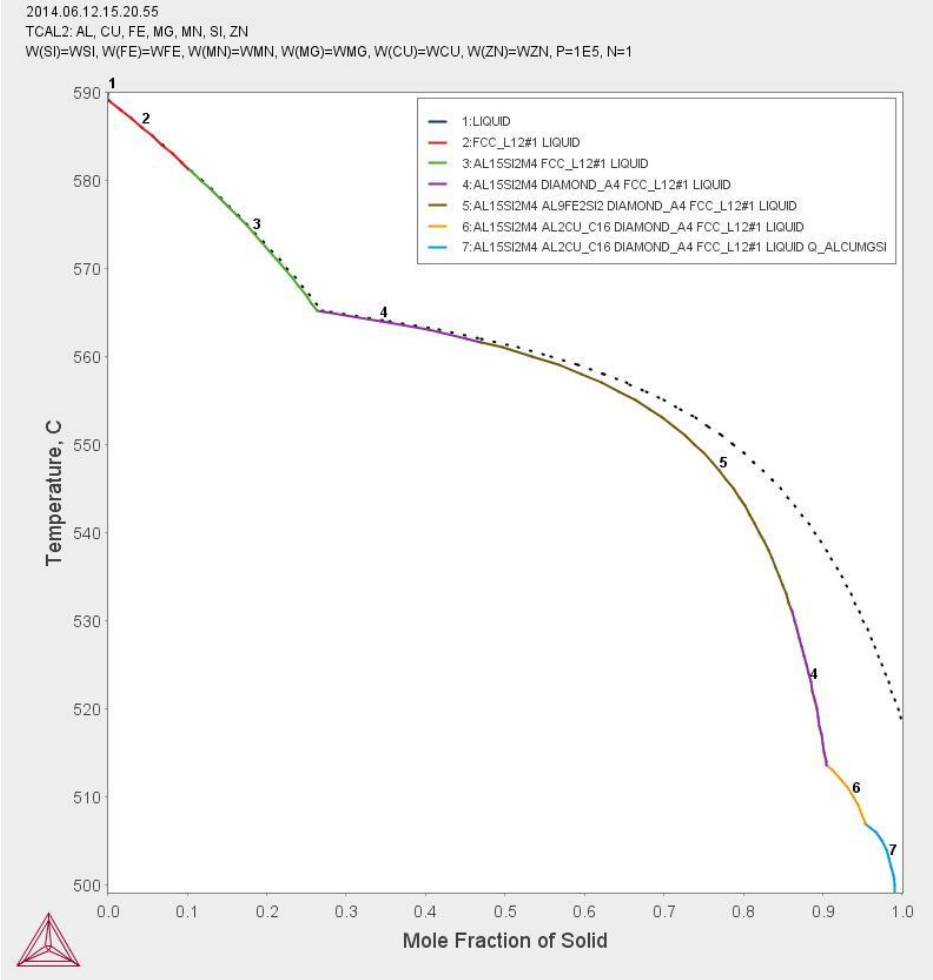
2014.06.12.15.20.55
TCAL2: AL, CU, FE, MG, MN, SI, ZN
W(SI)=WSI, W(FE)=WFE, W(MN)=WMN, W(MG)=WMG, W(CU)=WCU, W(ZN)=WZN, P=1E5, N=1
1:LIQUID
2:FCC_L12#1 LIQUID
3:AL15SI2M4 FCC_L12#1 LIQUID
4:AL15SI2M4 DIAMOND_A4 FCC_L12#1 LIQUID
5:AL15SI2M4 AL9FE2SI2 DIAMOND_A4 FCC_L12#1 LIQUID
6:AL15SI2M4 AL2CU_C16 DIAMOND_A4 FCC_L12#1 LIQUID
7:AL15SI2M4 AL2CU_C16 DIAMOND_A4 FCC_L12#1 LIQUID Q_ALCUMGSI
Temperature, C
590
580
570
560
550
540
530
520
510
500
0.0
0.1
0.2
0.3
0.4
0.5
0.6
0.7
0.8
0.9
1.0
Mole Fraction of Solid
1
2
3
4
5
4
6
7

(c)

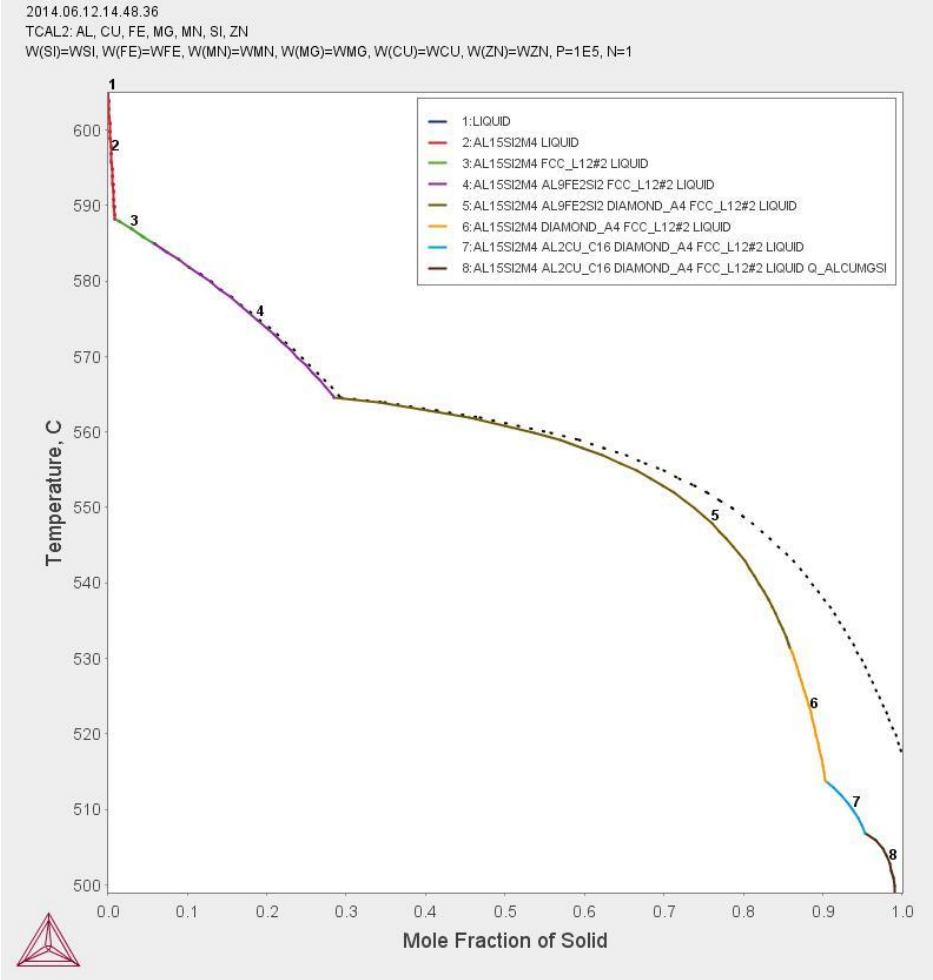
2014.06.12.14.48.36
TCAL2: AL, CU, FE, MG, MN, SI, ZN
W(SI)=WSI, W(FE)=WFE, W(MN)=WMN, W(MG)=WMG, W(CU)=WCU, W(ZN)=WZN, P=1E5, N=1
1:LIQUID
2:AL15SI2M4 LIQUID
3:AL15SI2M4 FCC_L12#2 LIQUID
4:AL15SI2M4 AL9FE2SI2 FCC_L12#2 LIQUID
5:AL15SI2M4 AL9FE2SI2 DIAMOND_A4 FCC_L12#2 LIQUID
6:AL15SI2M4 DIAMOND_A4 FCC_L12#2 LIQUID
7:AL15SI2M4 AL2CU_C16 DIAMOND_A4 FCC_L12#2 LIQUID
8:AL15SI2M4 AL2CU_C16 DIAMOND_A4 FCC_L12#2 LIQUID Q_ALCUMGSI
Temperature, C
600
590
580
570
560
550
540
530
520
510
500
0.0
0.1
0.2
0.3
0.4
0.5
0.6
0.7
0.8
0.9
1.0
Mole Fraction of Solid
1
2
3
4
5
6
7
8

(d)

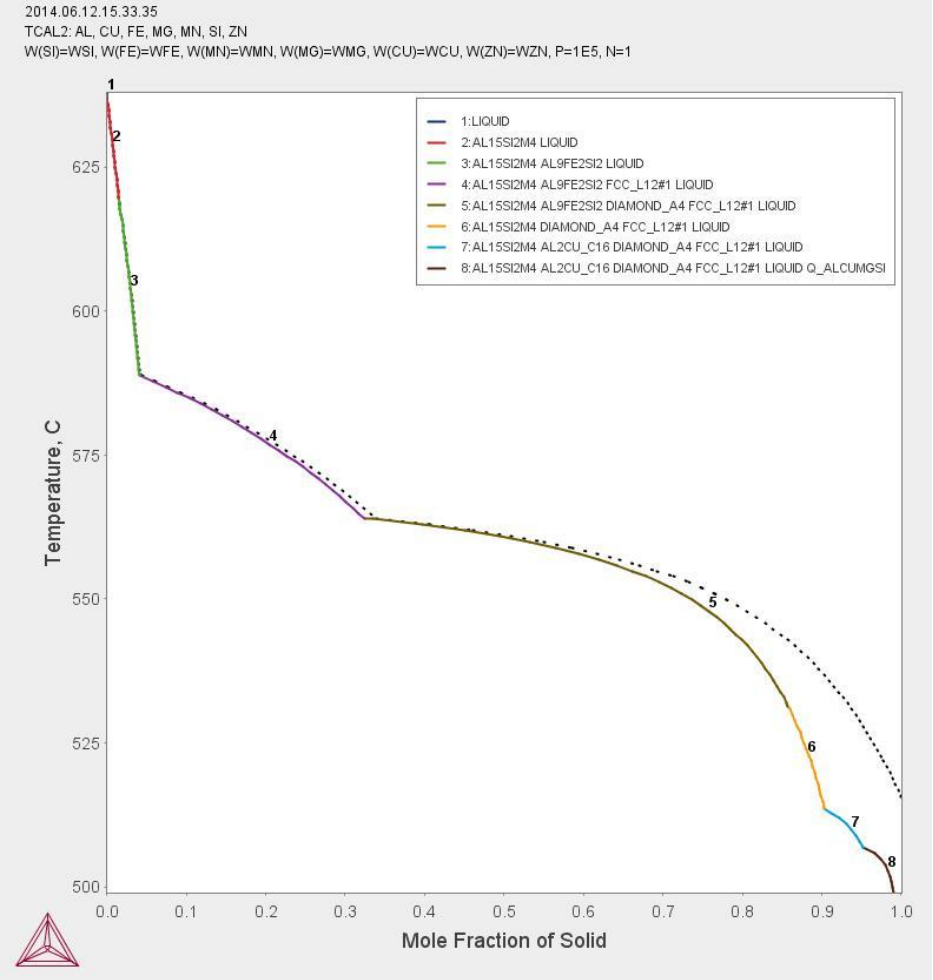


(e)

*Figure 4.18* Al-Si-Cu-xFe Scheil solidification curves
(a) Al-Si-Cu-0Fe; (b) Al-Si-Cu-0.2Fe; (c) Al-Si-Cu-0.4Fe; (d) Al-Si-Cu-1.0Fe(380) ;(e) Al-Si-Cu-2.0Fe.
(Si=9%, Cu=3.5%, Mn=0.5%, Mg=0.2%, Zn=0.35%, Al=bal.)

The Al-Si-Cu-xFe scheil solidification path has similar trend like Al-Si-Cu-xMn. The formation of α-AlFeSi and β-AlFeSi will bring forward with Fe addition will the increase of both formation temperature and fraction. The results are shown in Figure 4.18

With Fe addition, although the fraction of both α-AlFeSi and β-AlFeSi increases with the addition of Fe, however, only ternary β-AlFeSi can form even Fe contents goes up to 0.4%. On the other hand, the binary α-AlFeSi is only 0.5% even Fe content is up to

0.4%. Therefore we can conclude it Fe content is lower than 0.4%, no detrimental AlFeSi phase can form. This can be proved by the change of the number of the fraction point from one to two.

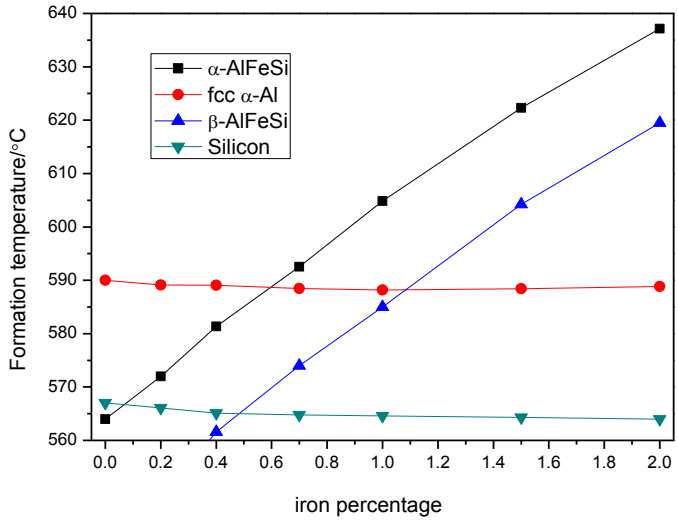


(a)

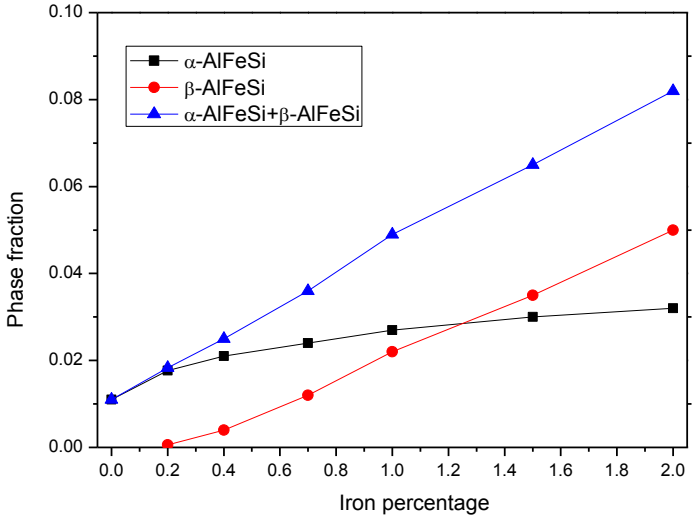


(b)

*Figure 4.19* Formation temperatures and fraction of different phases under different Fe percentage in Al-Si-Cu alloy by Scheil rule
(a) Formation temperature; (b) Fraction
(Si=9%, Cu=3.5%, Mn=0.5%, Mg=0.2%, Zn=0.35%, Al=bal.)

Similar to Mn addition, Fe content is related with the formation temperature of α-AlFeSi and β-AlFeSi. With the increase of Fe content, the fraction of both β-AlFeSi and α-AlFeSi increases. 0.6% and 1.3% are two critical points above which primary α-AlFeSi and β-AlFeSi will form respectively. The nominal Fe content in A380 is below 1.3%, which will guarantee no primary β-AlFeSi formation. It is also noticed that the addition of Fe will severely increase the fraction of β-AlFeSi while slightly facilitate the formation of α-AlFeSi. Thus the content of Fe in A380 should be strictly controlled.

## 4.2 Experimental Results

### 4.2.1 The Morphology and Phase Fraction of Original A380

The microstructure taken from original sample from A380 ingot is shown in Figure 4.20. The following phase information can be observed from the Figure 4.20: 1) fcc α-Al (matrix shown as a white color), 2) α-AlFeSi (Chinese script, polygon and other irregular shape), 3) β-AlFeSi (with needle or curve shape), 4) silicon phase (grey areas with polygon and script shape), 5) $Al_2Cu$ (small white bulk shape) and 6) final precipitate $Al_5Mg_8Si_6Cu_2$ phase (the little dark ones between $Al_2Cu$ phase). All the formation of these six phases is in agreement with the thermodynamic simulation results.

There are three types of α-AlFeSi in A380. The first has polygon shape. It is a primary α-AlFeSi phase which forms in advance of fcc α-Al dendrites. During the formation of primary α-AlFeSi, it is the first precipitated phase so α-AlFeSi phase grows freely to form bulk and large polygon shape. It is often referred as sludge. The secondary α-AlFeSi phase is formed during or after the formation of fcc α-Al dendrites. The size and growth direction here are restricted by α-Al dendrites so the intermetallic phase has

to nucleate and grow in the interdendrite area. This yields a Chinese script pattern for secondary α-AlFeSi. The third one is the binary eutectic α-AlFeSi phase which is formed in the eutectic stage with Al-Si eutectic phase. This type α-AlFeSi has an even smaller size and share the boundary with eutectic Si phase. There are reports of post-eutectic α-AlFeSi from the peritectic reaction of liquid and β-AlFeSi, which was not observed from this sample.

As to β-AlFeSi, no primary β-AlFeSi was found, that is in agreement with the thermo-calc simulation results. However, most of β-AlFeSi shares the boundary with eutectic silicon and $Al_2Cu$ phase. This phenomenon can be explained in two ways. One is both β-AlFeSi and silicon phase are formed during the eutectic stage and they are next to each other. The second explanation is that β-AlFeSi can be formed prior to the eutectic silicon and be the nucleation site for silicon and $Al_2Cu$.

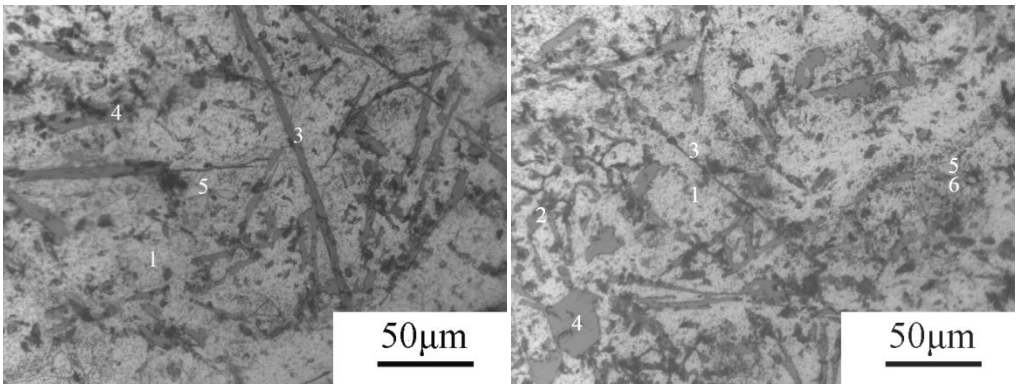


(a) (b)

*Figure 4.20* Optical images of original A380 ingot
(Note: The numbers represent the phase of 1)fcc-α-Al; 2)α-AlFeSi; 3)β-AlFeSi; 4)silicon; 5)$Al_2Cu$; 6) $Al_5Mg_8Si_6Cu_2$

In general, the original samples have large size α-AlFeSi and β-AlFeSi phases. Table 4.4 shows related parameters of α-AlFeSi and β-AlFeSi phases. The average length

of the β-AlFeSi phase is above 100 μm, a condition that typically leads to high stress concentration. Figure 4.20 also shows the presence of some α-AlFeSi. Most of that is polygonal sludge. From the thermodynamics calculation and the theory of sludge factor (the percentage of Fe + 2 ×percentage of Mn), primary α-AlFeSi will form in A380 alloy.

Table 4.4 *Parameters of α-AlFeSi and β-AlFeSi morphology in original A380 alloy*

| **β-length (μm)** | **β-width (μm)** | **Aspect ratio** | **β-fraction** | **α-fraction** |
|---|---|---|---|---|
| 267.2 | 8.66 | 30.854 | 1.31 | 2.24 |

### 4.2.2 The Effect of Cooling Rates on the Morphology and Phase Fraction of A380

Figure 4.21 shows the optical image of A380 alloy sample at different cooling rates. Figure 4.21 (a) shows the sample using a furnace at a rate of approximately 0.05 ℃/s. Figure 4.21 (b) shows the sample cast in a steel mold, with a cooling rate about 5 ℃/s. Figure 4.21 (c) shows the sample cast in a cooper mold and immersed in the water, with a cooling rates about 10 ℃/s. Figure 4.21 (d) shows the sample quenched in the water directly, with a cooling rate of roughly 20-30 ℃/s. Figure 4.21 (e) shows the sample cast in the tip of a V shape copper mold with cooling rates in the range of 50-100 ° C/s.The slow cooling (<0.1 ℃/s) rates can show the large size of AlFeSi phase, which simulates equilibrium cooling condition. The medium cooling rates(1-10 ℃/s) are used for study of the morphology and fraction of AlFeSi phase founded during permanent mold and sand casting conditions while the high cooling rates(>10 ℃/s) are typically used for simulating die-casting conditons.

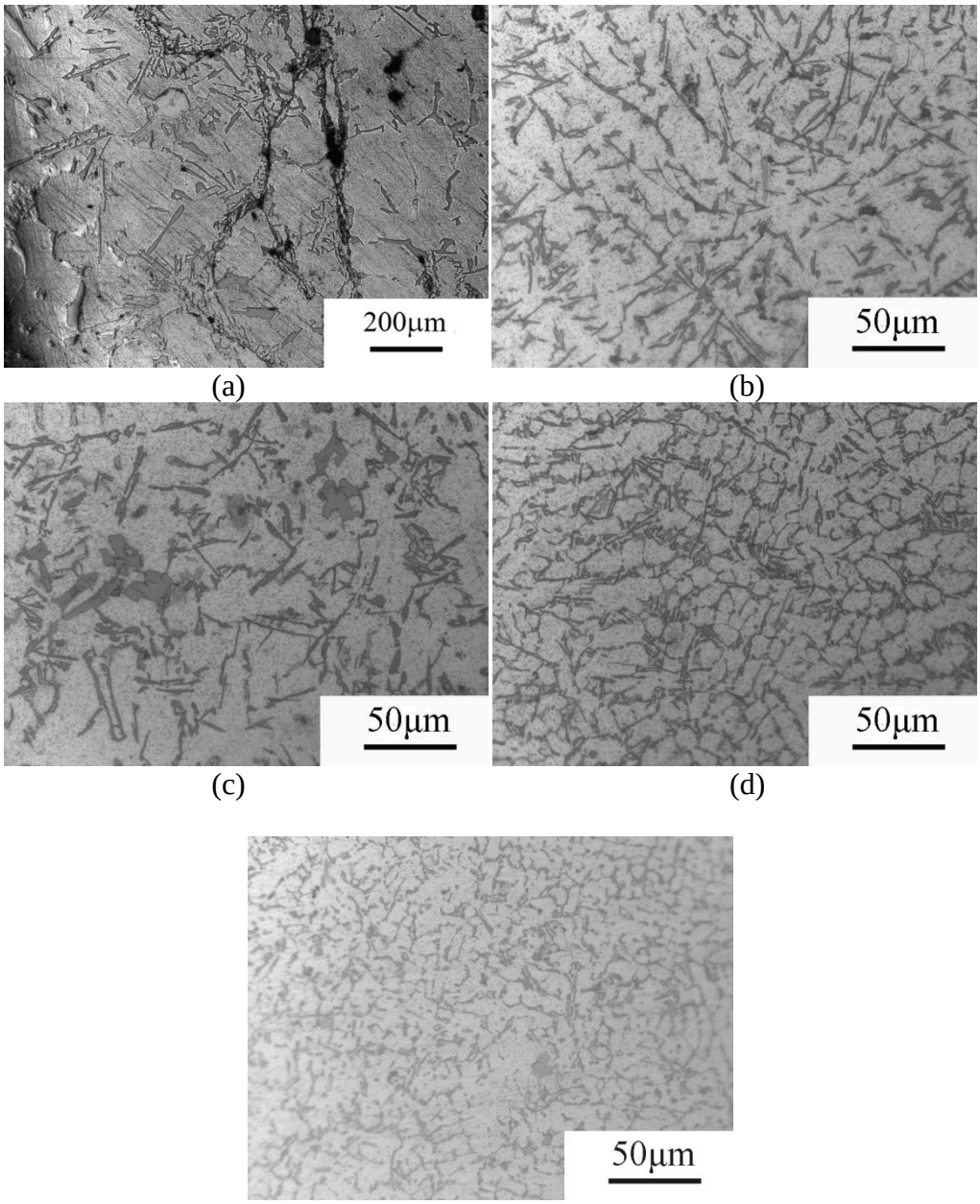


*Figure 4.21* Optical image of different A380 alloy with different cooling rates (a) 0.05 ℃/s; (b) 5 ℃/s; (c) 10 ℃/s; (d) 20-30 ℃/s; (e) 50-100 ℃/s.

From the five samples in Figure 4.21, we can see that the cooling rates not only have great impact on the morphology of AlFeSi phase, particularly in size, but also affect the fraction of α-AlFeSi phase. In Figure 4.21 a) large size of primary α-AlFeSi and secondary β-AlFeSi is predominating in A380. Figure 4.21 b) shows the predominating

β-AlFeSi with secondary α-AlFeSi phase. But if the cooling rates increase, the size and fraction of β-AlFeSi decreases, and α-AlFeSi are with the morphology of both Chinese script and polygon, as can be seen in Figure 4.21 c). In Figure 4.21 d), the Chinese script α-AlFeSi phase predominates and the size of β-AlFeSi phase is too small to be distinguished. For the highest cooling rate in Figure 4.21 e), no β-AlFeSi phase can be found, and the small size α-AlFeSi phase with both Chinese script and polygon shape is the only AlFeSi phase which can be found. The size and fraction of α-AlFeSi and β-AlFeSi phases are summarized in Table 4.5.

Table 4.5 *Parameters of α-AlFeSi and β-AlFeSi morphology in A380 alloy with different cooling rates*

| Cooling Rate (℃/s) | β-length (μm) | β-width (μm) | Aspect ratio | β-fraction(%) | α-fraction(%) |
|---|---|---|---|---|---|
| 0.05 | 213.21 | 7.14 | 29.86 | 1.31 | 2.20 |
| 5 | 30.12 | 1.72 | 17.51 | 0.70 | 2.71 |
| 10 | 20.13 | 1.58 | 12.74 | 0.51 | 2.92 |
| 20-30 | 10.07 | 1.13 | 8.91 | 0.08 | 3.42 |
| 50-100 | - | - | - | - | 3.45 |

### 4.2.3 The Effect of Mn Addition on the Morphology and Phase Fraction of A380

Figure 4.22 to Figure 4.24 show the microstructure obtained using different cooling rates and Mn addition. At low cooling rates (0.01 ℃/s), with Mn addition, the fraction of α-phase increases and that of β-phase decreases. This is in agreement with results from the thermodynamics simulation in Section 4.1. If the Mn content is 0.5%, increasing cooling rates results in replacement of the needle-like β-phase by the Chinese script α-phase ($Al_{15}(Fe,Mn)_8Si_2$). It is also seen that the fraction and the size of β-needles phase decreases while the portion of α-AlFeSi phase increases, thus leading to the increase of

the fraction of the total AlFeSi phase. However, when the Mn content goes up to 1.0%, a different situation is encountered, namely, that the increasing cooling rates favor the formation of β-needles phase. These seemingly apparent the contradictions are also reported by Gowri and Samuel (Gowri & Samuel, 1994).

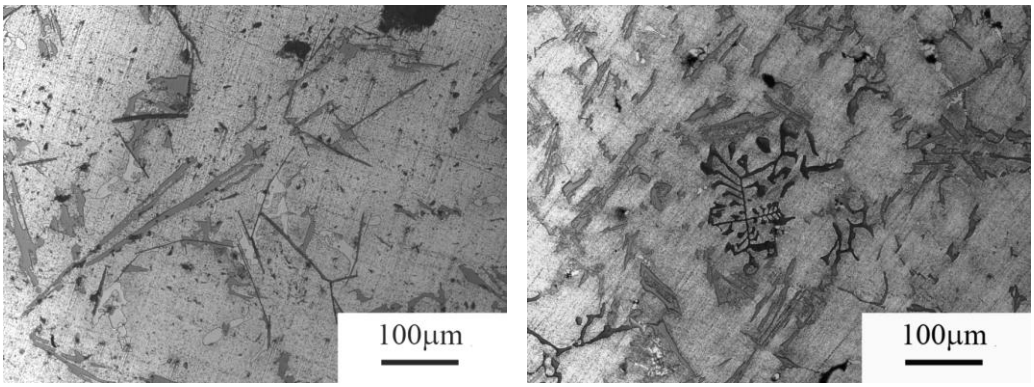


(a) (b)

*Figure 4.22* Microstructure of 380 alloy with different Mn content at 0.05 ℃/s (a) 0.5; (b)1

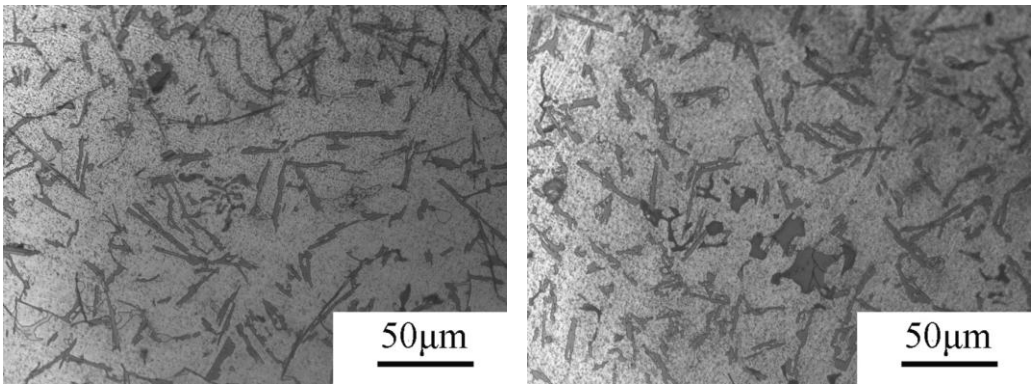


(a) (b)

*Figure 4.23* Microstructure of 380 alloy with different Mn content at 1-2 ℃/s (a) 0.5; (b)1

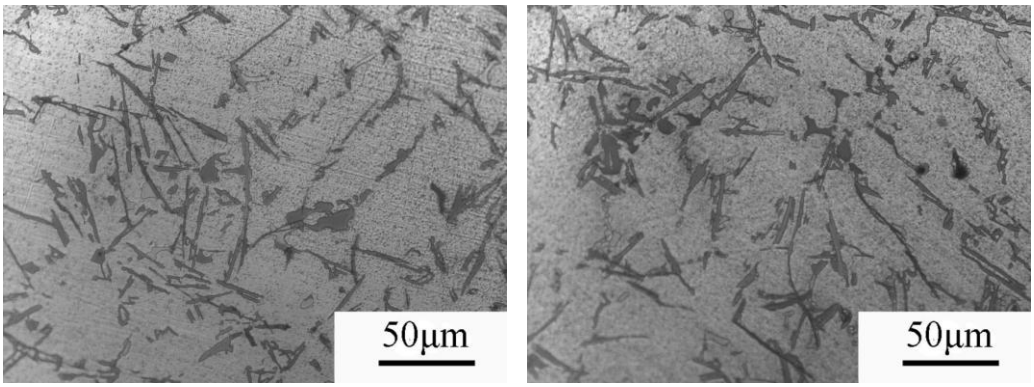


(a) (b)

*Figure 4.24* Microstructure of 380 alloy with different Mn content at 5 ℃/s (a) 0.5; (b)1

Samuel explains this situation as follows. According to the AlFeSi phase diagram, the β phase is a stable phase under equilibrium cooling conditions. However, when castings are manufactured using very high cooling rates, the compound crystallizes in the α-phase (Chinese script morphology) in metastable form. According to the Al-Fe-Mn-Si phase diagram, α phase is a stable phase under equilibrium cooling conditions (very low cooling rates). However in the presence of manganese, the iron compound crystallizes mainly in α phase (Chinese script morphology and polygon and star morphology) at low cooling rates and in both α and β phases (Chinese script morphology and needlelike morphology) at high cooling rates. This behavior is the reversed of that observed in the absence of manganese. From my experimental results, if Mn content is high (above 1.0%) , formation of β phase is favored in high cooling rates and is suppressed in low cooling rates, while with low Mn content, there is no this trend.

Table 4.6 *Parameters of α-AlFeSi and β-AlFeSi morphology in A380-0.5Mn alloy with different cooling rates*

| Cooling Rate( ℃/s) | β-length (μm) | β-width (μm) | Aspect ratio | β-fraction(%) | α-fraction(%) |
|---|---|---|---|---|---|
| 0.05 | 196.16 | 5.71 | 34.38 | 1.15 | 2.32 |
| 1 | 40.29 | 1.52 | 26.51 | 0.87 | 2.61 |
| 5 | 23.56 | 1.31 | 17.98 | 0.65 | 2.73 |

Table 4.7 *Parameters of α-AlFeSi and β-AlFeSi morphology in A380-1Mn alloy with different cooling rates*

| Cooling Rate( ℃/s) | β-length (μm) | β-width (μm) | Aspect ratio | β-fraction(%) | α-fraction(%) |
|---|---|---|---|---|---|
| 0.05 | - | - | - | - | 3.52 |
| 1 | - | - | - | - | 3.31 |
| 5 | 22.37 | 1.23 | 18.18 | 0.34 | 2.79 |

### 4.2.4 The Effect of Fe Addition on the Morphology and Phase Fraction of A380

From the literature, it can be seen that if the iron content is lower than 1%, the alloy may suffer die soldering. The best Fe content is within 1-1.3 wt %. However, if the Fe content still goes up, the primary AlFeSi phase will deteriorate the mechanical propertire. Fluidity of the alloys are also seriously impaired. (Samuel & Samuel, 1995).

Figure 4.25-4.27 shows the optical image of A380-1.5Fe and A380-2Fe. Here it can be seen that once the Fe: Mn ratio reaches 3:1 (A380-1.5Fe) to 4:1 (A380-2Fe), the β-AlFeSi phase predominates even with the fast cooling rates, which is shown in Figure 4.26, and 4.27. With a slow cooling rate, the size and quantity of β-AlFeSi phase increase compared to the original A380 alloy (Figure 4.22 a). Table 4.8 & 4.9 show the parameters of Al-Fe-Si phase. The size and fraction of β-AlFeSi phase increases tremendously with each cooling rate. The fraction of β-AlFeSi phase is above 2%. The length and width of β-AlFeSi phase increases at least 40%. Not only the length and width

of β-AlFeSi phase increases but also the shape changes to the branch morphology. It is mainly due to the formation of primary β-AlFeSi phase, which is not restricted by the dendritic α-Al phase. However, the high cooling rate surpresses the formation of α-AlFeSi phase.

Our results are similar to trends shown by Samuel et al. (1995). That is with the addition of Fe, more β phase forms and becomes the predominating phase. However, an abnormal trend is evident when with the slow cooling rates (0.05 ℃/s), where more α-AlFeSi phase forms compared to the higher cooling rates. This phenomeon is related to the formation sequence of the different phases.

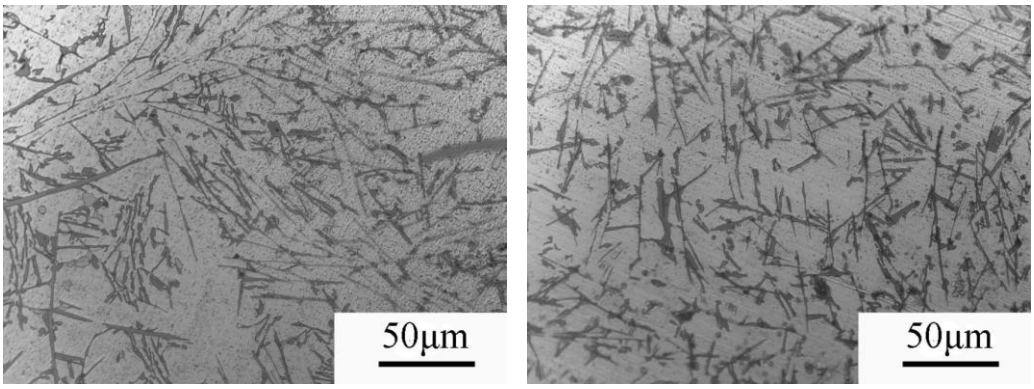


(a) (b)

*Figure 4.25* Microstructure of 380 alloy with different Fe addition at 5 °C/s (a) 1.5; (b)2

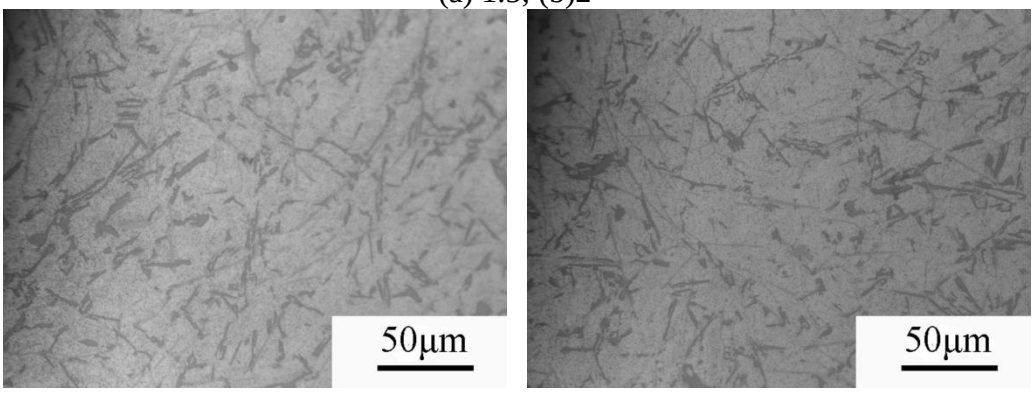


(a) (b)

*Figure 4.26* Microstructure of 380 alloy with different Fe addition at 1-2 ℃ /s (a) 1.5; (b)2

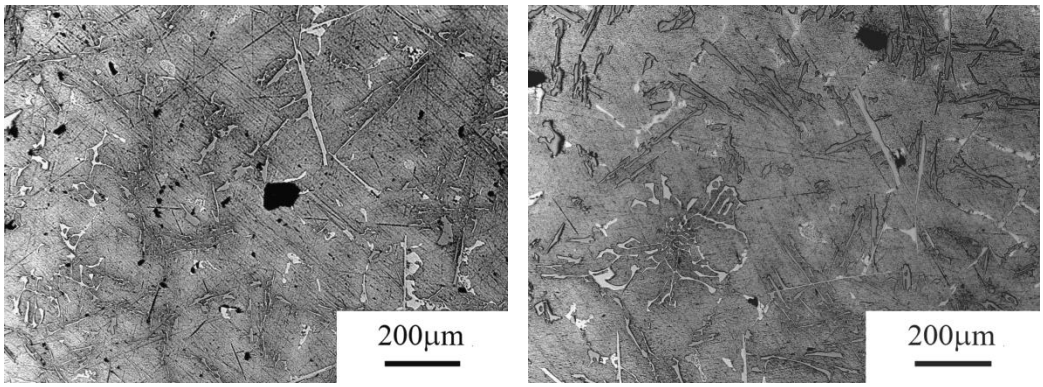


(a) (b)

*Figure 4.27* Microstructure of 380 alloy with different Fe addition at 0.05 ℃/s (a) 1.5; (b)2

Table 4.8 *Parameters of α-AlFeSi and β-AlFeSi morphology in A380-1.5Fe alloy with different cooling rates*

| Cooling Rate( ℃/s) | β-length (μm) | β-width (μm) | Aspect ratio | β-fraction(%) | α-fraction(%) |
|---|---|---|---|---|---|
| 0.05 | 396.16 | 9.17 | 43.21 | 2.3 | 2.21 |
| 1 | 50.17 | 2.35 | 21.35 | 2.53 | 2.02 |
| 5 | 40.81 | 2.12 | 19.25 | 2.7 | 0.53 |

Table 4.9 *Parameters of α-AlFeSi and β-AlFeSi morphology in A380-2Fe alloy with different cooling rates*

| Cooling Rate( ℃/s) | β-length (μm) | β-width (μm) | Aspect ratio | β-fraction(%) | α-fraction(%) |
|---|---|---|---|---|---|
| 0.05 | 410.70 | 10.32 | 39.79 | 2.6 | 2.13 |
| 1 | 55.33 | 2.57 | 21.52 | 2.8 | 1.85 |
| 5 | 45.93 | 2.15 | 21.36 | 3.5 | 0.15 |

### 4.2.5 The Effect of Mg Addition on the Morphology and Phase Fraction of A380

From the phase diagram and calculation results, it appears that Mg has no effect on AlFeSi phase. However, the experimental results seem to be controversial. With low cooling rates, there is neither obvious morphology nor quantity change of α-AlFeSi phase and β-AlFeSi phases (Fig. 4. 30). However, with higher cooling rates, most of plate and

needle phase change into the Chinese Script phase in both Figure 4.28 and 4.29. And also there is only a small fraction polygon and sludge formed.

Table 4.10 and 4.11 shows the parameters of α-AlFeSi and β-AlFeSi morphology. For the low cooling rates, the parameters show no obvious difference with original A380 sample. However, the fraction of β-AlFeSi decreased more than 2% for samples with 1 or 5 ℃/s cooling rates. Also, compared to the A380-0.3Mg sample, the A380-0.5Mg sample has an even smaller fraction of β-AlFeSi.

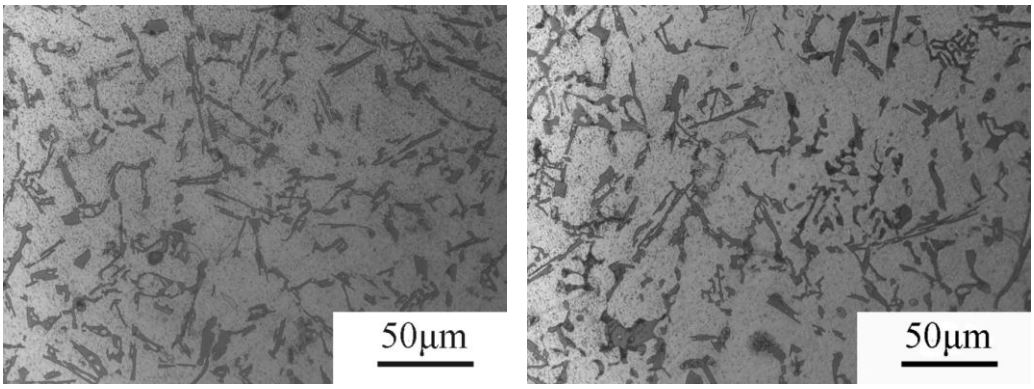


(a) (b)

*Figure 4.28* Microstructure of 380 alloy with different Mg addition at 5 ℃/s (a) 0.3; (b)0.5

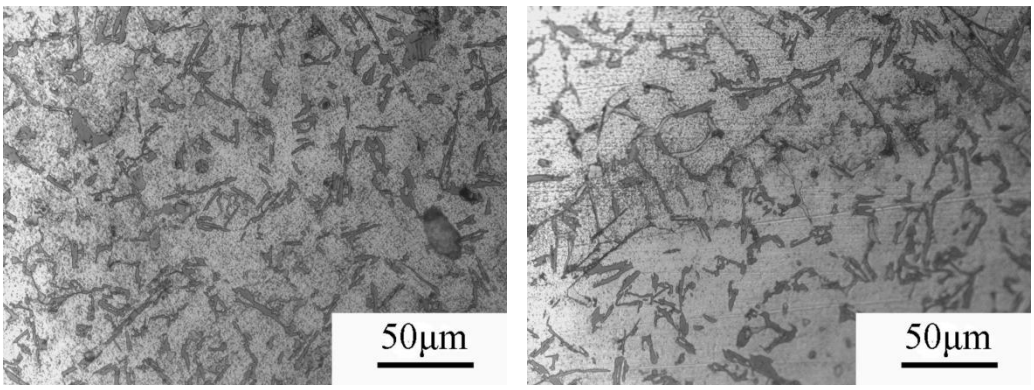


(a) (b)

*Figure 4.29* Microstructure of 380 alloy with different Mg addition at 1-2 ℃/s (a) 0.3; (b)0.5

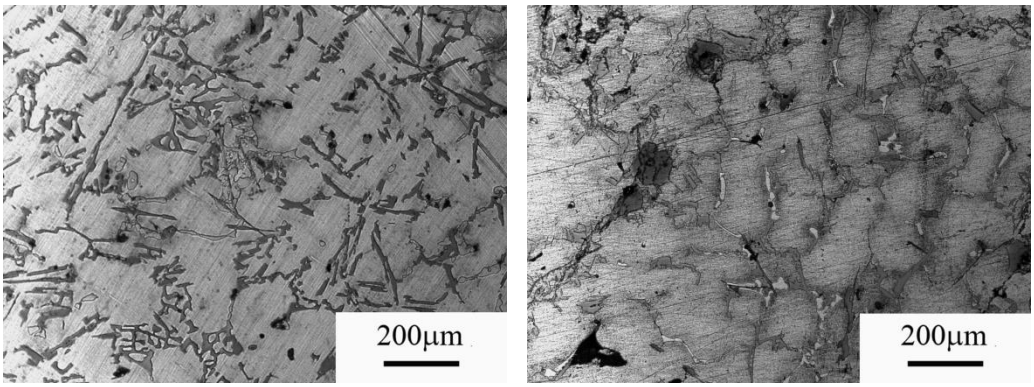


(a) (b)

*Figure 4.30* Microstructure of 380 alloy with different Mg addition at 0.05 ℃/s (a) 0.3; (b)0.5

Table 4.10 *Parameters of α-AlFeSi and β-AlFeSi morphology in A380-0.3Mg alloy with different cooling rates*

| Cooling Rate ( ℃/s) | β-length (μm) | β-width (μm) | Aspect ratio | β-fraction(%) | α-fraction(%) |
|---|---|---|---|---|---|
| 0.05 | 210.15 | 7.13 | 29.47 | 1.31 | 2.23 |
| 1 | 49.67 | 1.88 | 26.42 | 0.52 | 2.91 |
| 5 | 26.10 | 1.58 | 16.51 | 0.31 | 3.11 |

Table 4.11 *Parameters of α-AlFeSi and β-AlFeSi morphology in A380-0.5Mg alloy with different cooling rates*

| Cooling Rate ( ℃/s) | β-length (μm) | β-width (μm) | Aspect ratio | β-fraction(%) | α-fraction(%) |
|---|---|---|---|---|---|
| 0.05 | 160.13 | 5.41 | 29.59 | 1.15 | 2.73 |
| 1 | 41.19 | 1.76 | 23.40 | 0.32 | 3.51 |
| 5 | 23.13 | 1.49 | 15.52 | 0.30 | 3.70 |

### 4.2.6 The Effect of Ca Addition on the Morphology and Phase Fraction of A380

With the addition of Ca, the following phenomenon can be observed: (a) With increase of Ca, β-$Al_5FeSi$ phase transfers to the α-AlFeSi phase.(Figure 4.31) There is no obvious change in A380-0.01 Ca sample (Figure 4.31a) but the obvious β-$Al_5FeSi$ reduction in A380-0.05 Ca sample was observed (Figure 4.31b). If the Ca content goes up to 0.1%, nearly all β-$Al_5FeSi$ transfers to α-AlFeSi. (b) If the Ca contents goes up to

1.0%, polygon or needle-like $Al_2CaSi_2$ phase is formed. (Figure 4.31c, d) Polygon $Al_2CaSi_2$ tends to form with the low cooling rates and needle-like $Al_2CaSi_2$ phase is formed with high cooling rates (Figure 4.32a-d). (c) Ca can modify the eutectic Si. From table 4.12-4.15, it can be seen that once the Ca content goes up to 0.05%, the size and fraction of β-$Al_5FeSi$ is reduced significantly. Also no β-$Al_5FeSi$ can be detected at any cooling rate once the Ca content reaches 0.1%. See table 4.14 and 4.15.

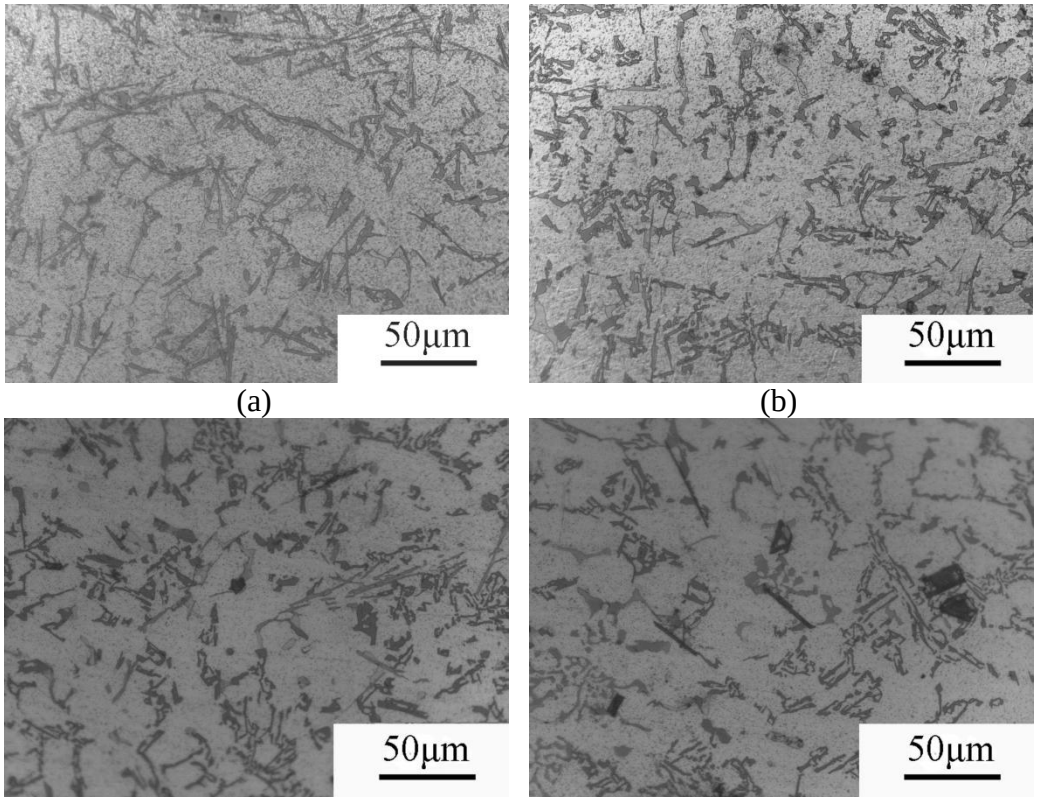


*Figure 4.31* Microstructure of 380 alloy with different Ca addition at 5 ℃/s (a)0.01; (b)0.05; (c) 0.1; (d) 0.3

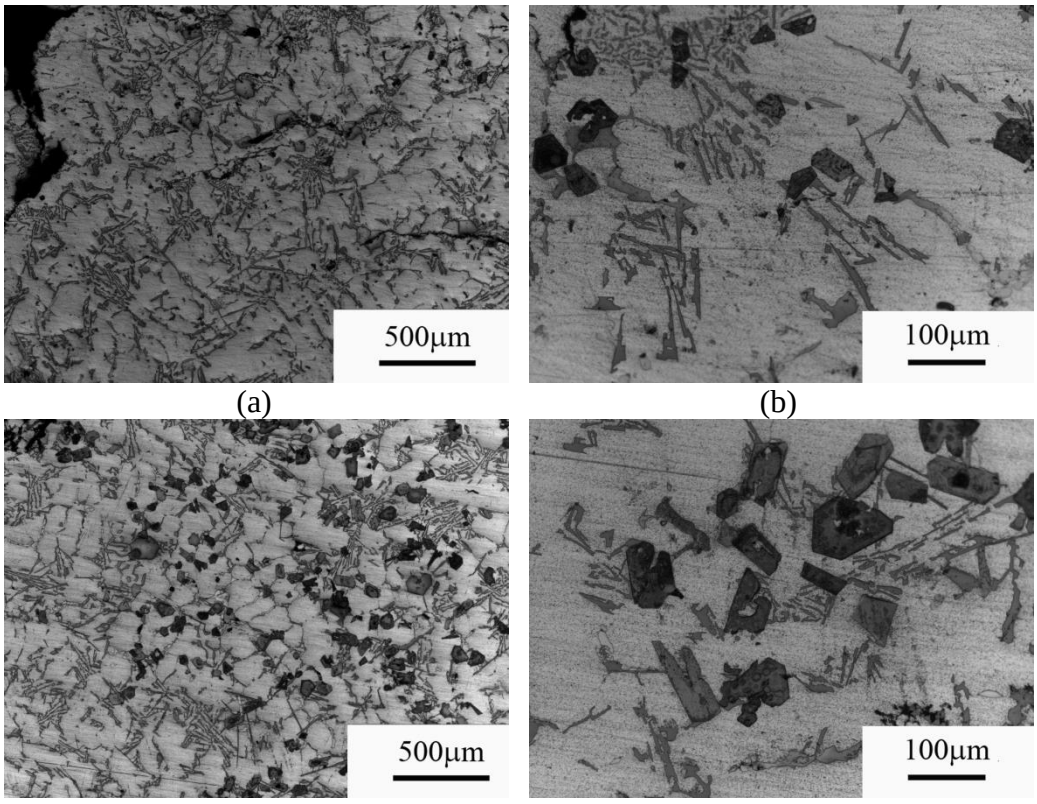


*Figure 4.32* Microstructure of 380 alloy with different Ca addition at 0.05 ℃/s (a) (b) 0.1; (c)(d) 0.3

Table 4.12 *Parameters of α-AlFeSi and β-AlFeSi morphology in A380 alloy with diferent cooling rates of 0.01Ca content*

| **Cooling Rate (℃/s)** | **β-length (μm)** | **β-width (μm)** | **Aspect ratio** | **β-fraction(%)** | **α-fraction(%)** |
|---|---|---|---|---|---|
| 0.05 | 213.42 | 7.23 | 29.52 | 1.31 | 2.22 |
| 5 | 30.15 | 1.75 | 17.23 | 0.68 | 2.69 |

Table 4.13 *Parameters of α-AlFeSi and β-AlFeSi morphology in A380 alloy with different cooling rates of 0.05Ca content*

| **Cooling Rate (℃/s)** | **β-length (μm)** | **β-width (μm)** | **Aspect ratio** | **β-fraction(%)** | **α-fraction(%)** |
|---|---|---|---|---|---|
| 0.05 | 198.65 | 6.84 | 29.04 | 1.06 | 2.41 |
| 5 | 18.73 | 1.41 | 13.28 | 0.50 | 2.80 |

Table 4.14 *Parameters of α-AlFeSi and β-AlFeSi morphology in A380 alloy with different cooling rates of 0.1Ca content*

| **Cooling Rate (℃/s)** | **β-length (μm)** | **β-width (μm)** | **Aspect ratio** | **β-fraction(%)** | **α-fraction(%)** |
|---|---|---|---|---|---|
| 0.05 | - | - | - | - | 3.42 |
| 5 | 16.73 | 2.41 | 6.94 | 0.05 | 3.51 |

Table 4.15 *Parameters of α-AlFeSi and β-AlFeSi morphology in A380 alloy with different cooling rates of 0.3Ca content*

| **Cooling Rate (℃/s)** | **β-length (μm)** | **β-width (μm)** | **Aspect ratio** | **β-fraction(%)** | **α-fraction(%)** |
|---|---|---|---|---|---|
| 0.05 | - | - | - | - | 3.32 |
| 5 | - | - | - | - | 3.35 |

### 4.2.7 The Effect of Sr Addition on the Morphology and Phase Fraction of A380

From the Figure 4.33-4.35, we can see that Sr is an effective modifier to reduce the amount of β-AlFeSi phase and transfer β-AlFeSi to α-AlFeSi phase. With tht addition of Sr, the following phenomenons have been observed:

1) The cooling rates affect the transformation of β-AlFeSi to the α-AlFeSi phase. With 5 ℃/s, even with 0.01% Sr addition, there no obvious β-AlFeSi can be found. (Figure 4.33) With 10 ℃/s, even 0.01% Sr addition can effeticvely reduce the fraction of β-AlFeSi formed. The optimized condition can be obtained when the Sr content is 0.1%. If the Sr contents go up, more platate phase would form (Figure 4.34). The 20 ℃/s cooling rate sample has a similar trend to that using 10 ℃/s cooling rate. However, even with the optimized condition (0.1 Sr %), obvious β-AlFeSi can still be viewed. (Figure 4.35) (2) It is noted that if the Sr conent is less than 0.1%, the size and fraction of β-AlFeSi reduced with Sr addition; however, if the Sr content is higher than 0.1%, the size

and fraction of β-AlFeSi is increased with Sr addition. So the high Sr content introduced more β-AlFeSi phase. (Table 4.16-4.19)

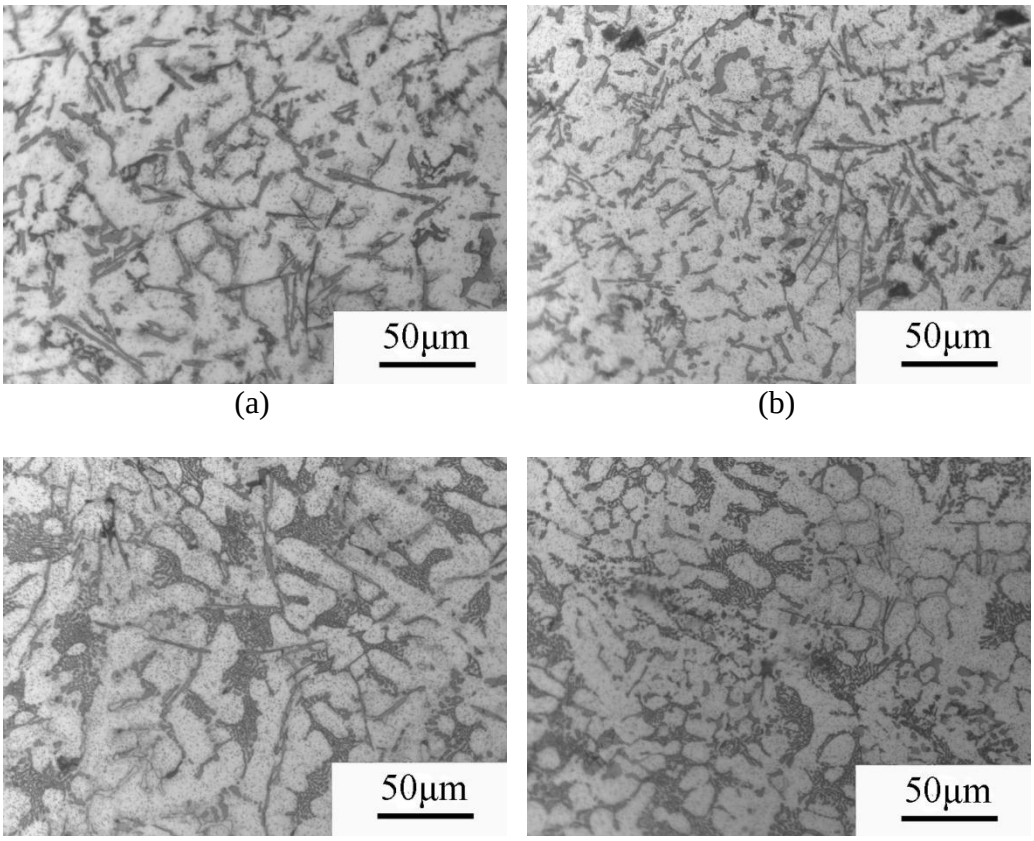


(a) (b)

(c) (d)

*Figure 4.33* Microstructure of 380 alloy with different Sr addition at 5 ℃/s (a) 0.01; (b) 0.05; (c) 0.1; (d) 0.3

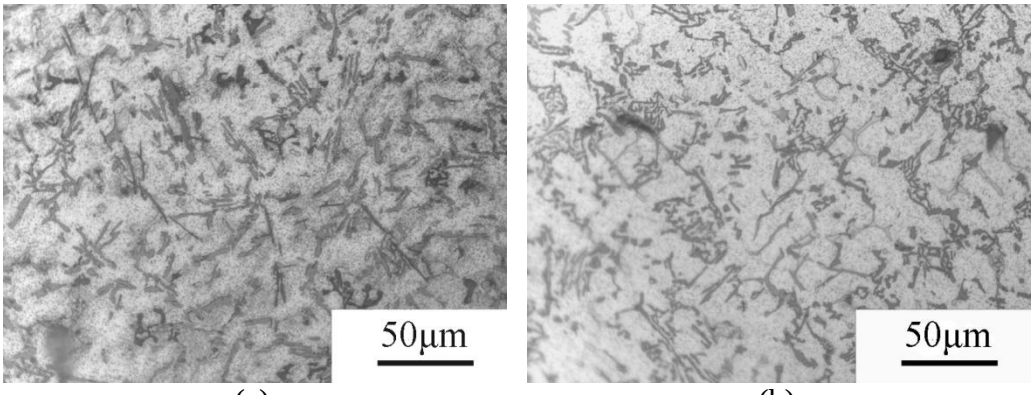


(a) (b)

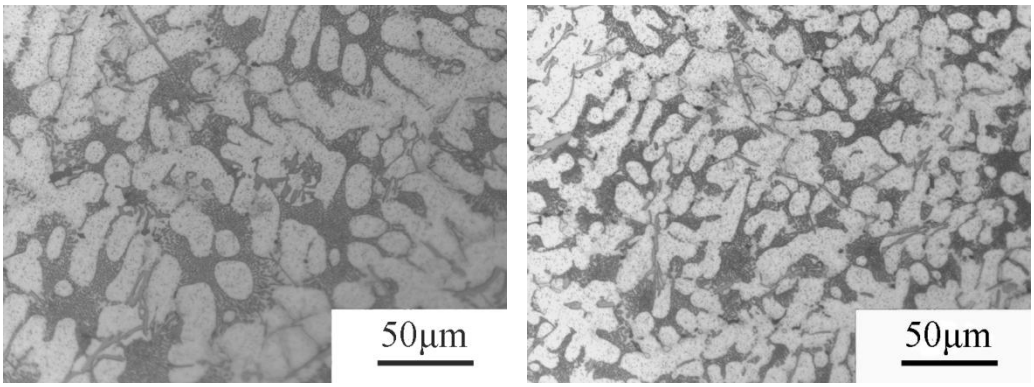


(c) (d)

*Figure 4.34* Microstructure of 380 alloy with different Sr addition at 10 ℃/s (a) 0.01; (b) 0.05; (c) 0.1; (d) 0.3;

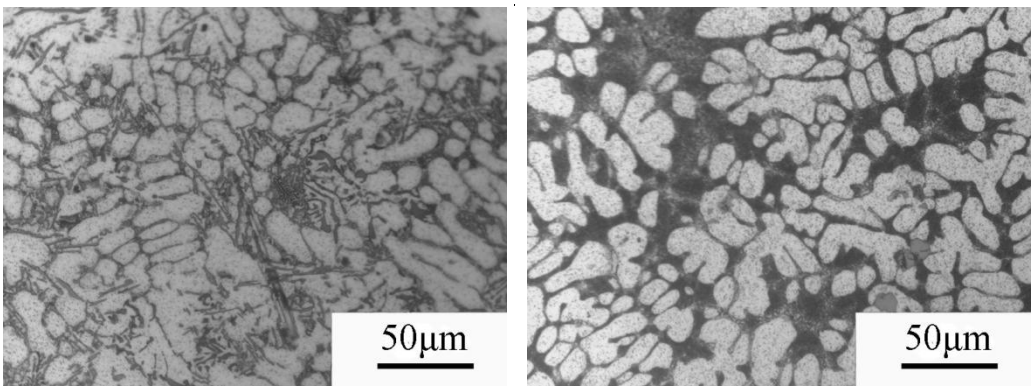


(a) (b)

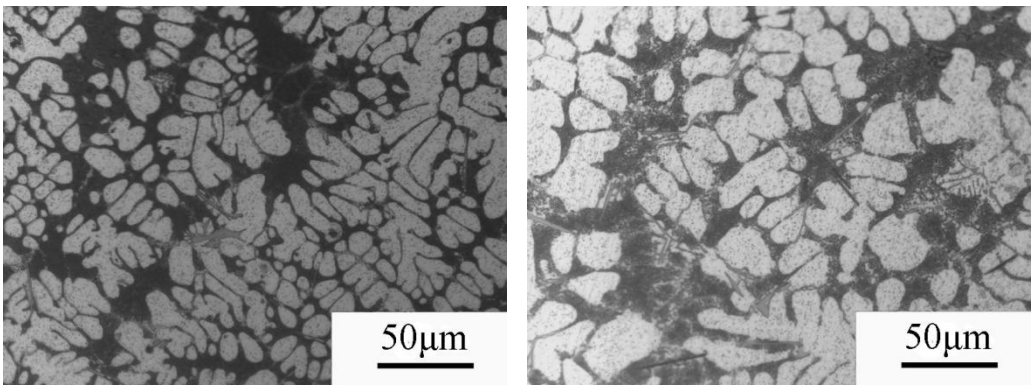


(c) (d)

*Figure 4.35* Microstructure of 380 alloy with different Sr addition at 20 ℃/s (a) 0.01; (b) 0.05; (c) 0.1; (d) 0.3

Table 4.16 *Parameters of α-AlFeSi and β-AlFeSi morphology in A380-0.01Sr alloy with different cooling rates*

| Cooling Rate (℃/s) | β-length (μm) | β-width (μm) | Aspect ratio | β-fraction(%) | α-fraction(%) |
|---|---|---|---|---|---|
| 5 | 28.95 | 1.87 | 15.48 | 1.12 | 2.22 |
| 10 | 16.87 | 1.88 | 8.97 | 0.73 | 2.51 |
| 20 | - | - | - | - | 3.13 |

Table 4.17 *Parameters of α-AlFeSi and β-AlFeSi morphology in A380-0.05Sr alloy with different cooling rates*

| Cooling Rate (℃/s) | β-length (μm) | β-width (μm) | Aspect ratio | β-fraction(%) | α-fraction(%) |
|---|---|---|---|---|---|
| 5 | 31.85 | 2.10 | 15.17 | 1.01 | 2.32 |
| 10 | 10.15 | 1.55 | 6.35 | 0.51 | 2.63 |
| 20 | - | - | - | - | 3.22 |

Table 4.18 *Parameters of α-AlFeSi and β-AlFeSi morphology in A380-0.1Sr alloy with different cooling rates*

| Cooling Rate (℃/s) | β-length (μm) | β-width (μm) | Aspect ratio | β-fraction(%) | α-fraction(%) |
|---|---|---|---|---|---|
| 5 | 23.67 | 1.64 | 14.43 | 0.62 | 2.68 |
| 10 | 20.56 | 1.79 | 11.49 | 0.31 | 3.12 |
| 20 | - | - | - | - | 3.31 |

Table 4.19 *Parameters of α-AlFeSi and β-AlFeSi morphology in A380-0.3Sr alloy with different cooling rates*

| Cooling Rate (℃/s) | β-length (μm) | β-width (μm) | Aspect ratio | β-fraction(%) | α-fraction(%) |
|---|---|---|---|---|---|
| 5 | 30.43 | 1.81 | 16.81 | 1.23 | 2.86 |
| 10 | 29.73 | 1.92 | 15.48 | 1.31 | 3.02 |
| 20 | - | - | - | - | 3.51 |

### 4.2.8 The Effect of K Addition on the Morphology and Phase Fraction of A380

From Figures 4.36-4.38, we can see that the addition of K effectively reduces the size of β-AlFeSi phase and its transfer into α-compound. With addition of K, the following phenomenos were observed. 1) High cooling rates can eliminate β-AlFeSi phase. If the cooling rates go up to 20 ℃/s, no obvious β-AlFeSi can be found (Fig. 4.36) and only α-AlFeSi can be seen. (Table 4.20-4.23); 2) the size of the α-AlFeSi phase reduced with K addtion. Compared with Figure 4.36 a) and e) and Figure 4.37 a) and e), we can see that the secondary dendrite arm spacing of 380 alloys is reduced significantly with K addition; 3) even with a lower cooling rate, K can effectively refine the β-AlFeSi phase. For the 5 ℃/s cooling rate sample (Figure 4.36), with 0.5K addition (Figure 4.36b), β-AlFeSi phase fraction goes down to 0.41% (Table 4.21) and no β-AlFeSi phase can be detected if the K content goes up to 2% (Figure 4.36d and Table 4.23). If the cooling rates are increased to 10 ℃/s, no β-AlFeSi phase can be seen with 1% K addition (Figure 4.36 c and Table 4.22); 4) addition of K does not introduce sludge under any cooling rates. It should be an ideal Fe modifier.

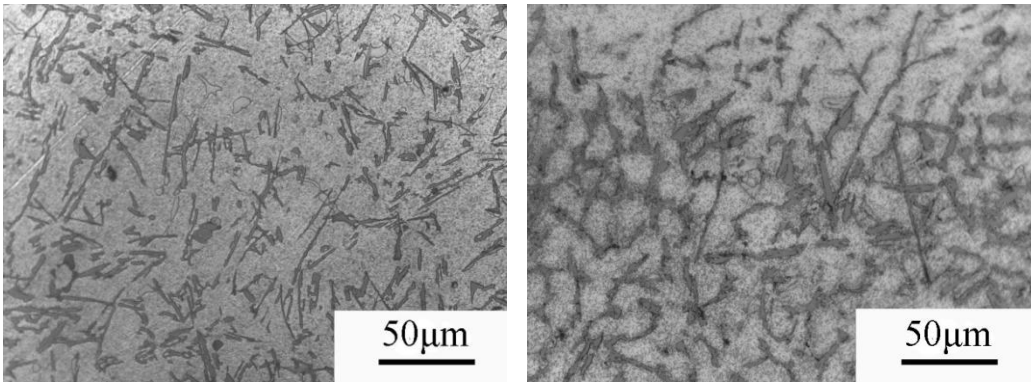


(a) (b)

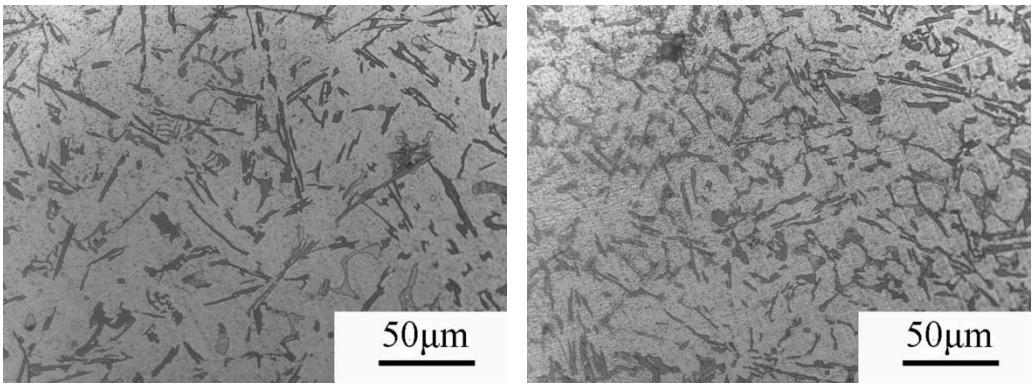


(c) (d)

*Figure 4.36* Microstructure of 380 alloy with different K addition at 5 ℃/s
(a) 0.1; (b) 0.5; (c)1; (d)2

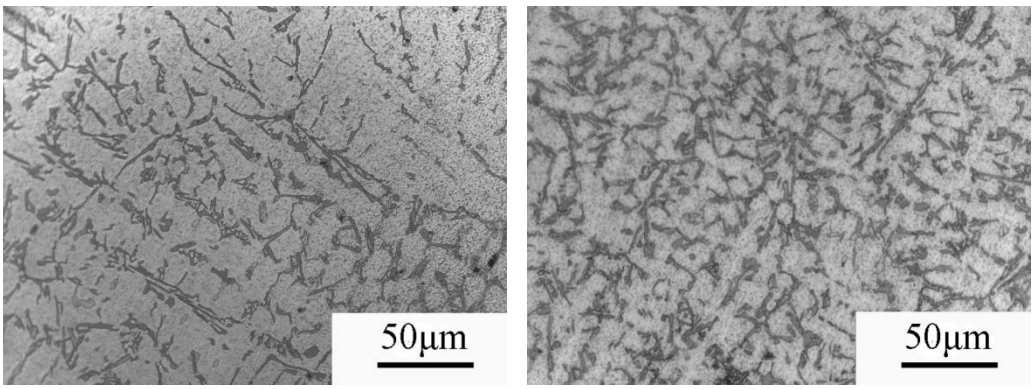


(a) (b)

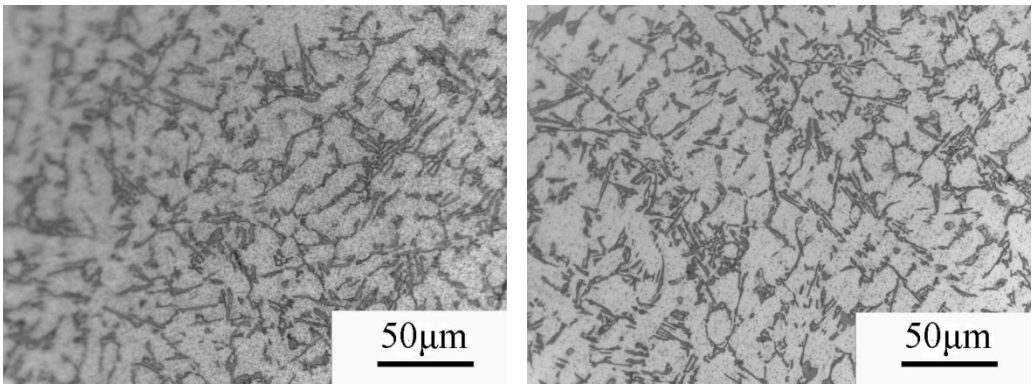


(c) (d)

*Figure 4.37* Microstructure of 380 alloy with different K addition at 10 ℃/s
(a) 0.1; (b) 0.5; (c)1; (d)2

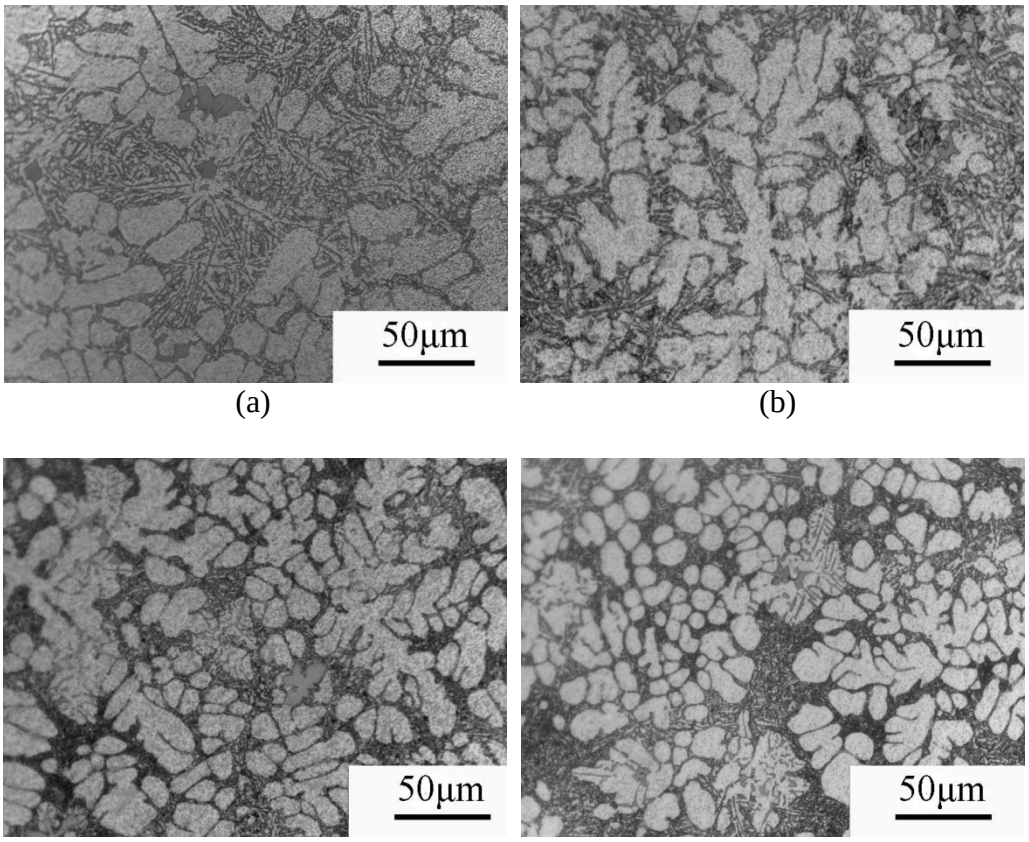


(a) (b)

(c) (d)

*Figure 4.38* Microstructure of 380 alloy with different K addition at 20 ℃/s
(a) 0.1; (b) 0.5; (c)1; (d)2

Table 4.20 *Parameters of α-AlFeSi and β-AlFeSi morphology in A380-0.1K alloy with different cooling rates*

| Cooling Rate ( ℃/s) | β-length (μm) | β-width (μm) | Aspect ratio | β-fraction(%) | α-fraction(%) |
|---|---|---|---|---|---|
| 5 | 28.71 | 1.53 | 18.77 | 1.21 | 2.43 |
| 10 | 10.17 | 1.32 | 7.70 | 0.91 | 2.65 |
| 20 | - | - | - | - | 3.61 |

Table 4.21 *Parameters of α-AlFeSi and β-AlFeSi morphology in A380-0.5K alloy with different cooling rates*

| Cooling Rate (℃/s) | β-length (μm) | β-width (μm) | Aspect ratio | β-fraction(%) | α-fraction(%) |
|---|---|---|---|---|---|
| 5 | 20.72 | 1.37 | 18.89 | 0.41 | 3.21 |
| 10 | 18.32 | 1.47 | 12.47 | 0.23 | 3.51 |
| 20 | - | - | - | - | 3.82 |

Table 4.22 *Parameters of α-AlFeSi and β-AlFeSi morphology in A380-1K alloy with different cooling rates*

| Cooling Rate (℃/s) | β-length (μm) | β-width (μm) | Aspect ratio | β-fraction(%) | α-fraction(%) |
|---|---|---|---|---|---|
| 5 | 10.83 | 0.91 | 11.90 | 0.32 | 3.31 |
| 10 | - | - | - | - | 3.63 |
| 20 | - | - | - | - | 3.53 |

Table 4.23 *Parameters of α-AlFeSi and β-AlFeSi morphology in A380-2K alloy with different cooling rates*

| Cooling Rate (℃/s) | β-length (μm) | β-width (μm) | Aspect ratio | β-fraction(%) | α-fraction(%) |
|---|---|---|---|---|---|
| 5 | - | - | - | - | 3.59 |
| 10 | - | - | - | - | 3.64 |
| 20 | - | - | - | - | 3.56 |

### 4.2.9 The Effect of Sr and Ca Addition on the Morphology and Phase Fraction of A380

Although the modification effect of Ca is less than that of Sr, no oxide film is introduced by Ca. Thus the combination of Ca and Sr will diminish the detrimental effect.

Figure 4.39 shows the optical images of A380 alloys with a combined content of 0.05%Sr and 0.1%Ca addition with different cooling rates. When compared to the sample of A380-0.1Ca using furnace cooling, it can be seen that the fraction of β-AlFeSi phase increases and the fraction of α-AlFeSi phase decreases.(Figure 4.39 a&b) This means that the combination of Sr and Ca diminishes the effect of modification of morphology of the

β-AlFeSi phase. It can also be seen that the size of polygon of AlCaSi phase and α-AlFeSi phase are reduced. That means the addition of Sr can also refine the AlCaSi phase and diminish the detrimental effect. In higher cooling rates, the combination of Sr and Ca addition can get rid of the β-AlFeSi phase and control the growth of AlCaSi phase. (Figure 4.39 c & d). Meanwhile, the introduction of Sr modifies the eutectic Si phase which also leads to improvement in the toughness of alloy. From table 4.24 we can see that the combination of Ca and Sr addition does not have obvious effect on the size of β-AlFeSi but leads to the reduction of its phase fraction.

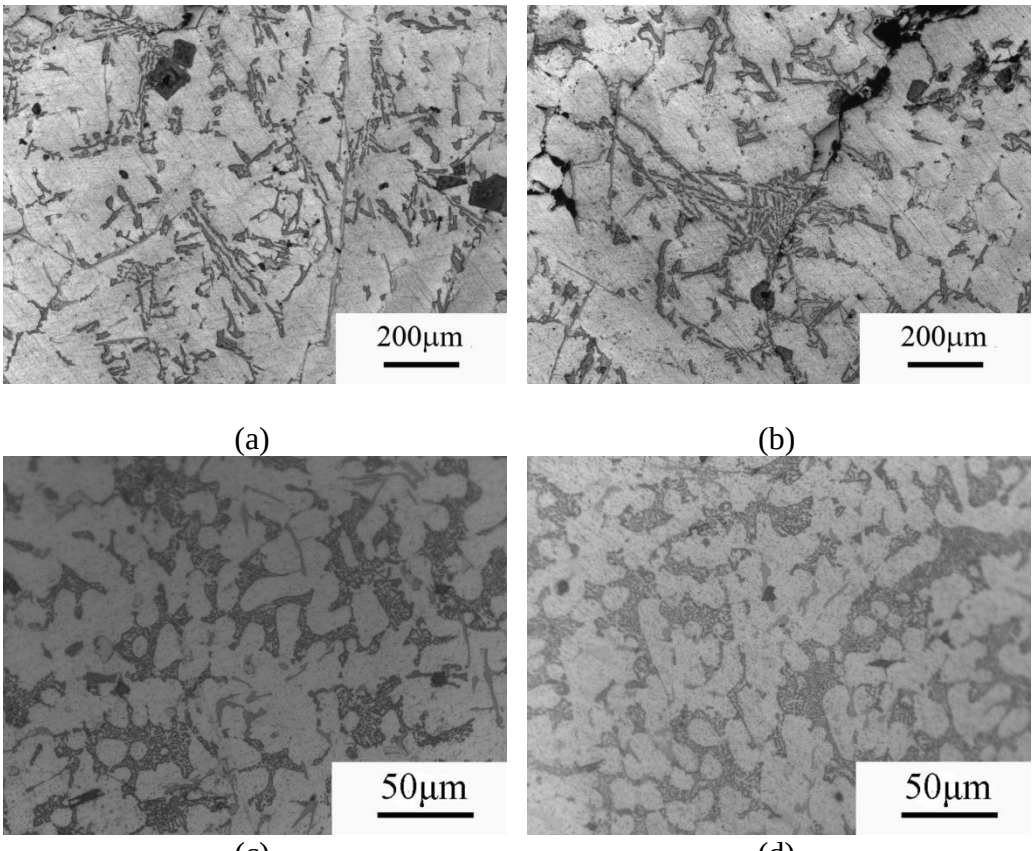


*Figure 4.39* Microstructure of A380+0.1Ca+0.05Sr with different cooling rates a) b) 0.05 °C/s; c) 1 ℃/s; d) 5 ℃/s

Table 4.24 *Parameters of α-AlFeSi and β-AlFeSi morphology in A380-0.1Ca+0.05Sr alloy with different cooling rates*

| Cooling Rate (℃/s) | β-length (μm) | β-width (μm) | Aspect ratio | β-fraction(%) | α-fraction(%) |
|---|---|---|---|---|---|
| 0.05 | 203.17 | 9.23 | 22.01 | 1.42 | 2.13 |
| 1 | 39.73 | 1.92 | 20.69 | 0.91 | 2.53 |
| 5 | 23.13 | 1.76 | 13.14 | 0.42 | 3.05 |

The addition of Sr reduces the size of $Al_2CaSi_2$ phase becase Sr can form $Al_2Sr_2Si$ prior to $Al_2CaSi_2$ thus reducing the Si content for $Al_2CaSi_2$ content. However, introduction of the oxide layer by Sr results in the formation of the nucleation site of β-AlFeSi. Thus there is no obvious advantage in using the combination of Ca and Sr addition compared to the use of A380 alloy having addition of only Ca or only Sr.

### 4.2.10 The Effect of Mn and Ca Addition on the Morphology and Phase Fraction of A380

The purpose in the combined addition of Ca and Mn addition lies in the reduction of the formation of the α-AlFeSi phase and the polygon $Al_2CaSi_2$ phase. In this dissertation, we adopt the combination of 0.1Ca and 1Mn. With low cooling rates, there is no obvious of reduction in demension of sludge α-AlFeSi phase, while the size of the polygon $Al_2CaSi_2$ phase reduces drastically.(Figure 4.40 a & b) compared with the A380-0.1Ca sample. However, with high cooling rates, the size of both α-AlFeSi and $Al_2CaSi_2$ phases is reduced. Even though most of the α-AlFeSi is still in a polygon shape, the size is smaller and its distribution is at the grain boundaries. The polygon shape is also noted around the grain boundary. This condition can lead to a reduction in the detrimental

effects of polygon sludge (Figure 4.40 c & d). In addition, no obvious β-AlFeSi phase can be found in the graphite and steel cooling samples, as shown in Table 4.25.

The combination of Ca and Mn further eliminated the β-AlFeSi phase and did not introduce any sludge at the high cooling rates (Figure 4.40 c & d). This situation will lead to an improvement in the ductility of the alloy. Finally, some $Al_2CaSi_2$ phase was pushed to the boundary of fcc α-Al. This condition may however affect the ductility of A380 alloy.

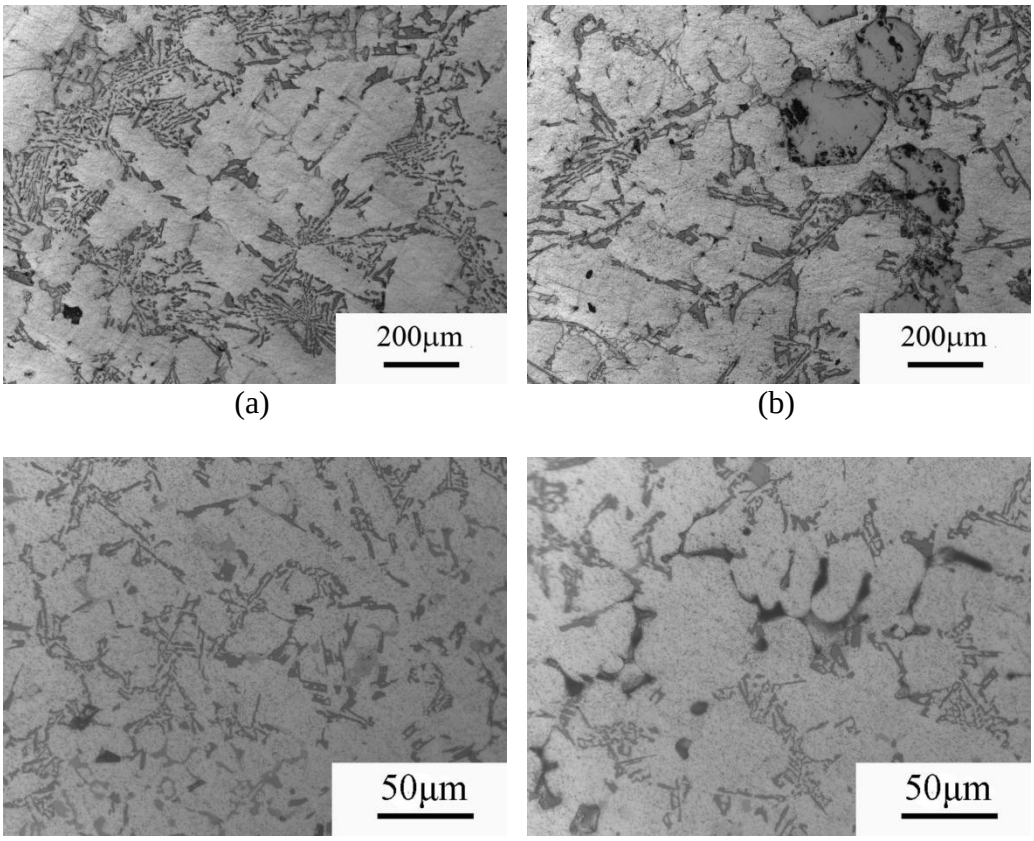


(a) (b)

(c) (d)

*Figure 4.40* Microstructure of A380+0.1Ca+1Mn
a) b) 0.05 °C/s; c) 1 ℃/s; d) 5 ℃/s

Table 4.25 *Parameters of α-AlFeSi and β-AlFeSi morphology in A380+0.1Ca+1Mn alloy with different cooling rates*

| Cooling Rate (℃/s) | β-length (μm) | β-width (μm) | Aspect ratio | β-fraction(%) | α-fraction(%) |
|---|---|---|---|---|---|
| 0.05 | - | - | - | - | 3.21 |
| 1 | - | - | - | - | 2.94 |
| 5 | - | - | - | - | 2.86 |

4.2.11 The Effect of Mn and Sr Addition on the Morphology and Phase Fraction of A380

Sr and Mn are two traditional elements used to reduce and refine the β-AlFeSi phase. In this dissertation two different combinations of Sr and Mn (0.1Sr+0.5Mn and 0.05Sr+1Mn) are used to test the effect of Mn and Sr with different ratio. With high Sr content and low Mn content, (0.1Sr +0.5Mn), and at low cooling rates, there is still plenty of β-AlFeSi phase.(Figure 4.41 a & b) But at higher cooling rates, no obvious β-AlFeSi phase is observed and most of the α-AlFeSi is in the form of Chinese script. (Figure 4.41 d). The polygon $AlSi_2Sr_2$ phase can still be observed. Table 4.26 shows the fraction of β-AlFeSi phase reduction. On the other hand, with low Sr content and high Mn content, (0.05Sr +1Mn), and at low cooling rates, sludge is formed (Figure 4.42 a & b). However, at high cooling rates, most α-AlFeSi is in the form of Chinese script and no obvious $Al_2Si_2Sr$ phase is observed (Figure 4.42 c & d). Therefore, it could be a good way for AlFeSi phase control.

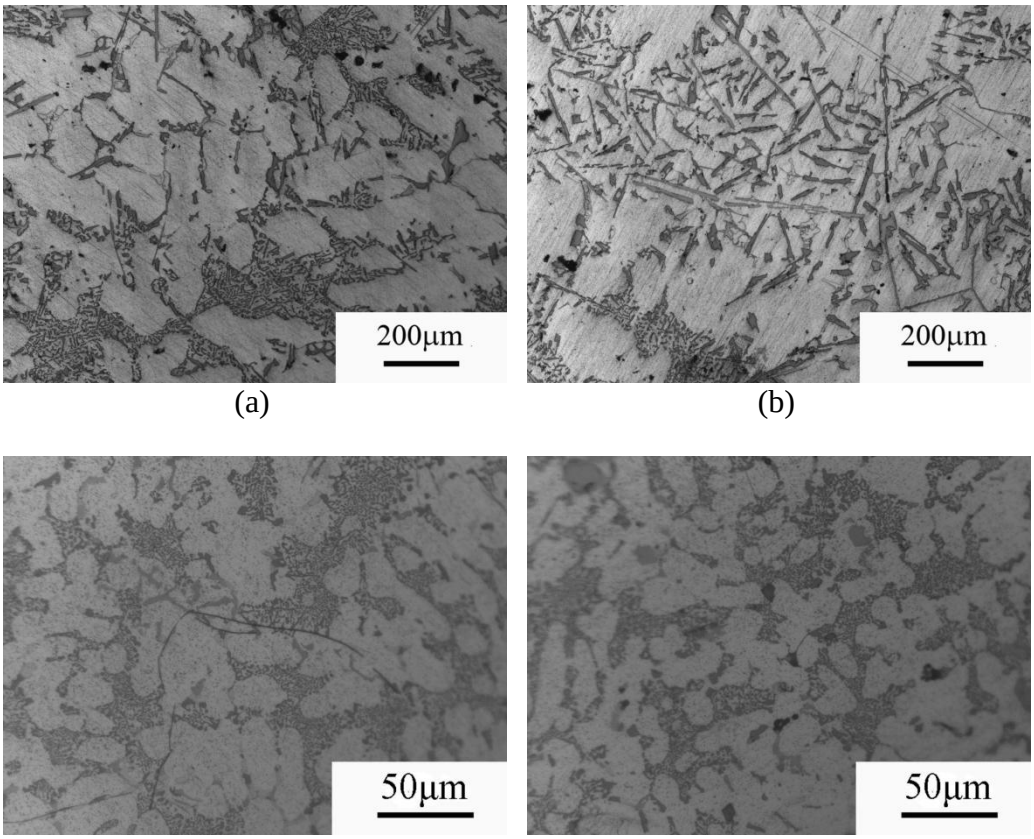


(a) (b)

(c) (d)

*Figure 4.41* Microstructure of A380+0.1Sr+0.5Mn
a) b) 0.05 ℃/s; c) 1 ℃/s; d) 5 ℃/s

Table 4.26 *Parameters of α-AlFeSi and β-AlFeSi morphology in A380+0.1Sr+0.5Mn alloy with different cooling rates*

| Cooling Rate ( ℃/s) | β-length (μm) | β-width (μm) | Aspect ratio | β-fraction(%) | α-fraction(%) |
|---|---|---|---|---|---|
| 0.05 | 198.71 | 7.14 | 27.83 | 1.05 | 2.31 |
| 1 | 45.3 | 1.23 | 57.97 | 0.63 | 2.53 |
| 5 | - | - | - | - | 3.61 |

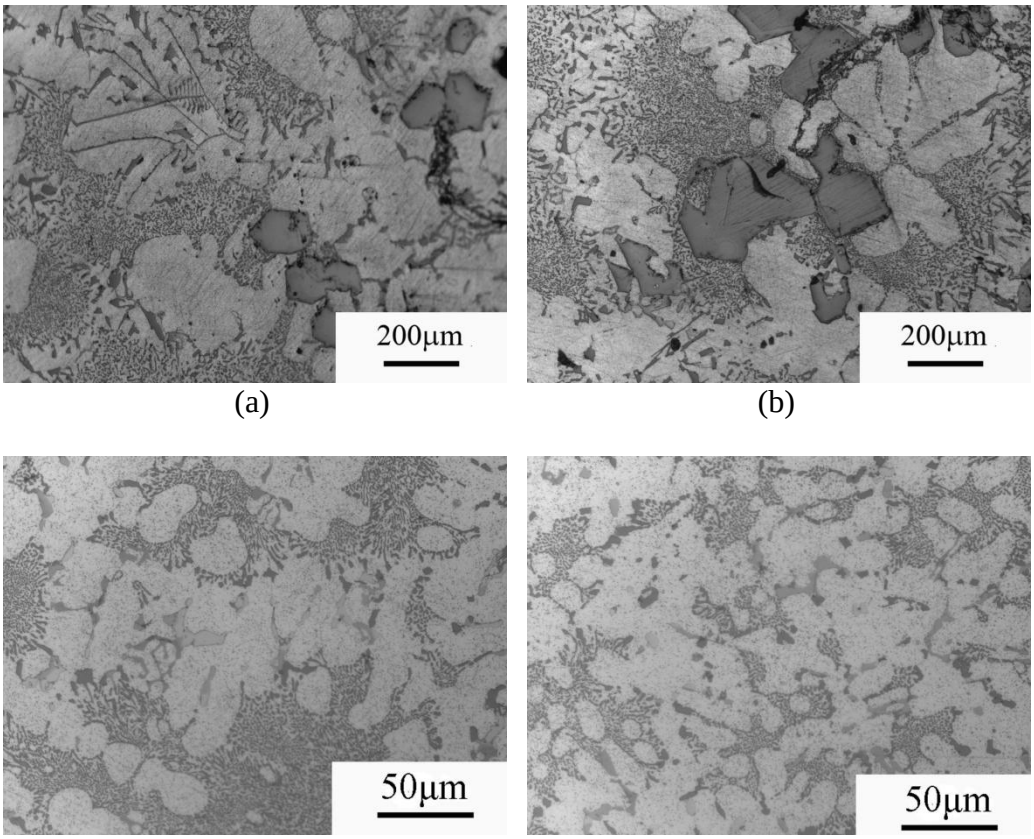


(a) (b)

(c) (d)

*Figure 4.42* Microstructure of A380+0.05Sr+1Mn
a) b) 0.05 ℃/s; c) 1 ℃/s; d) 5 ℃/s

Table 4.27 *Parameters of α-AlFeSi and β-AlFeSi morphology in A380+0.05Sr+1Mn alloy with different cooling rates*

| Cooling Rate ( ℃/s) | β-length (μm) | β-width (μm) | Aspect ratio | β-fraction(%) | α-fraction(%) |
|---|---|---|---|---|---|
| 0.05 | - | - | - | - | 2.0 |
| 1 | - | - | - | - | 2.9 |
| 5 | - | - | - | - | 3.5 |

In summary, to compare the three combination method, Ca+Sr addition is not an ideal choice, Ca+Mn addition can effectively reduce β-AlFeSi phase and Sr+Mn addtion can have the best effect. And high cooling rates can facilitate the transformation from β-AlFeSi to α-AlFeSi.

### 4.2.12 The Effect of Heat Treatment

The presence of the needle shape β-AlFeSi phase in the Al-Si alloy will severely reduce the mechanical properties of alloys. The element alloying method is introduced. However, with the benefit of element alloying method such as transferring β-AlFeSi to α-AlFeSi, some detrimental effects, especially introducing other intermetallics, will also adversely affect the properties of alloys.

Heat treatment of casting alloys is another effective method to minimize the detrimental effect of AlFeSi intermetallics. However, this method is not widely used in die casting Al-Si alloys for the following reasons: 1) during the die casting process, air will be absorbed and trapped in the solidified aluminum alloy. If heat treatment is needed, the entrapped gas will expand and bumps will form. 2) The diffusion rate of Fe in Al is very low. Because the diffusion coefficient of Fe in Al is only $4\times10^{-11}cm^2/s$, this means that the heat treatment temperature for solution of AlFeSi phase is comparatively higher than the normal solution temperatures. 3) Heat treatment can affect the formation of other phases. For example, coarsening of Si phase can result. In view of the reasons above, we studied high-temperature shot-time heat treatment method. In this way, it is possible that both refine Fe containing intermetallics phases and blistering can be avoided.

Narayanan (1994) adopted the non-equilibrium heat treatment method, which is above the regular solution in heat treatment temperature. This result in a reduction of the length of β phase, because of the dissolution effect. Meanwhile Yin (2001) conducted heat treatment on A319 alloys and considered that the disintergrity in β phase are the cause of dissolution. However, both individuals mentioned that α-AlFeSi phase is not influenced by heat treatment.

1) Influence of solution temperature

From Figure 4.43 with the increase of solution temperatures, the fraction and morphology of AlFeSi phases change significantly. In the 450 and 500 ℃ heat treatment samples, there is no obvious AlFeSi phase change, and β-AlFeSi phase predominates.(Figure 4.43 a & b) However, if the temperature rises to 515 °C, β-AlFeSi phase is dissolved and the fraction and average length of β-AlFeSi are reduced. (Figure 4.43c) Finally, if the temperature goes up to 525 °C, α-AlFeSi is predominates and the fraction and size of the α-AlFeSi phase increases. (Figure 4.28d)

From table 4.28, we can see that with the increasing solution temperatures, the size and the fraction of β-AlFeSi are decreased and the fraction of α-AlFeSi is increased. For the 450 °C sample, no β-AlFeSi morphology change is observed. However once the temperature goes up to 500 °C, decomposition of β-AlFeSi starts, so 500 ℃ is the lowest temperature at which decomposition of the β-AlFeSi phase.

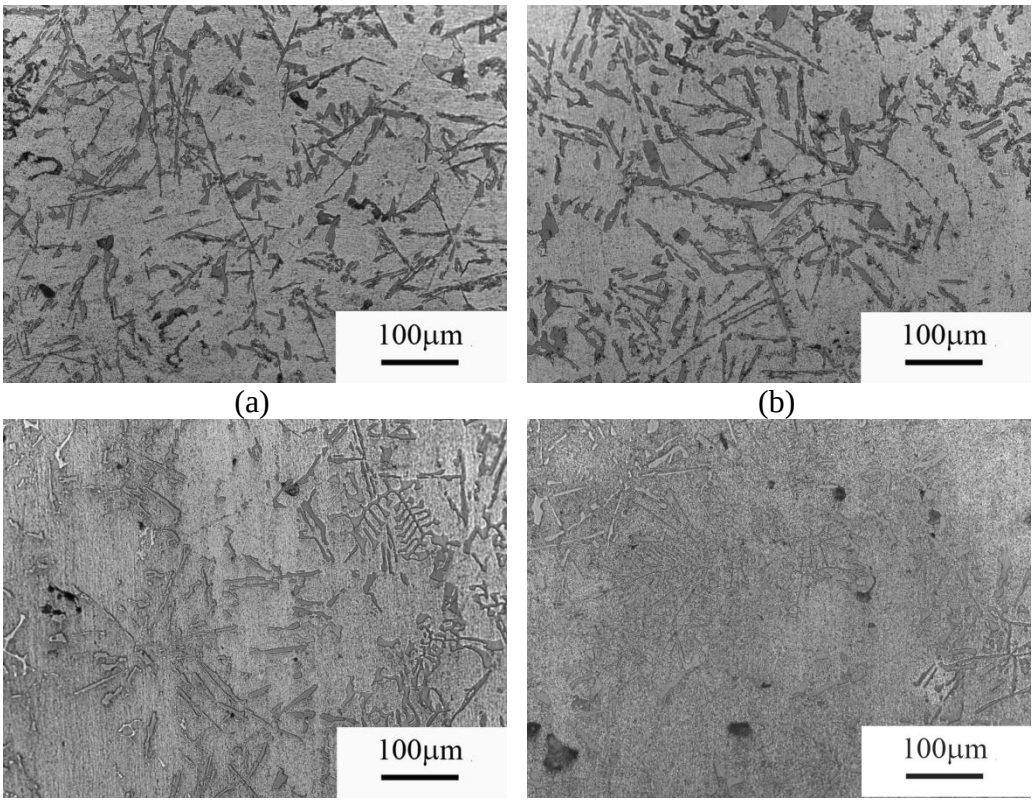


*Figure 4.43* Optical sample of different heat treatment temperatures for 4 hours a) 450 ℃; b)500 ℃; c)515 ℃; d)525 ℃

Table 4.28 *Parameters of α-AlFeSi and β-AlFeSi morphology 4h heat treatment samples with heat treatment temperatures*

| Heat treatment temperatures | β-length (μm) | β-width (μm) | Aspect ratio | β-fraction(%) | α-fraction(%) |
|---|---|---|---|---|---|
| 450 | 315.03 | 10.32 | 30.58 | 1.35 | 2.30 |
| 500 | 300.15 | 9.11 | 32.96 | 0.98 | 2.43 |
| 515 | 65.13 | 3.21 | 20.31 | 0.31 | 3.56 |
| 525 | - | - | - | - | 4.13 |

2) Influence of solution time

The solution time at a given solution temperature has a great effect on the morphology of AlFeSi intermetallics. At 450 ℃ (Figure 4.54), even after 24h heat treatment, there is no obvious change of the AlFeSi phase. (Figure 4.54 a-c) The

parameters of α and β phase do not have any change. (Table 4.29) It can therefore be said that no β phase transfers to α phase under 450 °C regardless the duration of heat treatment.

If the treatment is at 500 ℃, there is no obvious morphology change for the 0.5 h and 2 h sample (Figure 4.45 a & b). But once the heat treatment duration reaches 8 hours, the size of β phase begins to decrease (Figure 4.45 c). For 24 hour heat treatment, no β phase is detected, and that means all that β phase has changed to α-AlFeSi phase (Figure 4.45 d). Table 4.30 shows that after an 8 h treatment, the size and fraction of β phase begin to decrease.

For the sample with a 515 °C 1h heat treatment, the size of the β phase is reduced significantly, (Figure 4.46 b). After 4 hour heat treatment, nearly all the β phase was decomposited (Figure 4.46 d), which can be seen in Table 4.31.

Lastly, as to the 525 °C sample with only 0.5 h of heat treatment, β phase is reduced to 1.19% ( Figure 4.47 a). If the heat treatment time is longer, all β phase transfers to α phase (Figure 4.47 b, c & d, table 4.32).

In summary, 450 ℃ is too low to diminish β phase, and if the heat treatment temperature goes up to 500 °C, the higher temperature can reduce the β phase with shorter time. The reason is not only the decomposition of β phase but also the transformation of β to α phase.

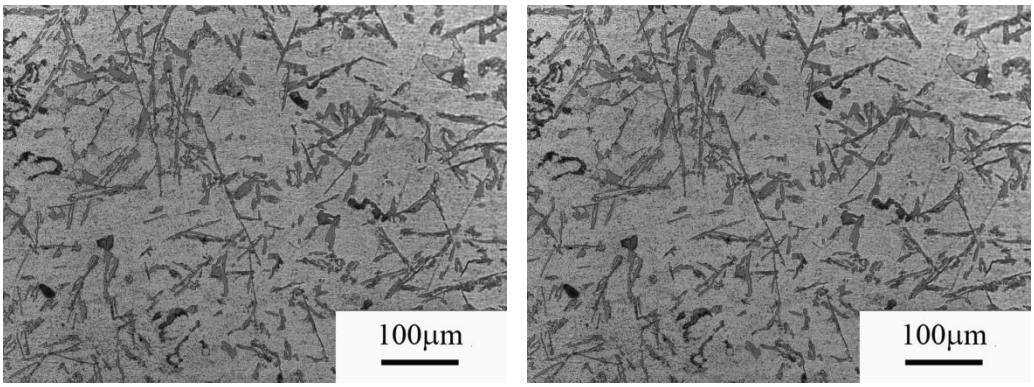


(a) (b)

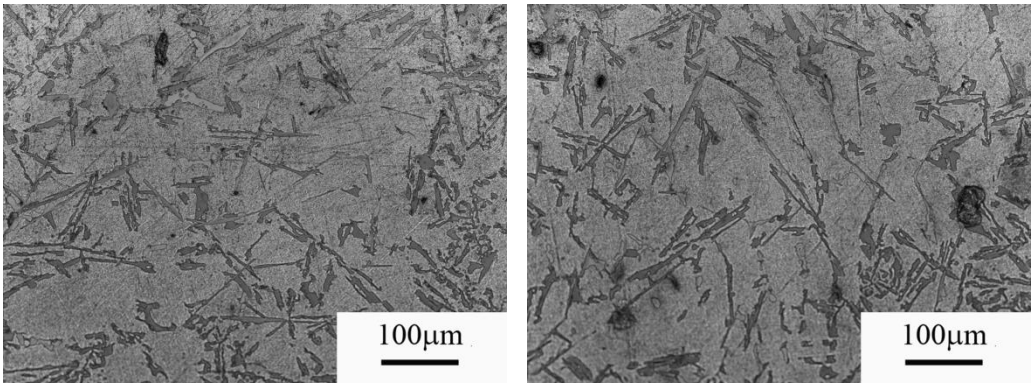


(c) (d)

*Figure 4.44* Optical sample of different heat treatment time at 450 ℃
a) 0.5 h; b)2 h; c)8 h; d)24h

Table 4.29 *Parameters of α-AlFeSi and β-AlFeSi morphology of 450 ℃ heat treatment samples with different heat treatment time*

| Heat treatment time | β-length (μm) | β-width (μm) | Aspect ratio | β-fraction(%) | α-fraction(%) |
|---|---|---|---|---|---|
| 0.5 h | 254.87 | 9.51 | 26.79 | 1.30 | 2.32 |
| 2 h | 265.44 | 9.91 | 26.76 | 1.42 | 2.26 |
| 8 h | 255.69 | 9.34 | 27.34 | 1.35 | 2.31 |
| 24 h | 253.98 | 9.18 | 27.64 | 1.46 | 2.19 |

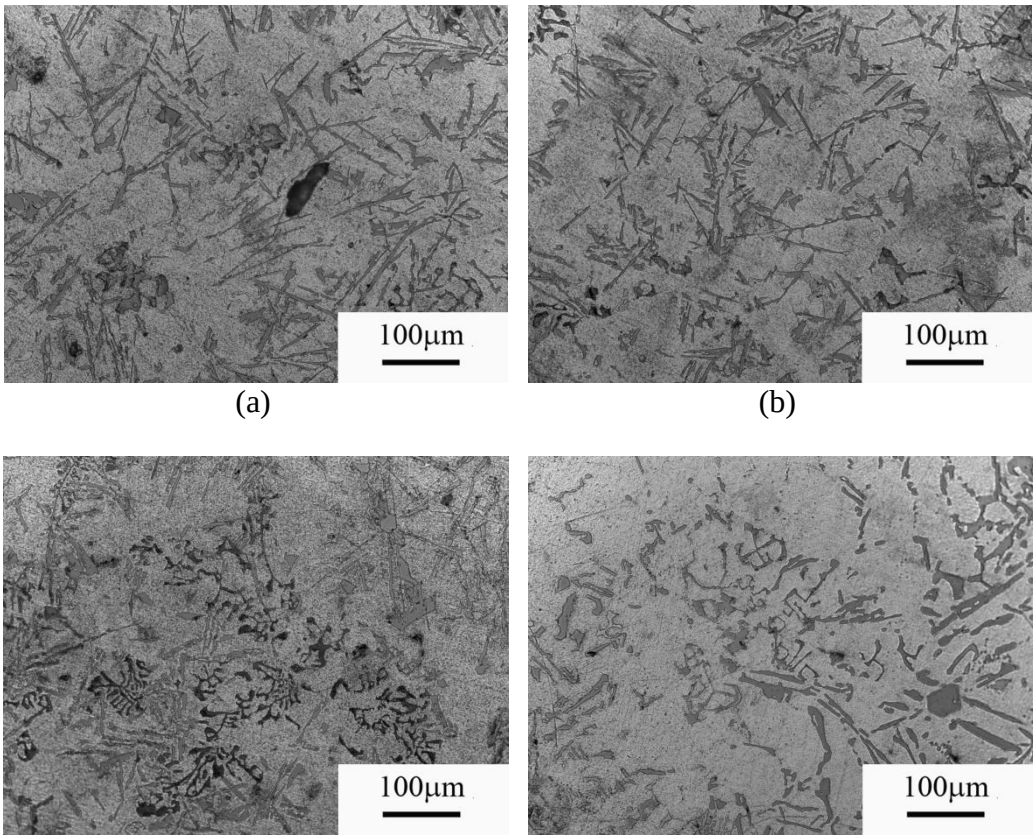


(a) (b)

(c) (d)

*Figure 4.45* Optical sample of different heat treatment time at 500 ℃
a) 0.5 h; b)2 h; c)8 h; d)24 h

Table 4.30 *Parameters of α-AlFeSi and β-AlFeSi morphology of 500 ℃ heat treatment samples with different heat treatment time*

| Heat treatment time | β-length (μm) | β-width (μm) | Aspect ratio | β-fraction(%) | α-fraction(%) |
|---|---|---|---|---|---|
| 0.5 h | 260.24 | 10.10 | 26.02 | 1.29 | 2.32 |
| 2 h | 258.04 | 10.65 | 24.23 | 1.20 | 2.31 |
| 8 h | 165.21 | 7.65 | 21.56 | 0.71 | 2.91 |
| 24 h | - | - | - | - | 3.56 |

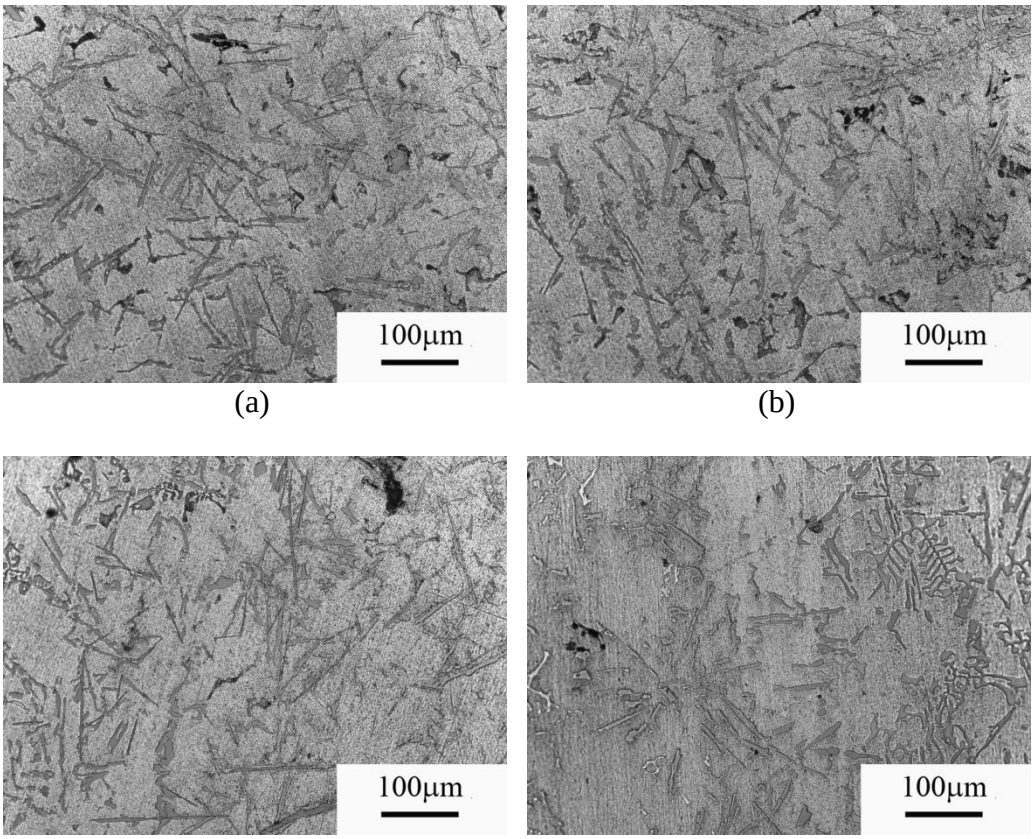


(a) (b)

(c) (d)

*Figure 4.46* Optical sample of different heat treatment time at 515 ℃
a) 0.5 h; b)1 h; c)2 h; d)4 h

Table 4.31 *Parameters of α-AlFeSi and β-AlFeSi morphology of 515 ℃ heat treatment samples with different heat treatment time*

| Heat treatment time | β-length (μm) | β-width (μm) | Aspect ratio | β-fraction(%) | α-fraction(%) |
|---|---|---|---|---|---|
| 0.5 h | 267.12 | 8.92 | 26.79 | 1.32 | 2.24 |
| 1 h | 261.34 | 9.13 | 28.62 | 1.09 | 2.46 |
| 2 h | 156.72 | 5.35 | 27.34 | 0.52 | 2.94 |
| 4 h | 65.13 | 3.21 | 20.31 | 0.31 | 3.26 |

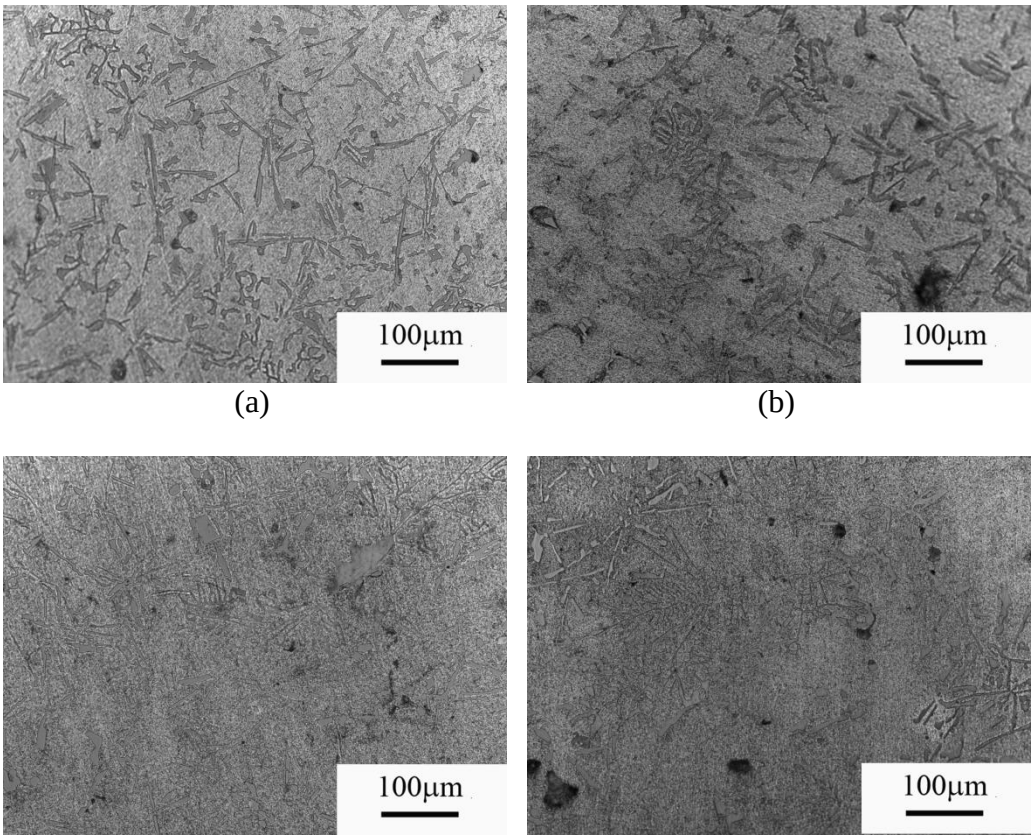


(a) (b)

(c) (d)

*Figure 4.47* Optical sample of different heat treatment time at 525 ℃
a) 0.5 h; b)1 h; c)2 h; d)4 h

Table 4.32 *Parameters of α-AlFeSi and β-AlFeSi morphology of 525 ℃ heat treatment samples with different heat treatment time*

| Heat treatment time | β-length (μm) | β-width (μm) | Aspect ratio | β-fraction(%) | α-fraction(%) |
|---|---|---|---|---|---|
| 0.5 h | 263.13 | 8.43 | 31.21 | 1.19 | 2.30 |
| 1 h | - | - | - | - | 3.17 |
| 2 h | - | - | - | - | 3.32 |
| 4 h | - | - | - | - | 3.28 |

### 4.2.13 Summary

The experimental results shows that increasing cooling rate can reduce the size of AlFeSi phase, while the transformation of α-AlFeSi and β-AlFeSi at different cooling

rates are related with Mn and Fe content in Al-Si alloy. Mn can introduce sludge. Ca and Sr can refine AlFeSi phase but propbably lead to the formation of AlSiCa or AlSiSr intermetallics. K is very effective to change β-AlFeSi to α-AlFeSi and no impurity is introduced. The combination of Mn/Ca and Mn/Sr can eliminate β-AlFeSi. Short-time high temperature heat treatment is another effective way to reduce β-AlFeSi phase.

# CHAPTER 5. DISCUSSION

## 5.1 Nucleation and Growth of β Phase

The basic problem in the study of the formation of AlFeSi phase is the nucleation and growth problem. Iglessis considers that the crystallization of AlFeSi phase is mainly controlled by growth undercooling. (Iglessis, Frantz, & Gantois, 1977). But Narayanan holds the opinion that for crystallization of the AlFeSi phase, of both the nucleation and the growth processes are essential. Therefore, if total undercooling, that is, the sum of nucleation undercooling (ΔTn) and growth undercooling (ΔTc) is greater than a certain critical value(ΔTc), the α phase will crystallize. Otherwise β phase will form. (Narayanan, Samuel, & Gruzleski, 1994). Yin (2001) considers that the greater one of the ΔTn and ΔTc values will determine the nucleate sequence.

As for our opinion, nucleation and growth problems are controlled by a series of factors. Generally speaking, nucleation of β-AlFeSi involves a heterogeneous nucleation process, and ΔTn is mainly controlled by a nucleation substrate such as $Al_2O_3$, MgO, AlP, etc. The growth of β-AlFeSi is in dendrite shape because of the monoclinic structure of β-AlFeSi phase. Thus the growth time (cooling rates) and temperature, crystal structure of substrate for nucleation of β-AlFeSi phase, and addition of other elements are also controlling factors. A brief discussion of these factors is presented.

1) The effect of cooling rates.

It is well known that increasing cooling rates will refine grain size. However, it will also facilitate the transformation of AlFeSi phase. When low cooling rates are used, the stable AlFeSi will have enough time to nucleate and grow. Increasing the cooling rates will suppress the growth time of first nucleate AlFeSi phase and increase the nucleation sites. The result of increasing cooling rates can effectively reduce the size of AlFeSi phase and change the nucleation sequence of different phases.

2) The Al-Fe-Si and Al-Fe-Mn-Si system

Because of the similarity of the Al-Fe-Si and Al-Fe-Mn-Si systems, Mn is usually added to the Al-Fe-Si system to form α-Al(Fe,Mn)Si. However, the stability of α-AlFeSi and β-AlFeSi changed with the addition of Mn.

3) The orientation discrepancy

Orientation discrepancy is very important factor to determine the nucleation suitability between the substrate and the nucleate AlFeSi phase.

4) Other factors

Other factors including the nucleation temperature, the interval of nucleation temperature and eutectic temperature of AlFeSi phase are studied. The effect of the elements on nucleation behavior will be discussed in the next session.

## 5.2 The Nucleation of AlFeSi Phase

There are two types of nucleation, namely homogeneous and heterogeneous. It is commonly known that the formation energy required for homogeneous nucleation is very large, according to the calculation a several hundred degree Kelvin undercooling is

required. Owing to this reason, homogeneous nucleation is seldom observed in our experiment.

In practical systems, the heterogeneous nucleation is the only nucleation format. The surface of the container or other foreign impurity particles in suspension may act as suitable nucleation sites, and hence reduce the nucleation of the sequent phase. This follows because fewer atoms are required to establish a stable nucleus and consequently a smaller nucleation energy barrier corresponds to a much reduced degree of undercooling.

Therefore, the nucleation substrate is an important factor for nucleation. In the beginning, the planner disregistry, that is the lattices of atom spacing between crystal nuclei and catalyst, is decisive. It is reported that some other factors may also control the nucleation effects. (Bramfitt, 1970; Tuttle and Lindsay, 1984). These include (i) the chemical property of the substrates; (ii) the morphology of the matrix (iii) electrostatic potential between interfaces. However, there is no doubt that the fitting of crystal registry is important and is the only quantitatively obtained factor.

Several nucleation agents for AlFeSi phase was proposed and found in this research. The first one is AlP. Sigworth (1987) suggested that P and AlP formed by P have effect on nucleation of AlFeSi phase. Samuel (1999) further suggested AlP is good nucleate substrate of β-AlFeSi phase.

Secondly, oxide layers can be a good substrate for nucleation of AlFeSi phase, which was discussed in detail in pretext. The desired oxide layer for AlFeSi phase includes $Al_2O$, MgO and $K_2O$.

Lastly, it is found some other intermetallics, namely $Al_2CaSi_2$ and $Al_2SrSi_2$, can also be nucleate substrate for AlFeSi phase. This is not reported before. Especially there

phase can only nucleate α-AlFeSi phase, which also a good way to reduce β-AlFeSi phase.

In this chapter, the theory study-planar disregistry will be calculated and the corresponding results will be analyzed. Then the experimental results are present and nucleation hierarchies are obtained.

### 5.2.1 Planar Disregistry

The effectiveness of nucleation of AlFeSi phase on oxide films can be calculated by the planar disregistry δ. As we discussed, it is the only way that be calculated quantitatively. For this reason, it was used as the main calculation of probable nucleation potential and also to evaluate the experimental results. The planar disregistry can be expressed as follows (Cao, 2004a):

$$\delta_{(hlk)_n}^{(hlk)_s} = \sum_{i=1}^{i=3} \frac{\frac{\left|d_{[uvw]_s}\cos\theta - d_{[uvw]_n}\right|}{d_{[uvw]_n}}}{3} \times 100 \qquad (5.1)$$

where $(hlk)_s$= a low-index plane of the substrate;

$[uvw]_s$= a low-index direction in$(hlk)_s$;

$(hlk)_n$= a low-index plane in the nucleated solid;

$[uvw]_n$= a low-index direction in $(hlk)_n$;

$d_{[uvw]_n}$= an interatomic spacing along $[uvw]_n$;

$d_{[uvw]_s}$= an interatomic spacing along $[uvw]_s$; and

θ= an angle between $[uvw]_s$ and $[uvw]_n$.

Campbell (1991) assumed that the electronic (bonding) contribution to the energy of the interface is favorable, if the planar disregistry is less than about 12 pct.

Table 5.1 to 5.9 show calculated results for planar disregistry in our study. A quick review of the data shows that MgO, α-$Al_2O$, $Al_2Si_2Sr$, $Al_2Si_2Ca$, and $K_2O$ are good nucleation substrates of α-AlFeSi. And γ-$Al_2O_3$, CaO and SrO are good substrate for β-AlFeSi. So this can explan why Sr, Ca and K can modify β-AlFeSi and sometimes excessive Sr may lead to formation of β-AlFeSi again.

Table 5.1 *Planar disregistries between $MgO.Al_2O_3$ and α-AlFeSi*

| Match Planes | $[hkl]_s$ | $[hkl]_n$ | $d_{[hkl]s(}$nm) | $d_{[hkl]n(}$nm) | θ | δ(Pct) |
|---|---|---|---|---|---|---|
| $(100)_s//(100)_n$ | [001] | [001] | 3×0.8080 | 2×1.2650 | 0 deg | **4.19** |
| | [011] | [011] | 3×1.1427 | 2×1.7890 | 0 deg | |
| | [010] | [010] | 3×0.8080 | 2×1.2650 | 0 deg | |
| $(100)_s//(111)_n$ | [001] | $[\bar{1}\bar{1}2]$ | 4×0.8080 | 3.0986 | 0 deg | **5.89** |
| | [011] | $[\bar{3}12]$ | 4×1.1427 | 4.7332 | 4.11 deg | |
| | [010] | $[\bar{1}10]$ | 4×0.8080 | 3.5780 | 0 deg | |
| $(111)_s//(110)_n$ | $[\bar{1}\bar{1}2]$ | $[1\bar{1}0]$ | 1.9792 | 1.7890 | 0 deg | **8.06** |
| | $[\bar{1}01]$ | $[1\bar{1}1]$ | 2.2854 | 2.1910 | 5.26deg | |
| | $[\bar{1}10]$ | [001] | 1.1427 | 1.2650 | 0 deg | |
| $(111)_s//(111)_n$ | $[\bar{1}01]$ | $[\bar{1}01]$ | 3×1.1427 | 2×1.7890 | 0 deg | **4.19** |
| | $[\bar{2}11]$ | $[\bar{2}11]$ | 3×1.9792 | 2×3.0986 | 0 deg | |
| | $[\bar{1}10]$ | $[\bar{1}10]]$ | 3×1.1427 | 2×1.7890 | 0 deg | |

Table 5.2 *Planar disregistries between MgO and α-AlFeSi*

| Match Planes | $[hkl]_s$ | $[hkl]_n$ | $d_{[hkl]s(}$nm) | $d_{[hkl]n(}$nm) | θ | δ(Pct) |
|---|---|---|---|---|---|---|
| $(100)_s//(100)_n$ | [001] | [001] | 3×0.4213 | 1.2650 | 0 deg | **0** |
| | [011] | [011] | 3×0.5985 | 1.7890 | 0 deg | |
| | [010] | [010] | 3×0.4213 | 1.2650 | 0 deg | |
| $(100)_s//(111)_n$ | [001] | $[\bar{1}\bar{1}2]$ | 8×0.4213 | 3.0986 | 0 deg | **5.00** |
| | [011] | $[\bar{3}12]$ | 8×0.5985 | 4.7332 | 4.11 deg | |
| | [010] | $[\bar{1}10]$ | 8×0.4213 | 3.5780 | 0 deg | |
| $(110)_s//(110)_n$ | [001] | [001] | 3×0.4213 | 1.2650 | 0 deg | **0.09** |
| | $[\bar{1}11]$ | $[\bar{1}11]$ | 3×0.7297 | 2.1910 | 0 deg | |
| | $[\bar{1}10]$ | $[\bar{1}10]$ | 3×0.5958 | 1.7890 | 0 deg | |
| $(110)_s//(111)_n$ | $[1\bar{1}0]$ | $[\bar{1}\bar{1}2]$ | 5×0.5958 | 3.0986 | 0 deg | **7.72** |
| | $[1\bar{1}1]$ | $[\bar{1}01]$ | 5×0.7297 | 3.5780 | 5.26 deg | |
| | [001] | $[\bar{1}10]$ | 5×0.4213 | 1.7890 | 0 deg | |
| $(111)_s//(110)_n$ | $[\bar{1}\bar{1}2]$ | $[1\bar{1}0]$ | 2×1.0320 | 1.7890 | 0 deg | **9.83** |
| | $[\bar{1}01]$ | $[1\bar{1}1]$ | 2×1.1916 | 2.1910 | 5.26deg | |
| | $[\bar{1}10]$ | [001] | 2×0.5958 | 1.2650 | 0 deg | |
| $(111)_s//(111)_n$ | $[\bar{1}01]$ | $[\bar{1}01]$ | 3×0.5958 | 1.7890 | 0 deg | **0.09** |
| | $[\bar{2}11]$ | $[\bar{2}11]$ | 3×1.0320 | 3.0986 | 0 deg | |
| | $[\bar{1}10]$ | $[\bar{1}10]]$ | 3×0.5958 | 1.7890 | 0 deg | |

Table 5.3 *Planar disregistries between α-$Al_2O_3$ and α-AlFeSi*

| Match Planes | $[hkl]_s$ | $[hkl]_n$ | $d_{[hkl]s(}$nm) | $d_{[hkl]n(}$nm) | θ | δ(Pct) |
|---|---|---|---|---|---|---|
| $(0001)_s//(100)_n$ | $[\bar{1}010]$ | [001] | 3×0.8241 | 2×1.2650 | 0 deg | **6.80** |
| | $[\bar{5}410]$ | [011] | 3×1.2588 | 2×1.7890 | 4.11 deg | |
| | $[\bar{1}2\bar{1}0]$ | [010] | 3×0.9516 | 2×1.2650 | 0 deg | |
| $(0001)_s//(111)_n$ | $[\bar{2}110]$ | $[\bar{1}01]$ | 4×0.4758 | 1.7890 | 0 deg | **6.38** |
| | $[\bar{1}110]$ | $[\bar{2}11]$ | 4×0.8241 | 3.0986 | 0 deg | |
| | $[\bar{1}2\bar{1}0]$ | $[\bar{1}10]$ | 4×0.4758 | 1.2650 | 0 deg | |

Table 5.4 *Planar disregistries between $K_2O$ and α-AlFe*Si

| Match Planes | [hkl]s | [hkl]n | d[hkl]s(nm) | d[hkl]n(nm) | θ | δ(Pct) |
|---|---|---|---|---|---|---|
| (001)s//(001)n | [100] | [100] | 0.7859 | 1.265 | 0 deg | **4.15** |
| | [110] | [110] | 1.11143 | 1.78898 | 0 deg | |
| | [010] | [010] | 0.7859 | 1.265 | 0 deg | |
| (110)s//(110)n | [001] | [001] | 0.7859 | 1.265 | 0 deg | **4.15** |
| | $[\bar{1}11]$ | $[\bar{1}11]$ | 1.361219 | 2.191044 | 0 deg | |
| | $[\bar{1}10]$ | $[\bar{1}10]$ | 1.11143 | 1.78898 | 0 deg | |
| (111)s//(111)n | $[\bar{1}\bar{1}2]$ | $[\bar{1}\bar{1}2]$ | 1.925054 | 3.098605 | 0 deg | **4.44** |
| | $[\bar{3}12]$ | $[\bar{3}12]$ | 2.940569 | 4.733197 | 7.68 deg | |
| | $[\bar{1}10]$ | $[\bar{1}10]$ | 1.11143 | 1.78898 | 0 deg | |

Table 5.5 *Planar disregistries between α-$Al_2Si_2Sr$ and α-AlFeSi*

| Match Planes | [hkl]s | [hkl]n | d[hkl]s(nm) | d[hkl]n(nm) | θ | δ(Pct) |
|---|---|---|---|---|---|---|
| (0001)s//(001)n | $[\bar{1}010]$ | [100] | 2.171472 | 2.53 | 0 deg | **8.39** |
| | $[\bar{5}410]$ | [110] | 3.695226 | 3.57796 | 4.10deg | |
| | $[\bar{1}2\bar{1}0]$ | [010] | 2.732376 | 2.53 | 0 deg | |

Table 5.6 *Planar disregistries between α-$Al_2Si_2Ca$ and α-AlFeSi*

| Match Planes | [hkl]s | [hkl]n | d[hkl]s(nm) | d[hkl]n(nm) | θ | δ(Pct) |
|---|---|---|---|---|---|---|
| (0001)s//(001)n | $[\bar{1}010]$ | [100] | 2.146011 | 2.53 | **0 deg** | **7.90** |
| | $[\bar{5}410]$ | [110] | 3.651899 | 3.57796 | 4.10deg | |
| | $[\bar{1}2\bar{1}0]$ | [010] | 2.700338 | 2.53 | 0 deg | |

Table 5.7 *Planar disregistries between γ-$Al_2O_3$ and β-AlFeSi*

| Match Planes | $[hkl]_s$ | $[hkl]_n$ | $d_{[hkl]s(}$nm) | $d_{[hkl]n(}$nm) | θ | δ(Pct) |
|---|---|---|---|---|---|---|
| $(001)_s$//$(001)_n$ | [100] | [100] | 0.6510 | 0.711 | 0 deg | **8.43** |
| | [110] | [110] | 0.9206 | 1.005 | 0 deg | |
| | [010] | [010] | 0.6510 | 0.711 | 0 deg | |

Table 5.8 *Planar disregistries between SrO and β-AlFeSi*

| Match Planes | [hkl]s | [hkl]n | d[hkl]s(nm) | d[hkl]n(nm) | θ | δ(Pct) |
|---|---|---|---|---|---|---|
| (001)s//(001)n | [100] | [100] | 0.615 | 0.611 | 0 deg | **0.65** |
| | [110] | [110] | 0.869741 | 0.864084 | 0 deg | |
| | [010] | [010] | 0.615 | 0.611 | 0 deg | |

Table 5.9 *Planar disregistries between CaO and β-AlFeSi*

| Match Planes | [hkl]s | [hkl]n | d[hkl]s(nm) | d[hkl]n(nm) | θ | δ(Pct) |
|---|---|---|---|---|---|---|
| (001)s//(001)n | [100] | [100] | 0.609 | 0.611 | 0 deg | **0.32** |
| | [110] | [110] | 0.861256 | 0.864084 | 0 deg | |
| | [010] | [010] | 0.609 | 0.611 | 0 deg | |

So it can be concluded:

$MgO.Al_2O_3 \leftrightarrow \alpha$-AlFeSi $(111)_{MgO.Al2O3}//(110)_{\alpha\text{-AlFeSi}}$

$MgO \leftrightarrow \alpha$-AlFeSi $(100)_{MgO}//(100)_{\alpha\text{-AlFeSi}}$

$\alpha\text{-}Al_2O_3 \leftrightarrow \alpha$-AlFeSi $(0001)_{\alpha\text{-}Al2O3}//(111)_{\alpha\text{-AlFeSi}}$

$K_2O \leftrightarrow \alpha$-AlFeSi $(001)_{K2O}//(001)_{\alpha\text{-AlFeSi}}$

$\alpha\text{-}Al_2Si_2Sr \leftrightarrow \alpha$-AlFeSi $(0001)_{Al2Si2Sr}//(001)_{\alpha\text{-AlFeSi}}$

$\alpha\text{-}Al_2Si_2Ca \leftrightarrow \alpha$-AlFeSi $(0001)_{Al2Si2Ca}//(001)_{\alpha\text{-AlFeSi}}$

$\gamma\text{-}Al_2O_3 \leftrightarrow \beta$-AlFeSi $(001)_{\gamma\text{-}Al2O3}//(001)_{\beta\text{-AlFeSi}}$

$SrO \leftrightarrow \beta$-AlFeSi $(001)_{SrO}//(001)_{\beta\text{-AlFeSi}}$

$CaO \leftrightarrow \beta$-AlFeSi $(001)_{CaO}//(001)_{AlFeSi}$

### 5.2.2 Possible Sequence of Phase Solidification in A380 Alloys

Figure 5.1 shows the nucleation hierarchy from our experiments and literature (Samuel, Samuel, & Doty, 1996; Cao & Cambell, 2004). Oxide layers can nucleate α-AlFeSi and β-AlFeSi. AlFeSi and β-AlFeSi can nucleate each other. $Al_2CaSi_2$, $Al_2SrSi_2$

and $K_2O$ can nucleate β-AlFeSi. Also, all phases mentioned above can nucleate the Si phase.

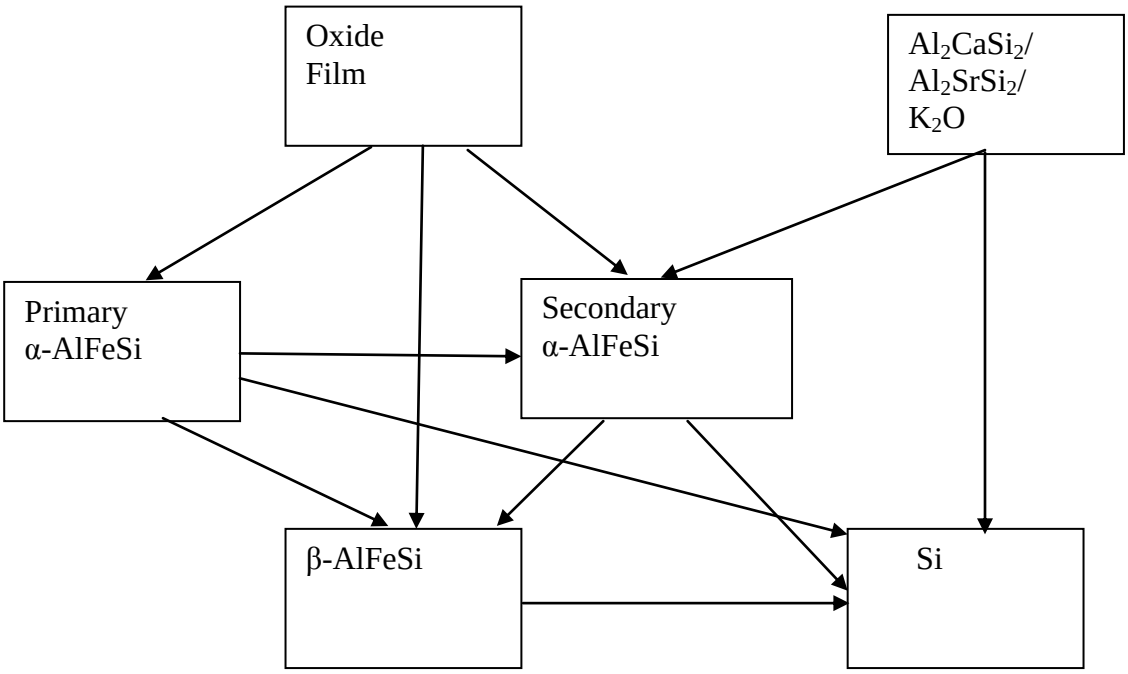


*Figure 5.1* Possible nucleation hierarchies in A380 (alloy arrows refer to the nucleated phase)

Figure 5.2 shows the nucleation relation of A380 alloy from our experiment. Fig 5.2 a-c shows both α-AlFeSi and β-AlFeSi can nucleate from the oxide layer (mainly $Al_2O_3$ or MgO). With K addition, it can be proved that $K_2O$ can be the the nucleation agent for α-AlFeSi, shown in 5.2 f. As for samples with Sr and Ca addition, $Al_2SrSi_2$ and $Al_2CaSi_2$ can be the nucleation substrate of α-AlFeSi, shown in Figure 5.2 d and e. Lastly, α-AlFeSi and β-AlFeSi can be the nucleation substate for each other, and they can also nucleate Si phase, which is shown in Figure 5.2 g-j.

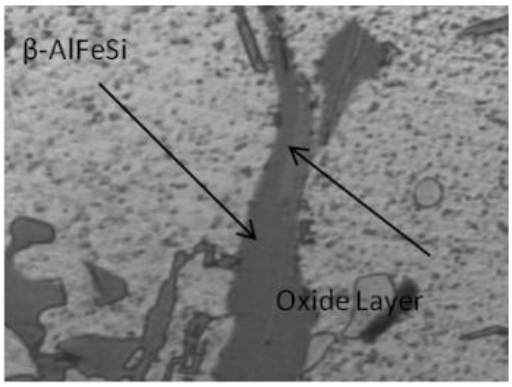
β-AlFeSi
Oxide Layer

(a)

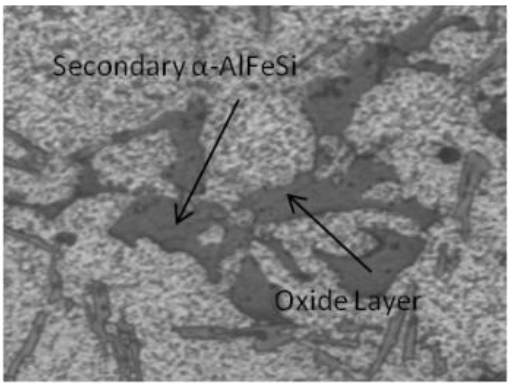
Secondary α-AlFeSi
Oxide Layer

(b)

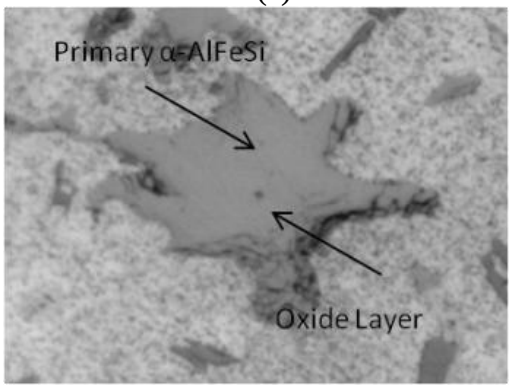
Primary α-AlFeSi
Oxide Layer

(c)

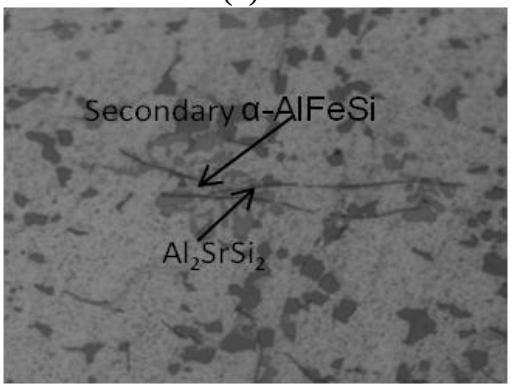
Secondary α-AlFeSi
Al2SrSi2

(d)

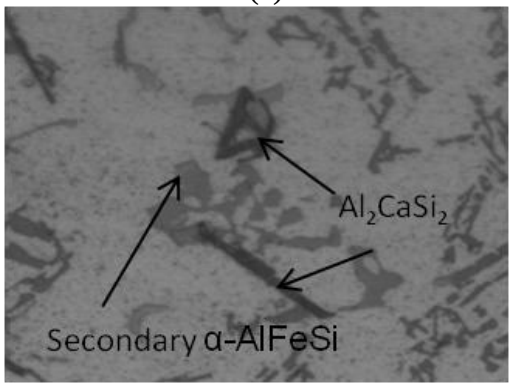
Al2CaSi2
Secondary α-AlFeSi

(e)

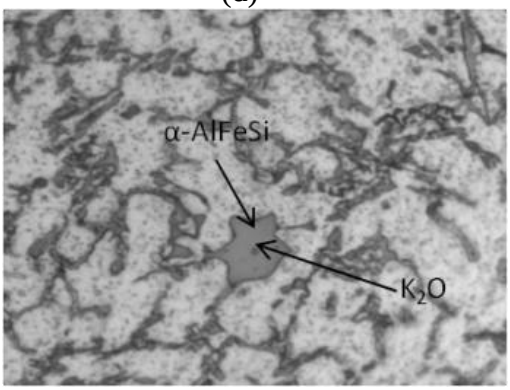
α-AlFeSi
K2O

(f)

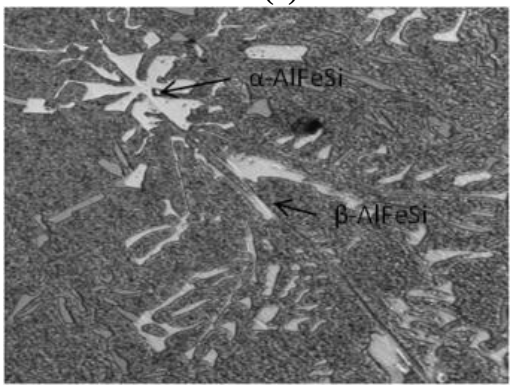
α-AlFeSi
β-AlFeSi

(g)

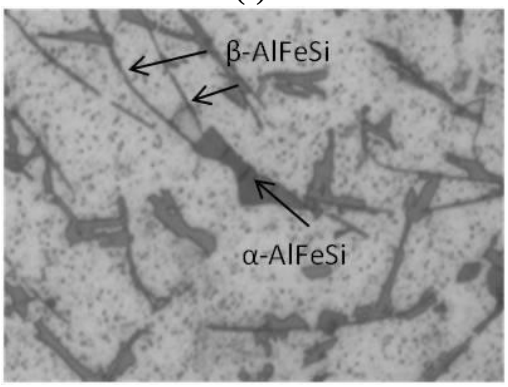
β-AlFeSi
α-AlFeSi

(h)

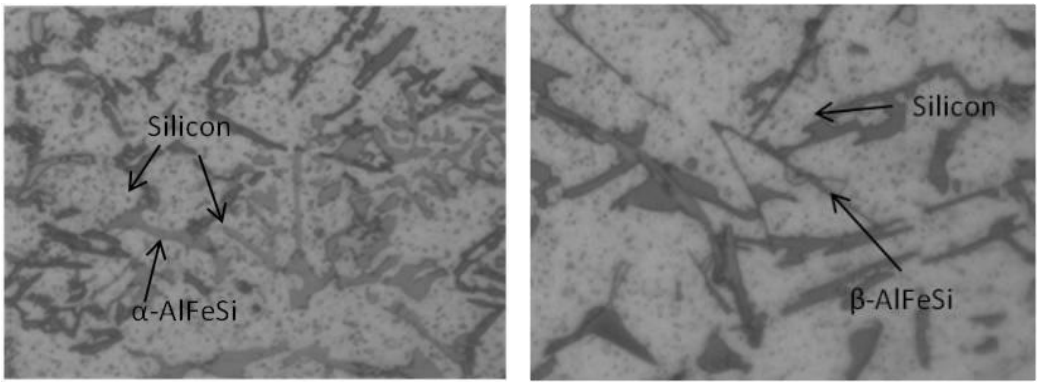


(i) (j)

*Figure 5.2* Nucleation relation in A380 (alloy arrows refer to the nucleated phase) a)oxide layer→ β-AlFeSi; b) oxide layer→ primary α-AlFeSi; c) oxide layer→ secondry α-AlFeSi; d) $Al_2SrSi_2$→ secondry α-AlFeSi; e) $Al_2CaSi_2$→ secondry α-AlFeSi; f) $K_2O$→ secondry α-AlFeSi; g) β-AlFeSi→ α-AlFeSi; (h) α-AlFeSi→β-AlFeSi; (i) α-AlFeSi→silicon; (j) β-AlFeSi →silicon

## 5.3 The Growth of AlFeSi Phase

The growth of the AlFeSi phase is mainly affected by the two factors. The first is the composition of the alloy, especially the content of the element Fe, Si and Mn. The second is the cooling rates. Cooling rates can both control the size and affect the stability of AlFeSi phase accompanying the composition of the alloy. In this section the Al-Si-Fe and Al-Si-Mn-Fe system will be discussed respectively.

### 5.3.1 Al-Fe-Si System

Al-Si-Fe system without Mn addition is different from Al-Fe-Mn-Si system. In Al-Si-Fe systems, β-AlFeSi is the stable phase which forms prior to the α-AlFeSi phase. Comparatively, α-AlFeSi is a metastable phase. At low cooling rate, β-AlFeSi will form first and will be the predominate phase. At a high cooling rate, α-AlFeSi will take place of β-AlFeSi (Narayanan, Samuel, & Gruzleski, 1993). Narayannan explained the reason

that the increasing cooling rates, leads to the decrease of staring nucleation temperature of β-AlFeSi phase. Hence the size of β-AlFeSi decreased. α-AlFeSi will be nucleate at the last stage of nucleation. From the results of the simulation, this explanation is reasonable. If Mn content is 0, under equilibrium condition, no α-AlFeSi can form.Figure 5.3 gives an example. Only at high cooling rates, the formation of β-AlFeSi is suppressed and α-AlFeSi can form.

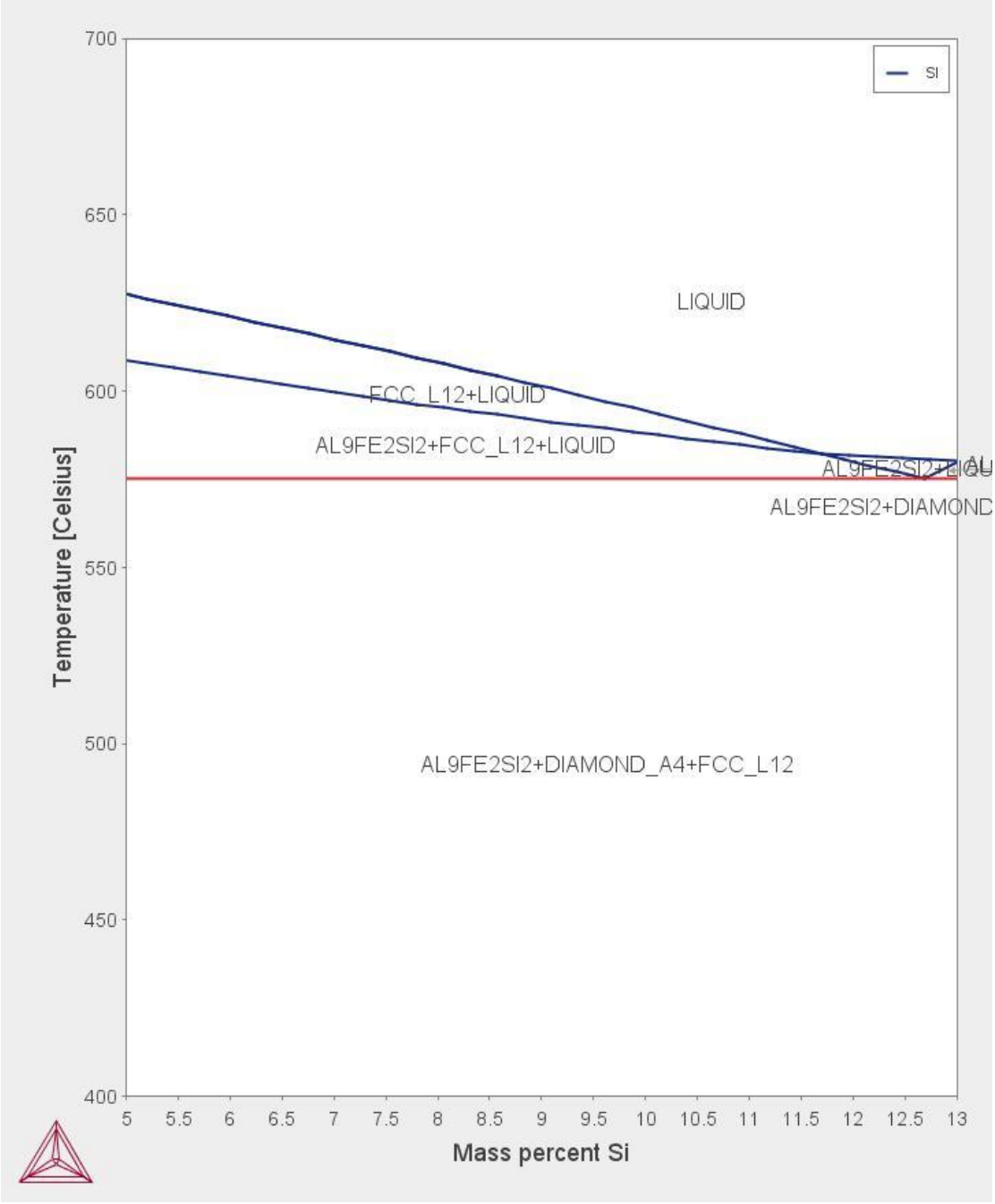


*Figure 5.3* Al-0.1Fe-xSi phase diagram

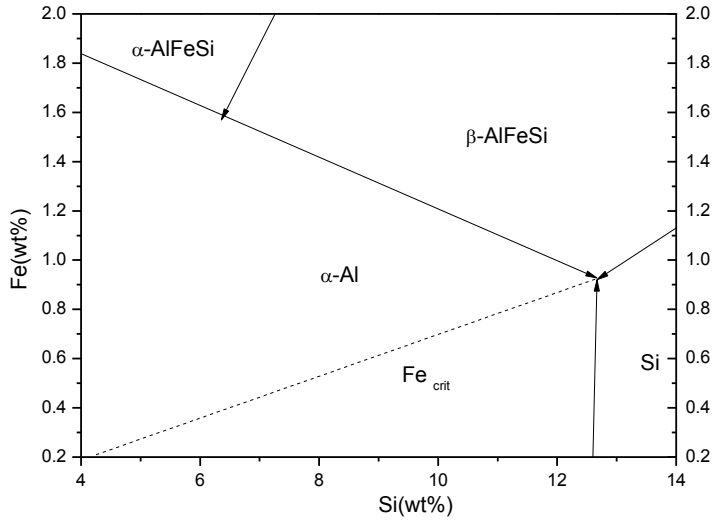


*Figure 5.4* AlFeSi liquidus projection

Figure 5.4 shows the AlFeSi liquidus projection. If the Fe content is less than 0.9%, there is no formation of primary AlFeSi phase. The dashed line is the critical Fe line. If the composition is under the dashed line, no pre-eutectic β-AlFeSi phase will form. However only if the alloy has a high Fe and low Si content, which means the composition is in the α-AlFeSi zone (left top part of the phase diagram), both primary α-AlFeSi and β-AlFeSi will precipitate prior to fcc α-Al. This condition would severely degrade the mechanical property of the Al-Si alloy. So typically, with the range of Si content of die-casting alloy (>7.5%), β-AlFeSi phase will be the stable phase and will form prior to the α-AlFeSi phase.

### 5.3.2 Al-Fe-Mn-Si System

In the presence of high manganese content, the iron compound crystallizes in the α phase (Chinese script morphology) at low cooling rates and in both the α and β phases

(Chinese script morphology and needlelike morphology) at high cooling rates. The reasons can be explained by the phase diagram of Figure 4.3.

If the Mn content is low, the situation is the same as that in Al-Fe-Si system. If the Mn content continues to increase, the primary α-AlFeSi predominates. The increasing cooling rate mainly suppresses the formation of the primary α-AlFeSi so that β-AlFeSi can appear. If the Fe content is high, the situation is similar. The primary α-AlFeSi phase is suppressed and thus it can be used to form β-AlFeSi at high cooling rates.

5.3.2.1 Phase fraction of AlFeSi vs Temperature

In this section, the change of the fraction of α-AlFeSi and β-AlFeSi phase vs temperature while varying the content of Si, Mn, Fe elements is discussed. The purpose is to determine the fraction of α-AlFeSi and β-AlFeSi formed before formation of fcc α-Al dendrite (primary phase), with formation of fcc α-Al dendrite (secondary phase) and with the formation of eutectic Si (ternary phase). With the formation termperatures of fcc α-Al and eutectic silicon from Figure 4.12, 4.15 and 4.19, the fraction of primary, secondary and ternary α-AlFeSi and β-AlFeSi can be decided from the diagrams of phase fraction of AlFeSi vs temperature (Figure 5.5-5.7). The effect of element variation on the formation of AlFeSi phase is analyzed in detail.

1) The change of Si

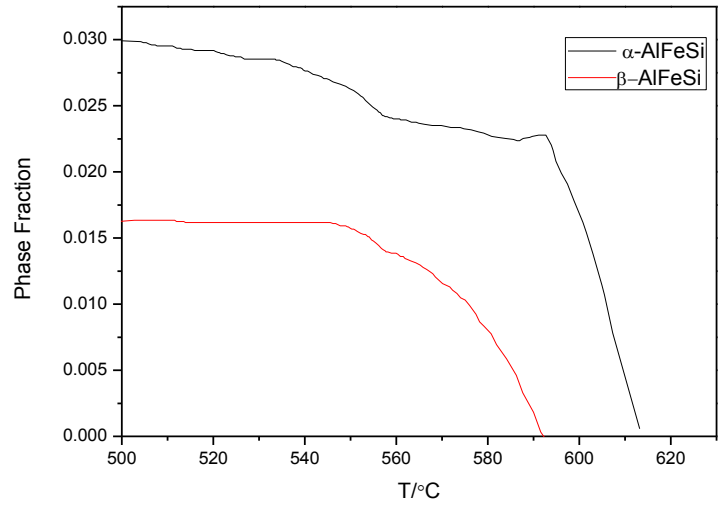
α-AlFeSi
β–AlFeSi
Phase Fraction
0.030
0.025
0.020
0.015
0.010
0.005
0.000
500
520
540
560
580
600
620
T/°C

a)

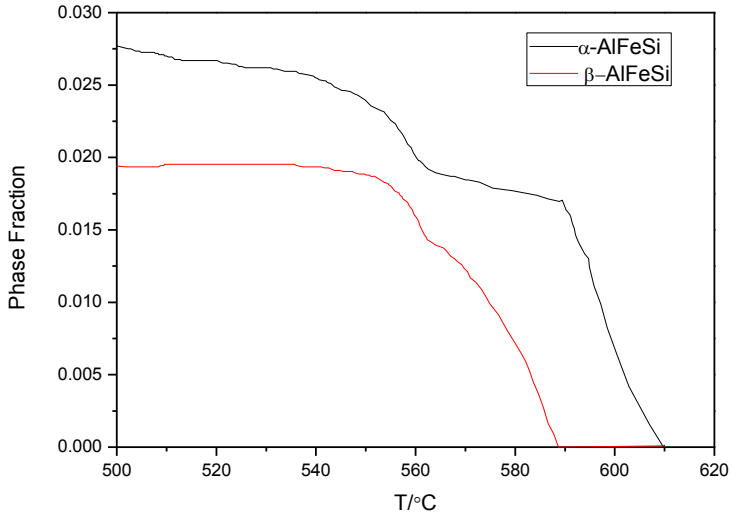
α-AlFeSi
β–AlFeSi
Phase Fraction
0.030
0.025
0.020
0.015
0.010
0.005
0.000
500
520
540
560
580
600
620
T/°C

b)

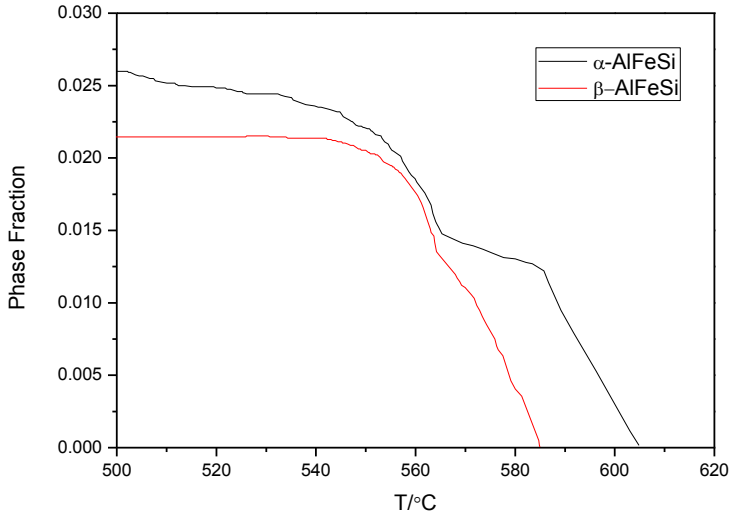
α-AlFeSi
β–AlFeSi
Phase Fraction
0.030
0.025
0.020
0.015
0.010
0.005
0.000
500
520
540
560
580
600
620
T/°C

c)

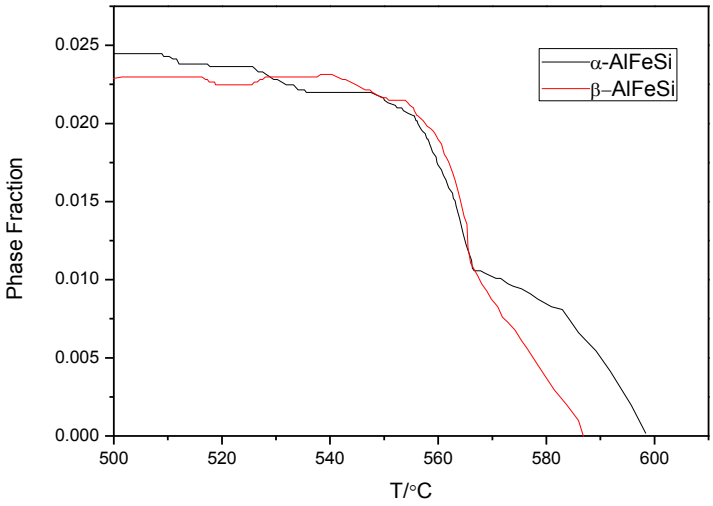


d)

*Figure 5.5* The diagram of phase fraction vs. temperature
a) 380 5Si b) 380 7Si; c) 380 9Si; d) 380 11Si

All graphs in Figure 5.5 have similar trends that indicate that α-AlFeSi increase rapidly in the predendrite and dendrite stage, until the starting formation of the β-AlFeSi phase, where the first inflection points can be found. After that, β-AlFeSi begins to form in large quantities while the formation of α-AlFeSi is slower. The other inflection point for α-AlFeSi is eutectic temperature. After that point, both α-AlFeSi and β-AlFeSi form rapidly until 540 ℃ where all Fe is consumed.

Table 5.10 *The percent of different styles α-AlFeSi and β-AlFeSi in A380-xSi alloy*

| Style | 380 5Si | 380 7Si | 380 9Si (380) | 380 11Si |
|---|---|---|---|---|
| Primary α | - | 0.5 | 1.25 | 1.2 |
| Secondary α | 2.5 | 1.4 | 0.25 | 0.2 |
| Ternary α | 0.5 | 0.85 | 1.2 | 1.2 |
| Total α | 3 | 2.75 | 2.7 | 2.6 |
| Primary β | - | - | - | 0.8 |
| Secondary β | 1.3 | 1.4 | 1.4 | 0.3 |
| Ternary β | 0.3 | 0.4 | 0.8 | 1 |
| Total β | 1.6 | 1.8 | 2.2 | 2.3 |

From table 5.10, it can be seen that with the increase of Si content, the total α phase decreases,the total amount of the primary and secondary α phase increase as Si content is increased. On the other hand both the total β phase and primary and secondary β phase increases. Thus the content of Si should be limited.

2) The change of Mn

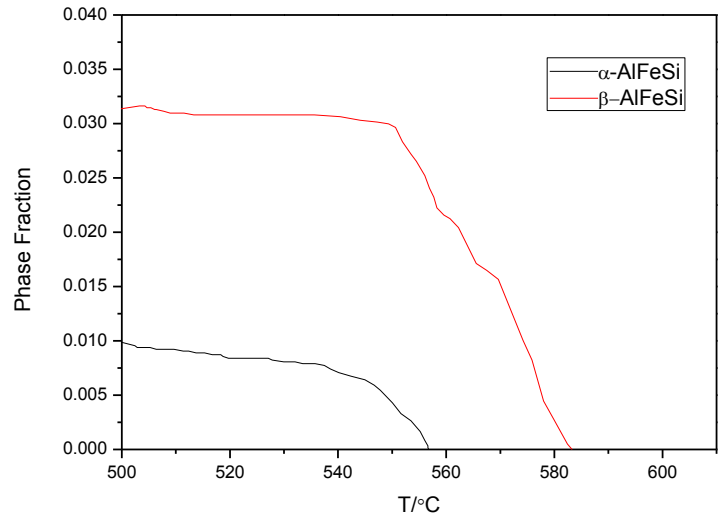


(a)

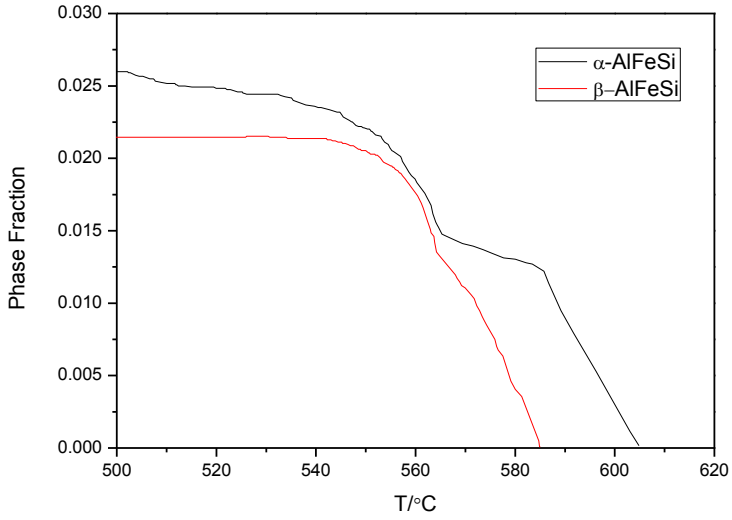


(b)

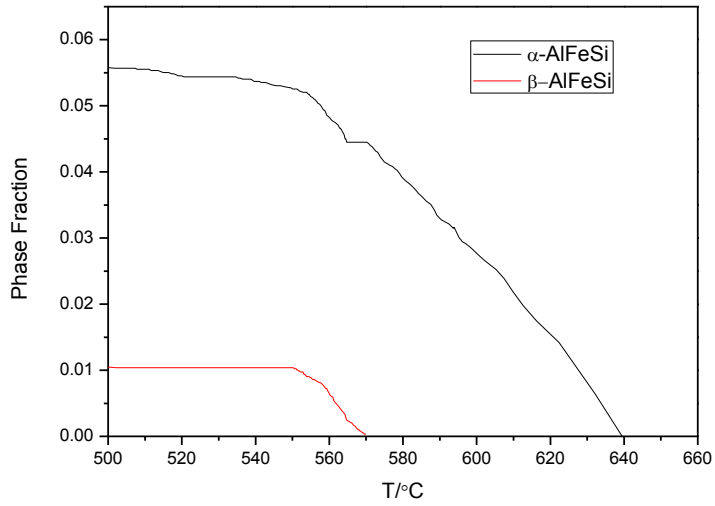


(c)

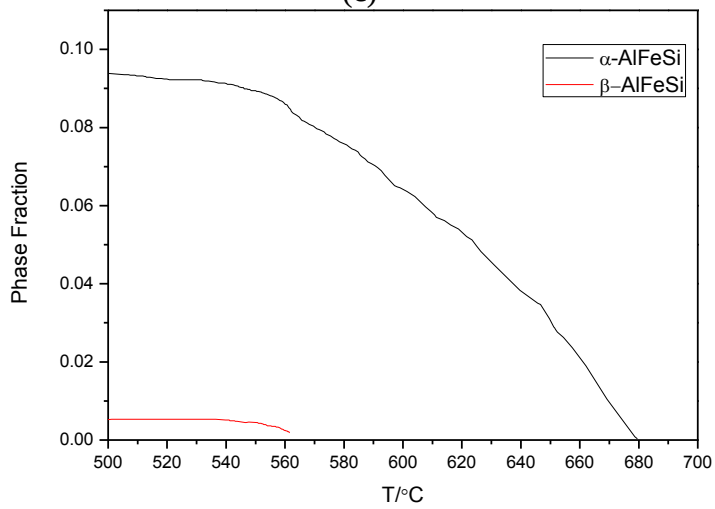


(d)

*Figure 5.6* The diagram of phase fraction vs. temperature
a) 380 0.2Mn b) 380 0.4Mn; c) 380 1Mn; d) 380 2Mn

The presence of the element Mn can postpone the starting formation temperature of β-AlFeSi phase. Figure 5.6 and Table 5.11 show that with Mn addition, the fraction of α-AlFeSi phase, especially the primary α-AlFeSi phase, increases as expected. Although the amount of β-AlFeSi phase is controlled, the primary α-AlFeSi can act as sludge and degrade the ductility of the alloys.

Table 5.11 *The percent of different styles α-AlFeSi and β-AlFeSi in A380-xMn alloy*

| Percent | 380 0.2mn | 380 0.4Mn(380) | 380 1Mn | 380 2Mn |
|---|---|---|---|---|
| Primary α | - | 1.25 | 3.5 | 7.5 |
| Secondary α | - | 0.25 | 1 | 0.7 |
| Ternary α | 0.75 | 1.2 | 1.1 | 1.2 |
| Total α | 0.75 | 2.7 | 5.6 | 8.4 |
| Primary β | 0.75 | - | - | - |
| Secondary β | 3.45 | 1.4 | 0.25 | |
| Ternary β | 0.7 | 0.8 | 0.85 | 0.5 |
| Total β | 4.9 | 2.2 | 1.1 | 0.5 |

3) The change of Fe

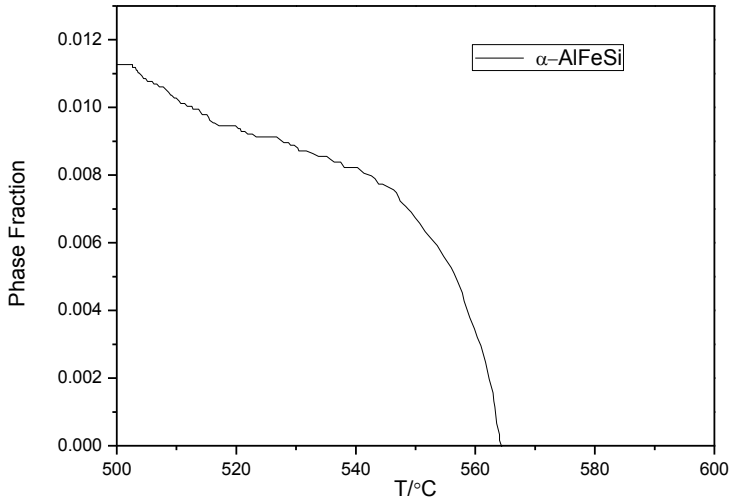


a)

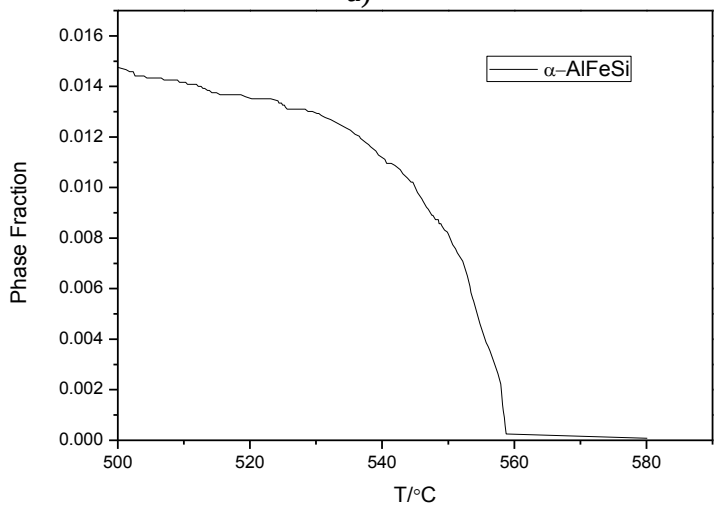


b)

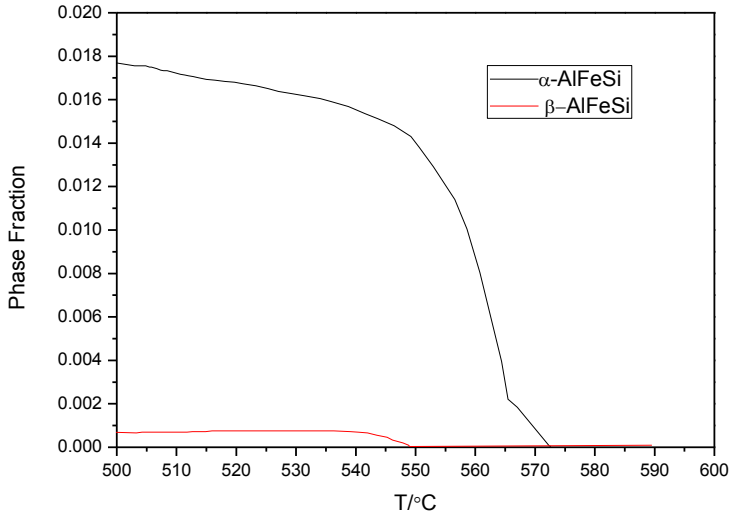
α-AlFeSi
β–AlFeSi
Phase Fraction
T/°C
0.020
0.018
0.016
0.014
0.012
0.010
0.008
0.006
0.004
0.002
0.000
500
510
520
530
540
550
560
570
580
590
600

(c)

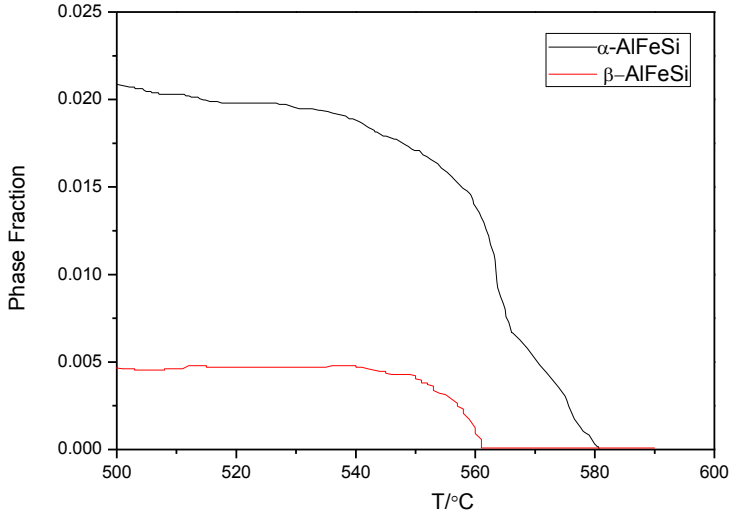
α-AlFeSi
β–AlFeSi
Phase Fraction
T/°C
0.025
0.020
0.015
0.010
0.005
0.000
500
520
540
560
580
600

(d)

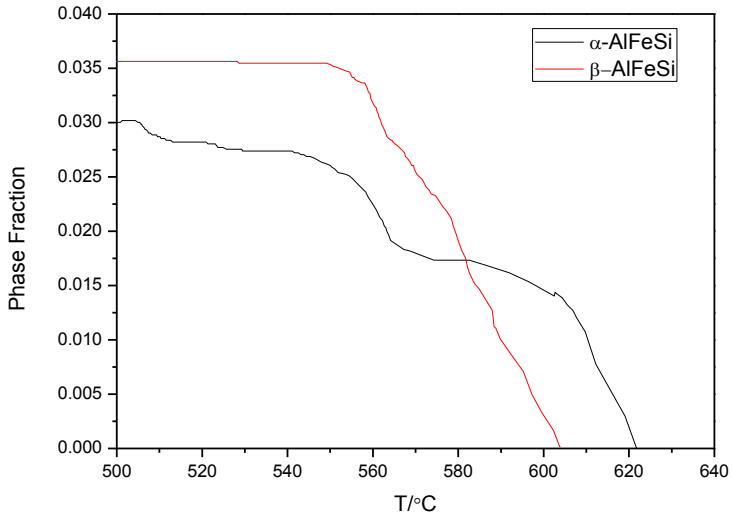


(e)

F*igure 5.7* The diagrams of phase fraction vs. temperature
a) 380 0Fe; b) 380 0.1Fe; c) 380 0.2Fe; d) 380 0.4Fe; e) 380 1.5Fe

From the diagrams of phase fraction and temperature in Figure 5.7, it can be seen that if the Fe content is lower than 0.2%, most α is ternary phase and that it forms in the range of 540-560 ℃, post-eutectic range. As the Fe content is increased to 0.4%, primary α-AlFeSi begins to form. However once the binary β-AlFeSi begins to form, the formation rate of α-AlFeSi is reduced. That means the formation of α-AlFeSi and β-AlFeSi is competing. A similar trend in the case of occurs. Here the first-nucleate α-AlFeSi is restricted by the following formation of the primary β-AlFeSi phase. It is also worthr noting that both the formation rate of α-AlFeSi and β-AlFeSi start to increase around 560 ℃, where eutectic reaction takes place.

Table 5.12 *The percent of different styles α-AlFeSi and β-AlFeSi in A380-xMn alloy*

| Fraction (%) | 380 0Fe | 380 0.1Fe | 380 0.2Fe | 380 0.4Fe | 380 0.7Fe | 380 1Fe (380) | 380 1.5Fe |
|---|---|---|---|---|---|---|---|
| Primary α | - | - | - | - | 0.3 | 1.25 | 3.3 |
| Secondary α | - | - | 0.25 | 0.75 | 1.0 | 0.25 | 0.2 |
| Ternary α | 0.6 | 1.5 | 1.5 | 1.35 | 1.0 | 1.2 | 0.2 |
| Total α | 0.6 | 1.5 | 1.75 | 2.1 | 2.3 | 2.7 | 3.5 |
| Primary β | - | - | - | - | - | - | 2.3 |
| Secondary β | - | - | - | - | 0.5 | 1.4 | 2.7 |
| Ternary β | - | - | 0.2 | 0.45 | 0.8 | 0.8 | 0.5 |
| Total β | - | - | 0.2 | 0.45 | 1.3 | 2.2 | 5.5 |

From table 5.12, it can be seen that at high levels of Fe concentration, the amount of α and β AlFeSi increases, especially the primary α and primary and secondary β increases. This condition will have a negative impact on the mechanical property of the aluminum diecasting alloy.

5.3.2.2 Al-Fe-Si-Mn Liquidus Projection

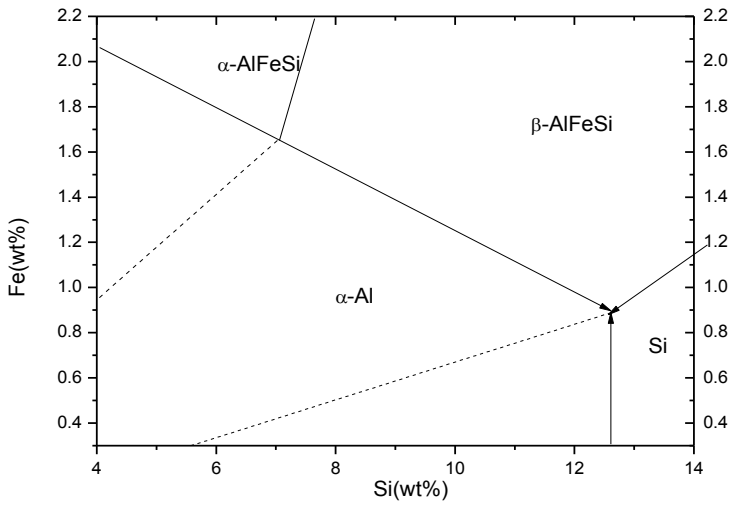


*Figure 5.8* Al-Fe-Si-0.1Mn liquidus projection

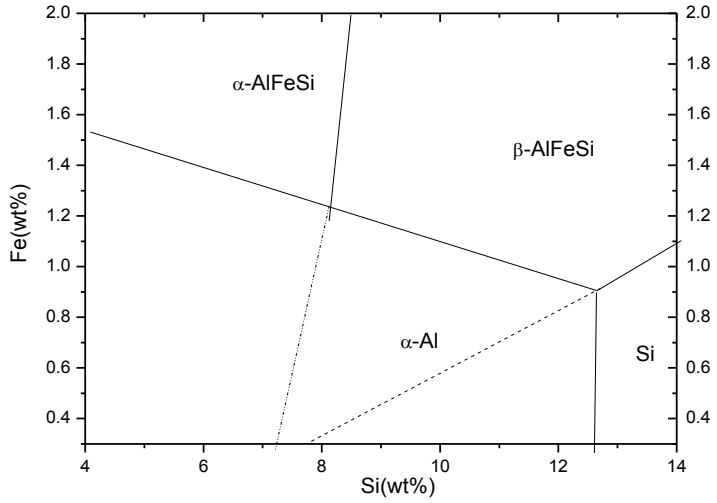


*Figure 5.9* Al-Fe-Si-0.2Mn liquidus projection

Figures 5.8 to 5.12 contain Al-Fe-Si-xMn liquidus projections, where Mn varies from 0.1 to 0.5. With the addition of Mn, β-AlFeSi phase are replaced by the α-AlFeSi, which can be seen from the Figure 5.8 and 5.9, where α-AlFeSi zone was enlarged.

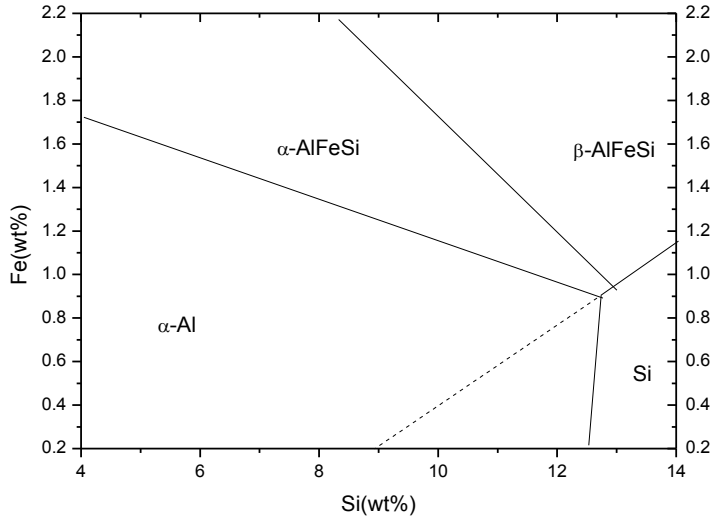


*Figure 5.10* Al-Fe-Si-0.3Mn liquidus projection

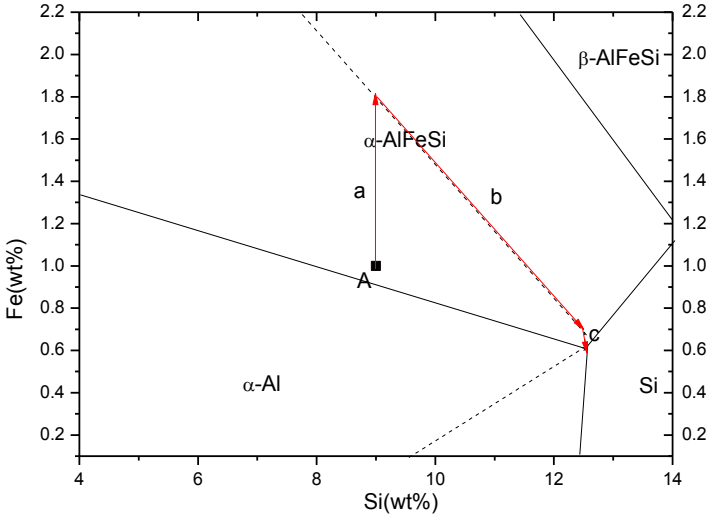


*Figure 5.11* Al-Fe-Si-0.4Mn liquidus projection

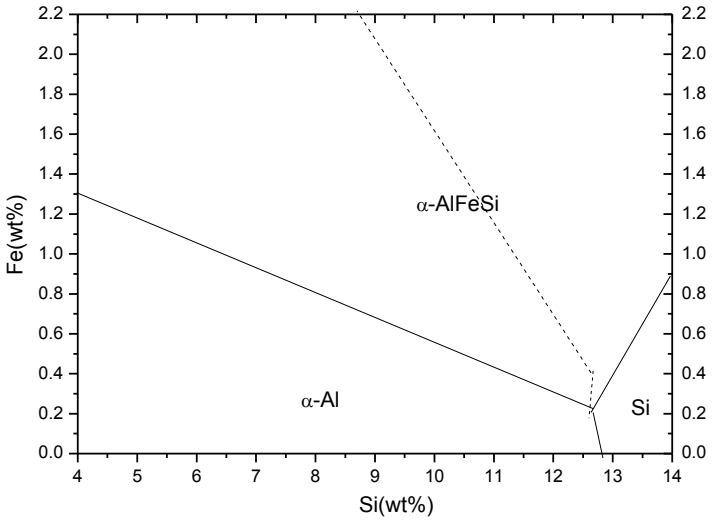


*Figure 5.12* Al-Fe-Si-0.5Mn liquidus projection

If the content of Mn elements goes up to 0.4 percent as shown in Figure 5.11, there is no direct boundary of α-Al and β-AlFeSi zone.Point A in Figure 5.11 represents the composition of A380, and the red line shows its solidification path. Line (a) indicates the formation of primary α-AlFeSi, which occurs until the trough between the α-AlFeSi and β-AlFeSi phases. The reaction continues involving the formation of secondary α-

AlFeSi and β-AlFeSi along the line (b) until the ternary eutectic composition is reached, and Al, Si and α-AlFeSi form together in the ternary eutectic along line (c).

5.3.2.3 Summary

According to the results from optical images and phase diagram in section 4.2.3 and 4.2.4, and this section, several phenomena and results can be observed. First, the higher cooling rates can reduce the size of both α and β-AlFeSi phase. It is well known that higher cooling rates can suppress the formation of the AlFeSi phase and reduce growth time. Thus there is insufficient time for AlFeSi phase to grow to a large size. Secondly, with different Mn addition, increasing cooling rates may either favor or oppose the formation of β-AlFeSi. Especially in the A380-1Mn sample, as cooling rates increase, almost all the β-AlFeSi phase transfers to α-AlFeSi. In the author's opinion, this situation must be considered as cooling rates, Mn content, Si content, Fe/Mn ratio are varied. Here Fe/Mn is considered as a critical parameter and three situations are examined.

1) If the Mn content is below 0.3wt%, or the Fe: Mn>3:1

If Mn content is low, the situation is similar to Al-Fe-Si system without the presence of Mn. Here β-AlFeSi is the primary stable phase and increasing cooling rate will suppress the formation of β-AlFeSi phase.Under this situation, from the simulation results and experimental results, in addition to some reference, β-AlFeSi is the predominant phase compared to α-AlFeSi. (Narayanan, Samuel, & Gruzleski, 1994) The relation of cooling rates and AlFeSi phase fraction is similar to that of the AlFeSi ternary alloys. Without the addition of Mn, β-AlFeSi is the stable phase and α-AlFeSi phase is the metastable phase. β-AlFeSi will be the primary phase and α-AlFeSi will form in the main eutectic stage. The higher cooling rates reduce the starting formation temperature of

the β-AlFeSi phase.With decreasing starting temperature of the β-AlFeSi phase, of the growth time of the β-AlFeSi phase is reduced and therefore the length and volume fraction of this phase decrease until the β-AlFeSi phase start temperature merges with the silicon eutectic temperature. At the end of the formation of the silicon eutectic stage, the remaining liquid, depleted in silicon, favors crystallization of the α-AlFeSi phase.

The equilibrium reaction subsequences are:

1)L→β-AlFeSi

2)L→Al+β-AlFeSi

3) L→Al+β-AlFeSi+Si

4) β-AlFeSi+L→α-AlFeSi+Al+Si

Thus with high cooling rates, reaction 1 is suppressed. So the fraction of α-AlFeSi is increased.

2) If the Mn content is between 0.3-0.9wt%, or the 1:1<Fe:Mn<3:1

In this range the stability of α-AlFeSi increases and that of β-AlFeSi decreases. At a cooing rate of 0.05°C/s, α-AlFeSi takes up a higher fraction. With increase in cooling rates, the size of α-AlFeSi and β-AlFeSi phases decrease. While the fraction of β-AlFeSi increases, and that of α-AlFeSi decreases. However, this change is not the dominate change observed for two reasons. First, the higher cooling rates mainly suppress formation of primary α-AlFeSi, while reducing the starting formation temperature of α-AlFeSi. Thus a fraction of α-AlFeSi is formed at the post dendrite and post main eutectic stages. Second the peritectic reaction can occur:

L+β-AlFeSi=Al+Si+α-AlFeSi can take place.

The equilibrium reaction subsequences are:

1)L→α-AlFeSi

2)L→Al+α-AlFeSi

3) L→Al+α-AlFeSi+β-AlFeSi

4) β-AlFeSi+L→α-AlFeSi+Al+Si

Thus with high cooling rates, reaction 1 is suppressed and reaction 4 is enhanced. While the fraction of α-AlFeSi and β-AlFeSi remains stable.

3) If the Mn content is more than 0.9wt%, or the Fe:Mn<1:1

Under low cooling rates, no visible β-AlFeSi can be seen from the 0.05 ℃/s and 1 ℃/s cooling rates. In the phase diagram, it is shown that only a negligible amount of eutectic β-AlFeSi can form. However, with higher cooling rates, the iron is not all consumed by α-AlFeSi in a short period. Thus the remaining high Fe in residual liquid favors the formation of β-AlFeSi, and of depressing the formation of α-AlFeSi.This situation makes the eutectic β-AlFeSi phase clearer to observe.

The resulting equilibrium reaction subsequences are:

1)L→α-AlFeSi

2)L→Al+α-AlFeSi

3) L→Al+α-AlFeSi+Si

4)L→Al+β-AlFeSi+Si

At high cooling rates, reaction 1 severely is suppressed. So the fraction of β-AlFeSi increases.

This also can be explained by the phase diagram shown in Figure 4.3. If the Mn content is lower than 0.3%, β-AlFeSi is the primary phase, and high cooling rates will suppress the formation of β-AlFeSi. With the addition of Mn content, α-AlFeSi phase

becomes the primary phase and its presence will change the stability of α-AlFeSi/β-AlFeSi. If the Mn content is over 0.9%, β-AlFeSi will only form in the eutectic stage. Thus, the low cooling rate will lead to the formation of a desirable amount of primary and secondary α-AlFeSi.

4) High Fe situation(Fe>1.1wt%)

If Fe content is further increased, the trend of the effect of cooling on the AlFeSi phase becomes similar to that of a high Mn A380 alloy. In the case of A380-1.5Fe and A380-2Fe alloys, if cooling rates are high, β phase predominates. Comparatively, polygon and Chinese script α-AlFeSi phase can be found in the slow cooling samples. From the phase diagram it can be seen that with Fe addition, primary β-AlFeSi phase can form if Fe content is greater than 1.1 %wt. However, under at Fe levels, primary α-AlFeSi phase is still the first phase to precipitate and Fe addition would increase its formation starting temperature. Therefore, in slow cooling situations, primary α-AlFeSi will consume Fe first and leave residual Fe for the formation of the primary β-AlFeSi and secondary AlFeSi phases. Since the higher cooling rates suppress the formation of primary α-AlFeSi, the β-AlFeSi will nake use of residual Fe. Primary β-AlFeSi, without competition from α-AlFeSi, will distribute itself freely and uniformly throughout the sample.

The equilibrium reaction subsequences are:

1)L→α-AlFeSi

2) L→α-AlFeSi+β-AlFeSi

3)L→Al+α-AlFeSi+β-AlFeSi

4) L→Al+α-AlFeSi+β-AlFeSi+Si

5)L→Al+α-AlFeSi+Si

6) β-AlFeSi+L→α-AlFeSi+Al+Si

Thus with high cooling rates, reaction 1 is severely suppressed. So the fraction of β-AlFeSi increases.

In summary, with low Mn and Fe, β-AlFeSi phase is a stable phase and can be formed using low cooling rates. With addition of Mn or Fe, the stability of α-AlFeSi increases and high cooling rates can obstrcuct the formation of α-AlFeSi phase.

## 5.4 The Element Addition

Addition of some minor element is another way to refine AlFeSi, especially β-AlFeSi. The elements Ca, Sr, K and Mg are used and their mechanism to refine the β-AlFeSi phase is examined in the section that follows.

(a) Ca

There is a report showing that a small amount of calcium addition is can improve the toughness of Al-Si alloy (Kobayashi, 1997). Another advantage of Ca addition is that Calcium can simultaneous refine both AlFeSi and eutectic Si.

Kumari proposed that the refine effect of Ca on β-AlFeSi is because of the fragmentation of β-platelet. With the addition of Ca, it was also proposed that the higher diffusion coefficient of Si than Fe would lead to the fragmentation of the β-$Al_5FeSi$ phase platelets in the presence of Ca. (Kumari, Pillai & Pai, 2008).

With low Ca content, the size of β-$Al_5FeSi$ is reduced. This is in agreement with the fragment theory. However, if Ca content reaches to 0.1%, more α-AlFeSi is formed and no apprarent β-$Al_5FeSi$ can be detected. This behavior cannot be explained by

fragment theory. However nucleation theory can explain this. We can see that $Al_2CaSi_2$ phase is connected with α-AlFeSi. Because large polygon and needle-like β-$Al_5FeSi$ can be seen, and some of the $Al_2CaSi_2$ phase is inside or throughout the dendrites, so $Al_2CaSi_2$ phase is designated as the primary phase. Because some secondary α-AlFeSi grows from the $Al_2CaSi_2$ phase, it consumes the Fe in the formation of β-$Al_5FeSi$. Also, the $Al_2CaSi_2$ phase can nucleate other phases, including Si and $Al_2Cu$.

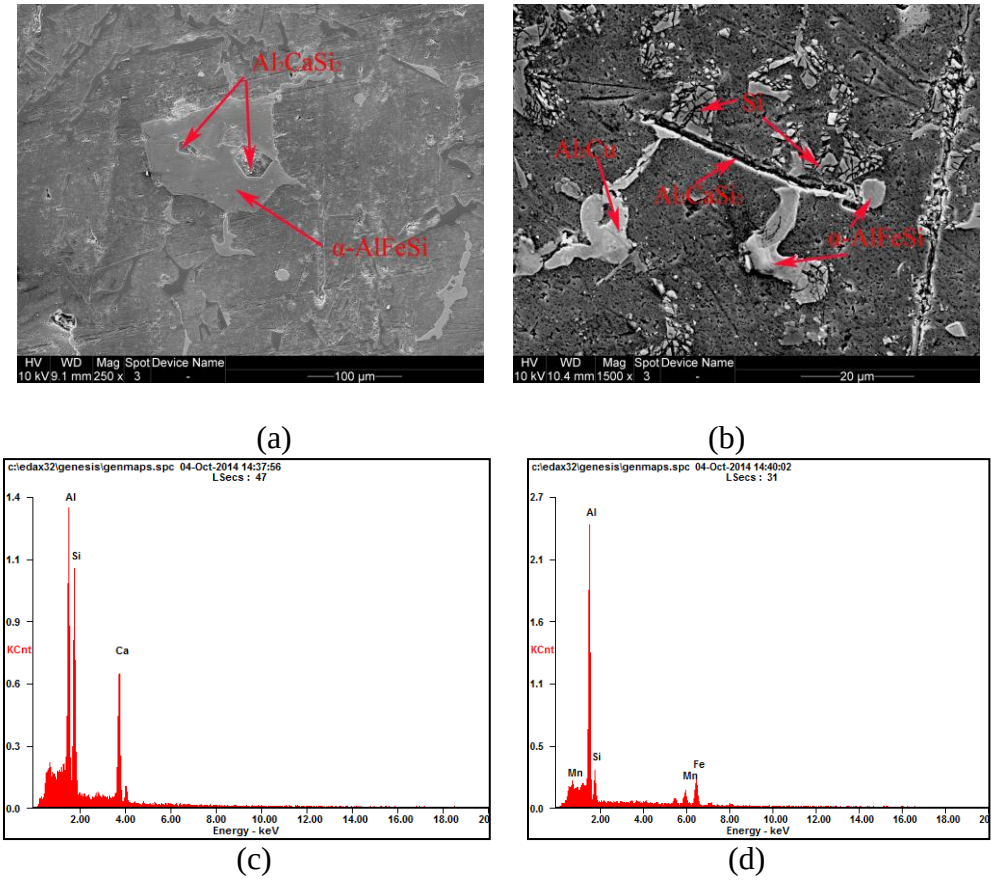


*Figure 5.13* Relations of $Al_2CaSi_2$ and α-AlFeSi
(a) (b) SEM images showing nucleation of α-AlFeSi from $Al_2CaSi_2$; (c) EDS of $Al_2CaSi_2$; (d) EDS of α-AlFeSi

Table 5.13 *Chemical composition of the phases indicated in Fig 5.13 (at.%)*

| Phase | Al | Si | Mn | Fe | Ca |
|---|---|---|---|---|---|
| $Al_2CaSi_2$ | 34.29 | 42.92 | - | - | 22.79 |
| α-AlFeSi | 69.90 | 13.87 | 5.32 | 10.90 | - |

From the SEM images, we can see that $Al_2CaSi_2$ phase has two morphologies, namely: polygon and platete. Here the polygon phase is the first precipate and becomes the nucleation substrate for a later precipitate phase, such as α-AlFeSi. On the other hand, $Al_2CaSi_2$ with the other morphology can also be the nucleation substrate of $Al_2Cu$, α-AlFeSi and Si phase. From the SEM images and calculation results, it can be seen that $Al_2CaSi_2$ is a good nulcleation substrate for α-AlFeSi, thus reducing the fraction of β-AlFeSi.

So in summary, the best Ca addition is 0.1% in A380 alloy to reduce the dentrimental β-AlFeSi phase and avoid the formation of $Al_2CaSi_2$ sludge.

(b) Sr

There are three hypotheses dealing with the effect of addition of Sr on the category and morphology of the AlFeSi phase.

1) Sr can be absorbed on the surface of primary α-AlFeSi phase to act as a barrier for dissolution. Thus, the peritectic reaction L+α-AlFeSi=Al+β-AlFeSi will be hindered. If this situation happens, α-AlFeSi phase can be the reactant of the peritectic reaction. But from the observation of samples without Sr addition, there is no β-AlFeSi to grow from and entrap α-AlFeSi. Thus no obvious peritectic reaction can be found. Except for the low cooling rates, there is not enough time for the primary α-AlFeSi phase to form, while fast cooling rates can contribute to better modification of β-AlFeSi. Thus this theory cannot support the current experimental results or explain the phenomenon observed in the experiment.

2) Sr can cause the super saturation of the elements Fe and Si. With the Supersaturated Si and Fe the primary β-AlFeSi phase will nucleate first prior to the

formation of α-Al. After that, α-Al begins to nucleate on the surface of the primary β-phase and Fe is rejected The secondary β-AlFeSi phase then grow on the interdendrite zone (Closset et al., 1996; Cho et al., 2008). The growth rate of the secondary phase is much lower than that of the primary phase, thus, the smaller β-AlFeSi phases can be found. However, no obvious primary β-AlFeSi phases can be found from the samples. For A380 alloys in general, the β-AlFeSi formation temperature is much lower than the liquidus temperature so that even with the assistance of Sr, primary β-AlFeSi phase cannot form.

3) It was another opinion that the Sr can be absorbed on the possible nucleation positions of the β-phase, which is named as poisoning. Therefore, the quantity of the β phase reduced. There is no observation of this situation from in experiment.

Instead, our experimental results indicate the presence of an increased double-size oxidation layer and the formation of $Al_2SrSi_2$ phase during solidification. Figure 5.14 shows α-AlFeSi grew from $Al_2SrSi_2$. The $Al_2SrSi_2$ has an effect similar to that of $Al_2CaSi_2$, which is also a good substrate of the α-AlFeSi phase. However, the Sr can also introduce an oxidation layer, which is a source of the nucleation of β-AlFeSi. Thus the amount of Sr addition should be controlled.

So in summary, the best Sr addition is 0.1% in A380 alloy to reduce the dentrimental β-AlFeSi phase and avoid the formation of $Al_2SrSi_2$ sludge and SrO oxide layer.

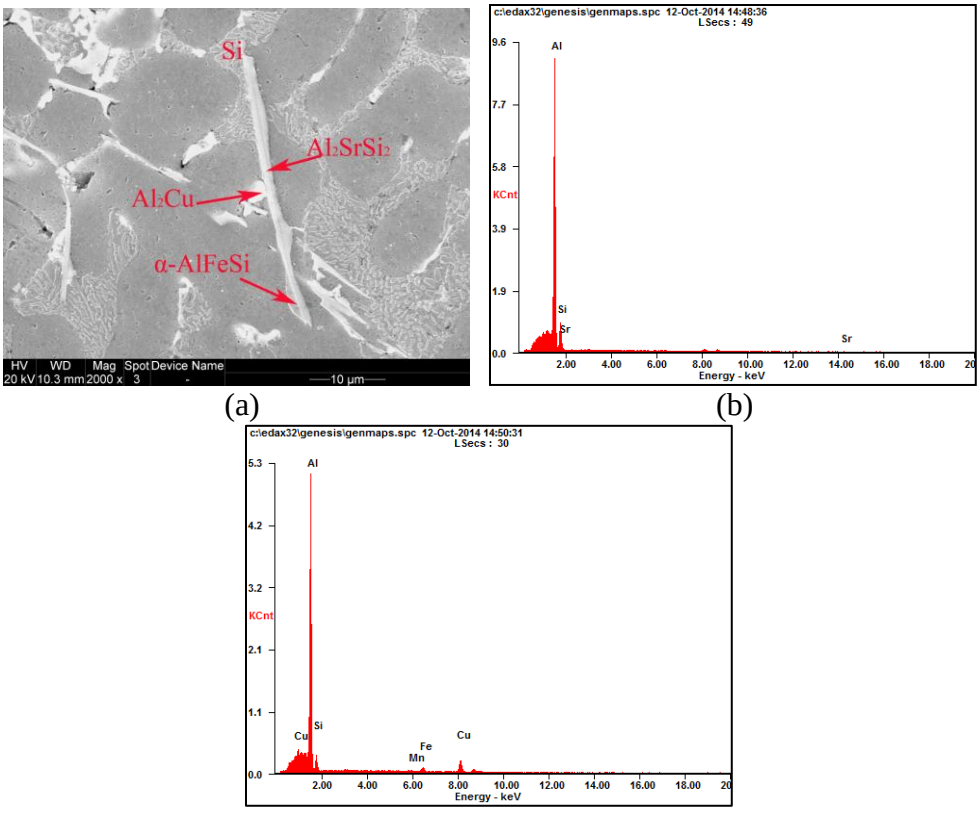


*Figure 5.14* Relations of $Al_2SrSi_2$ and α-AlFeSi
(a) SEM images showing nucleation of α-AlFeSi from $Al_2SrSi_2$; (b) EDS of $Al_2SrSi_2$; (c) EDS of α-AlFeSi

Table 5.14 *Chemical composition of the phases indicated in Fig. 5.14 (at.%)*

| Phase | Al | Si | Mn | Fe | Sr |
|---|---|---|---|---|---|
| $Al_2SrSi_2$ | 73.98 | 24.91 | - | - | 1.11 |
| α-AlFeSi | 82.81 | 10.21 | 0.17 | 1.45 | - |

c)K

Ashtari, Tezuka and Sato (2005) proposed several reasons why addition of K can lead to a refinement of the β-AlFeSi phase and transfer of β-AlFeSi to α-AlFeSi as follows. The addition of K lower eutectic Si formation temperature and increases fcc α-Al formation temperature and formation temperatures of the β-AlFeSi. It is because the

increase of nucleation site. The increasing nucleation sites are possibly $K_2O$. $K_2O$ let the α-AlFeSi to nucleate at a high cooling rate, while the β-AlFeSi at a low cooling rate.

From the experiment results it can be seen that most α-compound connects with some oxidation and according to literature review, it should be $K_2O$. But Ashtari suggests that $K_2O$ can be the nucleation site of the β-compound which increases the β-compound nucleation temperature and reduces the eutectic temperature. Because the size of β-compound is mainly controlled by the growth of the dendrite stage; in other words, it is controlled by the temperature between the nucleation temperature of β-compound and eutectic temperature. Then the size of the β-compound should be increased which is in contradiction with the experimental results. The reason for the increase is the nucleation of α-compound on $K_2O$. From the high magnification images, it can be seen that at the center of α-AlFeSi, a point nucleate center, there exists an oxide layer of $K_2O$. It should be the nucleate center for an α-compound.

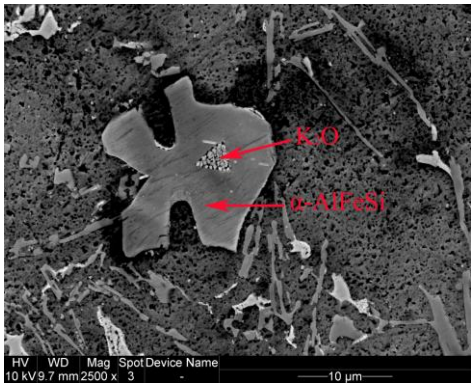


(a)

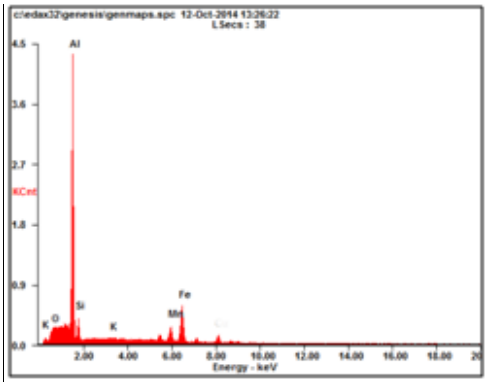


(b)

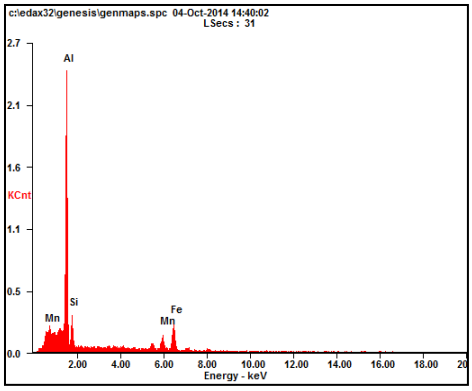


(c)

*Figure 5.15* Relation of $K_2O$ and α-AlFeSi
(a) SEM images showing nucleation of α-AlFeSi from $K_2O$; (b) EDS of $K_2O$ zone; (c)EDS of α-AlFeSi

Table 5.15 *Chemical composition of the phases indicated in Fig. 5.15 (at.%)*

| Phase | Al | Si | Mn | Fe | K | O |
|---|---|---|---|---|---|---|
| $K_2O$ zone | 72.29 | 9.06 | 1.58 | 4.45 | 0.29 | 12.32 |
| α-AlFeSi | 69.90 | 13.87 | 5.32 | 10.90 | - | - |

Table 5.15 shows the chemical analysis of the K compound and the α-AlFeSi in Fig. 5.15. It is possible that most of the K compound was removed during polishing. However, a trace of K and O remain. The chemical analysis of the α-AlFeSi does not exhibit any amount of K. So the K compounds are possibly $K_2O$.

In summary K is a good AlFeSi phase modifier for it does not introduce any intermetallics. The best K addition is 2% in A380 alloy

d) Mg

As previously noted, if Mg is added to A380 alloy, π-AlMgFeSi phase is formed. This is shown in Figure 5.16. Because this is a more detrimental phase, it should be avoided.

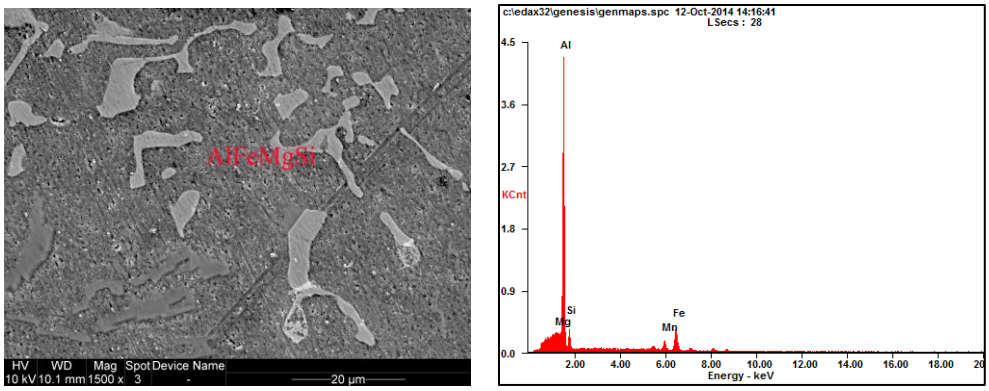


(a) (b)

*Figure 5.16* Relations of AlFeMgSi and α-AlFeSi
(a) SEM images showing nucleation of AlFeMgSi; (b) EDS of AlFeMgSi

Table 5.16 *Chemical composition of the phases indicated in Fig. 5.16 (at.%)*

| Phase | Al | Si | Mn | Mg | Fe |
|---|---|---|---|---|---|
| AlFeMgSi | 75.04 | 10.42 | 2.51 | 5.23 | 6.80 |

## 5.5 The Heat Treatment

Platelate Al-Fe-Si phase is relatively hazardeous due to its role in the formation of stress concentration and separation of the matrix. If the needle shape β-AlFeSi phase can be dissolved, the detrimental effect can be reduced. From that point on, the higher the heat treatment temperature, the shorter of the iron phase, the more help to improve the mechanical properties the alloy. It was found that during the heat treatment, and with the higher heat treatment temperature, the size of silicon particles will be further increased, which is called coarsening; and also the remelt will severely weaken the strength and ductility of the alloy. In the heat treatment process, it is more difficult to keep the temperature constant. Therefore in practical heat treatment application, temperature should not be too high. From the experimental results of section 4.2.12, although for a 525 ℃ heat treatment, 1 hour treat time is enough to get all visible β-AlFeSi diminished,

However, to avoid the problems mentioned above, one should control the heat treatment temperature around 515 ℃.

It is proved that β-AlFeSi phase can be dissolved during heat treatment. The higher the holding temperature, the greater the degree of iron phases shortened, which is due to the more favorable conditions of higher temperature dynamics. On the other hand, as the fraction of α-AlFeSi decreases, the fraction of β-AlFeSi is also decreased. This cannot be fully explained by the theory of dissolving. The only explanation that can be offered is that β-AlFeSi transfer to α-AlFeSi. Figure 5.17 shows that heat treatment can facilitate the trand transformation of β-AlFeSi to α-AlFeSi.

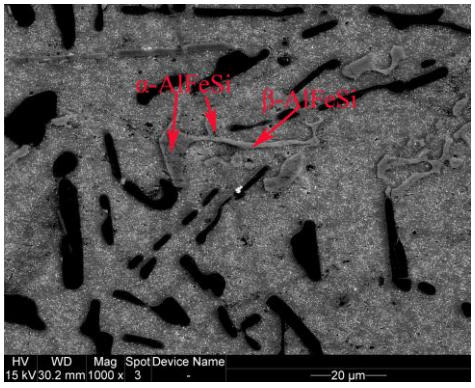


*Figure 5.17* A380 heated at 515°C for 2 hours, β phase transferred to α phase

## 5.6 The Regression Results of Elements on β-AlFeSi phase

According to the experimental results, the results of a regression analysis between β-AlFeSi phase formation and element content in 380-x(x=Ca, Sr, Ti, K) can be expressed as follows:

380 system:

$$f_{\beta(\mathrm{AlFeSi})} = 0.001\mathrm{Si} + 0.022\mathrm{Fe} - 0.012\mathrm{Mn} \quad (5.2)$$

380-Ca system:

$$f_{\beta(AlFeSi)} = 0.001Si + 0.022Fe - 0.012Mn - 0.014Ca \quad (5.3)$$

380-Sr system:

$$f_{\beta(AlFeSi)} = 0.001Si + 0.022Fe - 0.012Mn - 0.006Sr \quad (5.4)$$

380-K system:

$$f_{\beta(AlFeSi)} = 0.001Si + 0.022Fe - 0.012Mn - 0.0012K \quad (5.5)$$

## 5.7 The Suggestion of β-AlFeSi Phase Control

Based on this work, the following suggestions for controlling of β-AlFeSi phase formation are presented:

1) Increase the cooling rate

According to the cooling rate study of the A380 alloy, both size and fraction of β-AlFeSi decrease with increasing cooling rates. This is a common way to reduce the detrimental effect of β-AlFeSi phase.

2) Control the content Fe and Mn

Fe will facilitate the formation of β-AlFeSi phases. However, excessive Mn not only introduces sludge, but is also prone to form β-AlFeSi phases at high cooling rates.

3) Element addition

K is the best candidate to avoid the introduction of sludge. Meanwhile, Mn+Ca, Mn+Sr are good choices to get rid of the adverse effect of β-AlFeSi phases.

4) Heat treatment

High temperature and short duration heat treating can provide yet another option to modify the AlFeSi phase. However, the treatment termperature cannot be too high.

# CHAPTER 6. CONCLUSION

1. From the thermodynamics simulation results, Mn can suppress and Fe, Si, Zn can facilitate the formation of β-AlFeSi phases. The experiment at slow cooling rates proved this.
2. With low Mn and Fe, β-AlFeSi phase is a stable phase and can be formed using low cooling rates. With increasing amounts Mn or Fe, α-AlFeSi is more stable and high cooling rates can facilitate the formation of β-AlFeSi phase in reverse.
3. Ca and Sr can accelerate the fragmentation of β-AlFeSi phase and introduce $Al_2Sr$ $Si_2$ and $Al_2CaSi_2$, which act as the nucleation substrate of α-AlFeSi. However, excessive $Al_2SrSi_2$ and $Al_2CaSi_2$ can results in the formation of sludge
4. K can effectively reduce and even get rid of the β-AlFeSi phase. The introduced $K_2O$ can be the nucleation substrate of α-AlFeSi without the introduction of any other intermetallics.
5. The combination Sr and Mn, and Ca and Sr can reduce the formation of β-AlFeSi phase and sludge.
6. Short time high temperature heat treatment can both dissolve β-AlFeSi and transfer β-AlFeSi to α-AlFeSi.

7. The optimum method for reducing β-AlFeSi phase is to increase the cooling rate, control the content Fe and Mn, K, Ca or Sr addition, and short time high temperature heat treatment.

# LIST OF REFERENCES

# LIST OF REFERENCES

Allen, C. M., O'reilly, K. A. Q., Cantor, B., & Evans, P. V. (1998). Intermetallic phase selection in 1XXX Al alloys. *Progress in Materials Science, 43*(2), 89-170.

Anderson, J. C. (1970). *Materials Science.* New York: Wiley.

Apelian, D. (2009). *Aluminum cast alloys: enabling tools for improved performance*. North American Die Casting Association. Wheeling, Illinois.

Ashtari, P., Tezuka, H., & Sato, T. (2003). Influence of Sr and Mn additions on intermetallic compound morphologies in Al-Si-Cu-Fe cast alloys. *Materials Transactions*, *44*(12), 2611-2616.

Ashtari, P., Tezuka, H., & Sato, T. (2005). Modification of Fe-containing intermetallic compounds by K addition to Fe-rich AA319 aluminum alloys.*Scripta materialia*, *53*(8), 937-942.

Awano, Y., & Shimizu, Y. (1990). Non-equilibrium crystallization of alfesi compound in melt-superheated Al-Si alloy castings. *AFS Transactions*, *98*, 889-895.

Backerud, L., Chai, G., and Tamminen, J. (1990). *Solidification Characteristics of Aluminum Alloys. Vol. 2. Foundry Alloys*. Detroit: American Foundrymen's Society.

Bramfitt, B. L. (1970). The effect of carbide and nitride additions on the heterogeneous nucleation behavior of liquid iron. *Metallurgical Transactions*, *1*(7), 1987-1995.

Brandt, M. K., Glazoff, M. V., Grasmo, G., Jacobsen, P. S., Johnsen, T., Jorgensen, S., & Zhang, W. (2006). *U.S. Patent No. 7,087,125*. Washington, DC: U.S. Patent and Trademark Office.

Buzea, C., Pacheco, I. I., & Robbie, K. (2007). Nanomaterials and nanoparticles: sources and toxicity. *Biointerphases*, *2*(4), MR17-MR71.

Campbell, J. (1991). *Casting*. Oxford, United Kingdom: Butterworth-Heinemann.

Cao, X., & Campbell, J. (2004). Effect of Sr on primary α-Fe phase in liquid Al-11.5 Si-0.4 Mg cast alloy. *Materials Science and Technology, 20*(4), 514-520.

Cao, X., & Campbell, J. (2004). The solidification characteristics of Fe-rich intermetallics in Al-11.5 Si-0.4 Mg cast alloys. *Metallurgical and Materials Transactions A, 35*(5), 1425-1435.

Cao, X., & Campbell, J. (2006). Morphology of Beta-$Al_5FeSi$ Phase in Al-Si Cast Alloys. *Materials Transactions, 47*, 1303–1312.

Carpenter, G. J. C. & Lepage, Y. (1993) Revised Cell Data for the Beta-FeSiAl Phase in Aluminum Alloys. *Scripta Metallurgica et Materialia, 28*, 733–736.

Cho, Y. H., Lee, H. C., Oh, K. H., & Dahle, A. K. (2008). Effect of Strontium and Phosphorus on Eutectic Al-Si Nucleation and Formation of β-Al5FeSi in Hypoeutectic Al-Si Foundry Alloys. *Metallurgical and Materials Transactions A, 39*(10), 2435-2448.

Closset, B., & Gruzleski, J. E. (1982). Mechanical properties of A356.0 alloys modified with pure strontium. *AFS Transactions, 31*, 453-464.

Closset, B., & Gruzleski, J. E. (1982). Structure and properties of hypoeutectic Al-Si-Mg alloys modified with pure strontium.*Metallurgical Transactions A, 13*(6), 945-951.

Closset, B., Paray, F., Gruzleski, J., & Mulazimoglu, H. (1996). Microstructures and properties of strontium treated aluminium electrical conductor alloys. *Light Metals*, 737–744.

Cooper, M. (1967). The crystal structure of the ternary alloy (AlFeSi). *Acta Crystallographica, 23*(6), 1106-1107.

Cooper, M., & Robinson, K. (1966). The crystal structure of the ternary alloy (AlMnSi). *Acta Crystallographica, 20*(5), 614-617.

Colwell, D. L. & Kissling, R. J. (1961). Die and permanent mold casting aluminum alloy minor elements. *AFS Transactions, 69*, 610–615.

Crepeau, P. N. (1995). Effect of iron in Al-Si casting alloys: A critical review. *Transactions of the American Foundrymen's Society, 103*, 361–366.

Czikel, J., Pfeiffer, W. D., Sabath, G., & Steinhaufl, B. (1985). Effects of zinc, iron and manganese on the properties of AlSi8Cu3 type alloys. *Aluminium, 61*, 917–922.

Couture, A. (1981) Iron in aluminum casting alloys–a literature survey. *International Cast Metals Journal, 6*, 9–17.

Dichtl, H. J. (1970) Use of molybedenum to compensate for the adverse effect of iron in aluminium-silicon alloys. *Aluminium, 46*, 362–364.

Dinnis, C. M., Taylor, J. A., & Dahle, A. K. (2005). As-cast morphology of iron intermetallics in Al-Si foundry alloys. *Scripta Materialia, 53*, 955–958.

Doehler, H. H. (1951). *Die Casting.* New York: McGraw-Hill

Donahue, R. H. (2011). Proposed environmentally green high pressure die casting alloys with low Iron for improved mechanical properties and Strontium for die soldering resistance. *NADCA*

Gobrecht, J. (1975). Settling-out of Fe, Mn and Cr in Al-Si casting alloys. pt. 1. *Giesserei, 62*, 263-266.

Granger, D. A., Sawtell, R. R., & Kersker, M. M. (1984). Effect of beryllium on the properties of A357.0 castings. (Retroactive coverage). *Transactions of the American Foundrymen's Society, 92*, 579-586.

Gowri, S., & Samuel, F. H. (1994). Effect of alloying elements on the solidification characteristics and microstructure of Al-Si-Cu-Mg-Fe 380 alloy.*Metallurgical and Materials Transactions A, 25*(2), 437-448.

Green, J. A. (2007). *Aluminum recycling and processing for energy conservation and sustainability*. ASM International.

Groover, Mikell P. *Fundamentals of modern manufacturing: materials processes, and systems*. John Wiley & Sons, 2007.

Gustafsson, G., Thorvaldsson, T., & Dunlop, G. L. (1986).The influence of iron and chromium on the microstructure of cast Al–Si–Mg alloys. *Metallurgical Transactions A, 17*, 45-52.

Hanna, M. D., Lu, S. Z., & Hellawell, A. (1984). Modification in the aluminum silicon system. *Metallurgical Transactions A, 15*(3), 459-469.

Hartlieb, M. (2013). Aluminum Alloys for Structural Die Casting. *Die Casting Engineer, 57*(3), 40-43.

Iglessis, J., Frantz, C., & Gantois, M. (1977). Conditions for the formation of the Fe phases in commercial purity Al-Si alloys. *Memoires Et Etudes Scientifiques De La Revue De Metallurgie, 74*, 237-242.

Jones, H. (1969). Observations on a structural transition in aluminium alloys hardened by rapid solidification. *Materials Science and Engineering*, *5*(1), 1-18.

Karamouz, M., Azarbarmas, M., Emamy, M., & Alipour, M. (2013). Microstructure, hardness and tensile properties of A380 aluminum alloy with and without Li additions. *Materials Science and Engineering: A*, *582*, 409-414.

Khalifa, W., Samuel, F. H., & Gruzleski, J. E. (2003). Iron intermetallic phases in the Al corner of the Al-Si-Fe system. *Metallurgical and Materials Transactions A*, *34*(3), 807-825.

Kim, H. Y., Park, T. Y., Han, S. W., & Lee, H. M. (2006). Effects of Mn on the crystal structure of α-Al (Mn, Fe) Si particles in A356 alloys. *Journal of Crystal Growth*, *291*(1), 207-211.

Kosuge, H., & Mizukami, I. (1975). Formation of 'Fir-Tree' structure in D.C. Cast ingots of Al-0.6percent Fe alloys. *Journal of Japan Institute of Light Metals*, *25*, 48-58.

Kral, M. V. (2005). A crystallographic identification of intermetallic phases in Al-Si alloys. *Materials Letters, 59*, 2271-2276.

Kral, M. V., Mcintyre, H. R., & Smillie, M. J. (2004) Identification of intermetallic phases in a eutectic Al-Si casting alloy using electron backscatter diffraction pattern analysis. *Scripta Materialia, 51*, 215-219.

Kral, M. V., Nakashima, P. N. H., & Mitchell, D. R. G. (2006). Electron microscope studies of Al-Fe-Si intermetallics in an Al-11 Pct Si alloy. *Metallurgical and Materials Transactions A, 37*, 1987-1997.

Kumari, S. S., Pillai, R. M., & Pai, B. C. (2008). A study on the structural, age hardening and mechanical characteristics of Mn and Ca added Al-7Si-0.3Mg-0.6Fe alloy. *Journal of Alloys and Compounds, 453*, 167-173

Lakshmanan, A. N., Shabestari, S. G., & Gruzleski, J. E. (1995). Microstructure control of iron intermetallics in Al-Si casting alloys. *Zeitschrift für Metallkunde*, *86*(7), 457-464.

Liu, P., Thorvaldsson, T., & Dunlop, G. L. (1986). Formation of intermetallic compounds during solidification of dilute Al–Fe–Si alloys. *Materials Science and Technology*, *2*, 1009-1018.

Lu, L. & Dahle, A. K. (2005). Iron-rich intermetallic phases and their role in casting defect formation in hypoeutectic Al-Si alloys. *Metallurgical and Materials Transactions A, 36*, 819-835.

Mahta, M., Emamy, M., Daman, A., Keyvani, A., & Campbell, J. (2005). Precipitation of Fe rich intermetallics in Cr- and Co-modified A413 alloy. *International Journal of Cast Metals Research, 18*, 73-79.

Mascre, C. (1955). Influence of iron and manganese on type A-S13 (Alpax) alloys. *Fonderie, 108*, 4330-4336.

Mbuya, T. O., Odera, B. O., & Ng'ang'a, S. P. (2003). Influence of iron on castability and properties of aluminium silicon alloys: literature review. I*nternational Journal of Cast Metals Research, 16*(5), 451-465.

Miki, I., Kosuge, H., & Nagahama, K. (1975). Supersaturation and decomposition of Al-Fe alloys during solidification. *J. Japan Inst. Light Metals, 25*(1), 1-9.

Mondolfo, L. F. (1976). *Aluminum Alloys: Structure and Properties.* London: Butterworths.

Morris, L. R. & Miners, F. B. (1975). *Aluminum Alloys*. Montreal, QC: Alcan Research and Development Limited.

Murali, S., Raman, K. S., & Murthy, K. S. S. (1994). Morphological studies on beta-FeSiAl5 phase in Al- 7Si-0.3Mg alloy with trace additions of Be, Mn, Cr, and Co. *Materials Characterization, 33*, 99–112.

Mulazimoglu, M. H., Gruzleski, J. E., & Closset, B. (1992). Evaluation of the metallurgical effects of strontium on cast 6000 series aluminum alloys. *Aluminium, 68*, 489–493.

Mulazimoglu, M. H., Paray, F., Gruzleski, J. E., & Kulunk, B. (1994). Modification of intermetallic phases by strontium in aluminum wrought alloys. *Light Metals, 27*,1047–1056.

Narayanan, L. A., Samuel, F. H., & Gruzleski, J. E. (1994). Crystallization behavior of iron-containing intermetallic compounds in 319 aluminum-alloy. *Metallurgical and Materials Transactions a-Physical Metallurgy and Materials Science, 25*, 1761-1773.

Novelline, R. (1997). *Squire's Fundamentals of Radiology*. Massachusetts: Harvard University Press.

Pan, Q. Y., Wang, L., Apelian, D., & Makhlouf, D. (2005). Optimization of 380 Alloy for Semi-Solid Processing. *NADCA.*

Pennors, A., Samuel, A. M., Samuel, F. H., & Doty, H. W. (1998). Precipitation of beta-Al sub 5 FeSi iron intermetallic in Al-6% Si-3. 5% Cu(319) type alloys: role of Sr and P. *American Foundrymen's Society, Inc, Transactions of the American Foundrymen's Society,, 106*, 251-264..

Philips, H. W. (1976). *Annotated Equilibrium Diagrams of Some Aluminum Alloy Systems*. London: The Institute of Metal.

Phragmen, G. (1950). On the phases occurring in alloys of aluminium with copper, magnesium, manganese, iron, and silicon. *Journal of the Institute of Metals*, *77*(6), 489-551.

Roy, N., Samuel, A. M., & Samuel, F. H. (1996). Porosity formation in Al-9 wt% Si-3 wt% Cu alloy systems: metallographic observations. *Metallurgical and Materials Transactions A*, 27, 415–429.

Samuel, A. M. & Samuel, F. H. (1995). Effect of alloying elements and dendrite arm spacing on the microstructure and hardness of an Al-Si-Cu-Mg-Mg-Fe-Mn (380). *Journal of Materials Science, 301*, 698-1708.

Samuel, A. M., Samuel, F. H., Villeneuve, C., Doty, H. W., & Valtierra, S. (2001) Effect of trace elements on Al5FeSi characteristics, porosity and tensile properties in Al-Si-Cu (319) cast alloys. *International Journal of Cast Metals*, *14*, 97-120.

Samuel, A. M., Samuel, F. H., & Doty, H. W. (1996) Observations on the formation of β-AlFeSi phase in 319 type Al-Si alloys. *Journal of Materials Science, 31*, 5529-5539.

Schulze, G. E. (1967). *Metallphysik*. Berlin: Akademie-Verlag.

Shabestari, S. G., & Gruzleski, J. E. (1995). Modification of Iron Intermetallics by Strontium in 413 Aluminum Alloys (95-26). *Transactions of the American Foundrymen's Society, 103*, 285-294.

Shabestari, S. G. (2004). The effect of iron and manganese on the formation of intermetallic compounds in aluminum-silicon alloys. *Materials Science and Engineering A, 383*, 289–298.

Shabestari, S. G. and Shahri, F. (2004). Influence of modification, solidification conditions and heat treatment on the microstructure and mechanical properties of A356 aluminum alloy. *Journal of Materials Science, 39*, 2023–2032.

Sigworth, G. K., Wang, C., Huang, H., and Berry, J. T. (1994). Porosity formation in modified and unmodified Al-Si alloy casting, *AFS Transactions*, *102*, 245-261.

Skjerpe, P. (1987). Intermetallic phases formed during DC-casting of an Al–0.25Fe–0.13Si alloy. *Metallurgical Transactions A, 18*, 189–200.

Stefaniay, V., Griger, A., & Turmezey, T. (1987) Intermetallic phases in the aluminium-side corner of the AlFeSi-alloy system. *Journal of Materials Science, 22*, 539–546.

Suarez-Pena, B. & Asensio-Lozano, J. (2006). Influence of Sr modification and Ti grain refinement on the morphology of Fe-rich precipitates in eutectic Al-Si die cast alloys. *Scripta Materialia, 54*, 1543–1548.

Tang, S. K., & Sritharan, T. (1998). Morphology of beta-AlFeSi intermetallic in Al-7Si alloy castings. *Materials Science and Technology, 14*, 738–742.

Taylor, J. A. (1995). Metal related castability effects in aluminium foundry alloy. *Cast Metals, 8*(4), 225-252.

Tuttle, B. L., and Lindsay, R. W. (1984). Principles of solidification control in cast metals. *AFS Transactions, 92*, 681-692

Wang, Y., & Xiong, Y. (2000). Effects of beryllium in Al-Si-Mg-Ti cast alloy. *Materials Science and Engineering α-Structural Materials Properties Microstructure and Processing, 280*, 124–127.

William, D. V. & Bernard, W. (1987). Aluminum base alloys of the Al-Cu-Mg-Zn type. US Patent No. 4711762.

Yie, S. N., Lee, S. L., Lin, Y. H., & Lin, J. C. (1999). Mechanical properties of Al-11% Si casting alloys containing trace Be and Sr. *Materials Transactions, JIM, 40*, 294–300

Yoo, J. E., Shan, A., & Moon, I. G. (1999). A study on composition and crystal structure of dispersoids in AlMgSi alloys. *Journal of Materials Science, 34*, 2679–2683.

Yin, F. (2001). Study on the morphology of Iron-rich phase and its solidification Behavior in Aluminum-silicon Alloy. Dissertation of Shanhai Jiaotong University.

Young, R. M. K., & Clyne, T. W. (1981). An Al–Fe intermetallic phase formed during controlled solidification. *Scripta Metallurgica,15*, 1211–1216.

Zald ívar-Cadena, A. A., & Flores-Vald és, A.(2007). Prediction and identification of calcium-rich phases in Al–Si alloys by electron backscatter diffraction EBSD/SEM. *Materials Characterization, 58*, 834–841.

Zheng, J. G., Vincent, R., & Steeds, J. W. (2000). *Philosophical Magazine A*, *80*, 493–500.

Zhang, H. (2007). Effect of iron on the microstructure and mechanical properties of Al-Si alloys. *Light Metals*, 775–780.

Zhang, L., Gao, J., Damoha, L., & Robertson, D. G. (2012). Removal of iron from aluminum: a review. *Mineral Processing and Extractive Metallurgy Review, 39*, 99-157.

# APPENDIX

# APPENDIX

## The Statistics Results

Table A.1 *Tests of the content of elements on fraction of α-Al-Fe-Si*

| Source | Type III Sum of Squares | df | Mean Square | F | Sig. |
|---|---|---|---|---|---|
| Corrected Model | .030[a] | 20 | .002 | 57.628 | .000 |
| Intercept | .053 | 1 | .053 | 2042.072 | .000 |
| Si | .000 | 4 | 7.963E-5 | 3.048 | .036 |
| Fe | .002 | 4 | .001 | 20.169 | .000 |
| Mn | .022 | 4 | .006 | 211.277 | .000 |
| Mg | 7.910E-5 | 4 | 1.977E-5 | .757 | .563 |
| Cu | .000 | 4 | 4.192E-5 | 1.604 | .206 |
| Error | .001 | 24 | 2.613E-5 | | |
| Total | .096 | 45 | | | |
| Corrected Total | .031 | 44 | | | |

Table A.2 *Tests of the content of elements on formation temperature of α-Al-Fe-Si*

| Source | Type III Sum of Squares | df | Mean Square | F | Sig. |
|---|---|---|---|---|---|
| Corrected Model | 49434.342[a] | 20 | 2471.717 | 39.473 | .000 |
| Intercept | 19958005.781 | 1 | 19958005.781 | 318729.290 | .000 |
| Si | 1487.328 | 4 | 371.832 | 5.938 | .002 |
| Fe | 8541.629 | 4 | 2135.407 | 34.102 | .000 |
| Mn | 29190.983 | 4 | 7297.746 | 116.545 | .000 |
| Mg | 113.701 | 4 | 28.425 | .454 | .769 |
| Cu | 795.079 | 4 | 198.770 | 3.174 | .032 |
| Error | 1502.818 | 24 | 62.617 | | |
| Total | 35672183.474 | 45 | | | |
| Corrected Total | 50937.160 | 44 | | | |

Table A.3 *Tests of the content of elements on fraction of β-Al-Fe-Si*

| Source | Type III Sum of Squares | df | Mean Square | F | Sig. |
|---|---|---|---|---|---|
| Corrected Model | .008[a] | 20 | .000 | 24.895 | .000 |
| Intercept | .010 | 1 | .010 | 566.341 | .000 |
| si | .001 | 4 | .000 | 8.366 | .000 |
| fe | .005 | 4 | .001 | 73.115 | .000 |
| mn | .002 | 4 | .000 | 29.222 | .000 |
| mg | 7.024E-5 | 4 | 1.756E-5 | 1.035 | .410 |
| cu | 6.704E-5 | 4 | 1.676E-5 | .987 | .433 |
| Error | .000 | 24 | 1.697E-5 | | |
| Total | .028 | 45 | | | |
| Corrected Total | .009 | 44 | | | |

Table A.4 T*ests of the content of elements on formation temperature of β-Al-Fe-Si*

| Source | Type III Sum of Squares | df | Mean Square | F | Sig. |
|---|---|---|---|---|---|
| Corrected Model | 14203.406[a] | 20 | 710.170 | 26.452 | .000 |
| Intercept | 18120662.015 | 1 | 18120662.015 | 674955.999 | .000 |
| si | 170.442 | 4 | 42.611 | 1.587 | .210 |
| fe | 9189.371 | 4 | 2297.343 | 85.571 | .000 |
| mn | 2751.723 | 4 | 687.931 | 25.624 | .000 |
| mg | 229.664 | 4 | 57.416 | 2.139 | .107 |
| cu | 33.450 | 4 | 8.363 | .311 | .867 |
| Error | 644.332 | 24 | 26.847 | | |
| Total | 33084560.936 | 45 | | | |
| Corrected Total | 14847.738 | 44 | | | |

Table A.5 *Tests of the content of elements on formation temperature of fcc α-Al*

| Source | Type III Sum of Squares | df | Mean Square | F | Sig. |
|---|---|---|---|---|---|
| Corrected Model | 10860.024[a] | 20 | 543.001 | 310.160 | .000 |
| Intercept | 18425515.314 | 1 | 18425515.314 | 10524565.989 | .000 |
| si | 9430.411 | 4 | 2357.603 | 1346.651 | .000 |
| fe | .237 | 4 | .059 | .034 | .998 |
| mn | 6.976 | 4 | 1.744 | .996 | .429 |
| mg | 60.623 | 4 | 15.156 | 8.657 | .000 |
| cu | 280.135 | 4 | 70.034 | 40.003 | .000 |
| Error | 42.017 | 24 | 1.751 | | |
| Total | 33486854.067 | 45 | | | |
| Corrected Total | 10902.041 | 44 | | | |

Table A.6 *Tests of the content of elements on fraction of Si*

| Source | Type III Sum of Squares | df | Mean Square | F | Sig. |
|---|---|---|---|---|---|
| Corrected Model | .023[a] | 20 | .001 | 120.916 | .000 |
| Intercept | .123 | 1 | .123 | 12932.816 | .000 |
| si | .021 | 4 | .005 | 547.934 | .000 |
| fe | .000 | 4 | 7.636E-5 | 8.027 | .000 |
| mn | 1.833E-5 | 4 | 4.583E-6 | .482 | .749 |
| mg | .000 | 4 | 3.027E-5 | 3.182 | .031 |
| cu | 2.470E-5 | 4 | 6.174E-6 | .649 | .633 |
| Error | .000 | 24 | 9.513E-6 | | |
| Total | .254 | 45 | | | |
| Corrected Total | .023 | 44 | | | |

Table A.7 *Tests of the content of elements on formation temperature of Si*

| Source | Type III Sum of Squares | df | Mean Square | F | Sig. |
|---|---|---|---|---|---|
| Corrected Model | 2934.371[a] | 20 | 146.719 | 13.808 | .000 |
| Intercept | 17454739.733 | 1 | 17454739.733 | 1642737.320 | .000 |
| si | 2182.141 | 4 | 545.535 | 51.343 | .000 |
| fe | 140.903 | 4 | 35.226 | 3.315 | .027 |
| mn | 39.162 | 4 | 9.790 | .921 | .468 |
| mg | 172.947 | 4 | 43.237 | 4.069 | .012 |
| cu | 238.747 | 4 | 59.687 | 5.617 | .002 |
| Error | 255.010 | 24 | 10.625 | | |
| Total | 31728603.907 | 45 | | | |
| Corrected Total | 3189.380 | 44 | | | |

VITA

# VITA

Meng Wang earned degrees Bachelor in Materials Science and Engineering, and Masters in Science in Materials Science, both from Harbin Institute of Technology, in Harbin, China. Then he studied on the development of Aluminum alloy in Purdue University for Ph. D. work under the supervision of Dr. Qingyou Han from August 2010.